BINDING INTERACTION OF QUINOLINE DERIVATIVES TO SERUM ALBUMIN USING MULTISPECTROSCOPY, MOLECULAR DOCKING AND MOLECULAR DYNAMICS SIMULATIONS

NATCHAPHON NGUEANNGAM

Graduate School Srinakharinwirot University

2023

การศึกษาอันตรกิริยาระหว่างอนุพันธ์ควิโนลีนกับซีรั่มอัลบูมีนโดยใช้มัลติสเปกโตรสโกปี โมเลกุลลาร์ด็อกกิ้ง และการจำลองพลวัตเชิงโมเลกุล

ณัชพล เงื่อนงาม

ปริญญานิพนธ์นี้เป็นส่วนหนึ่งของการศึกษาตามหลักสูตร
วิทยาศาสตรมหาบัณฑิต สาขาวิชาเคมี
คณะวิทยาศาสตร์ มหาวิทยาลัยศรีนครินทรวิโรฒ
ปีการศึกษา 2566

BINDING INTERACTION OF QUINOLINE DERIVATIVES TO SERUM ALBUMIN USING MULTISPECTROSCOPY, MOLECULAR DOCKING AND MOLECULAR DYNAMICS SIMULATIONS

NATCHAPHON NGUEANNGAM

A Thesis Submitted in Partial Fulfillment of the Requirements

for the Degree of MASTER OF SCIENCE

(Chemistry)

Faculty of Science, Srinakharinwirot University

2023

THE THESIS TITLED

BINDING INTERACTION OF QUINOLINE DERIVATIVES TO SERUM ALBUMIN USING MULTISPECTROSCOPY, MOLECULAR DOCKING AND MOLECULAR DYNAMICS SIMULATIONS

BY

NATCHAPHON NGUEANNGAM

HAS BEEN APPROVED BY THE GRADUATE SCHOOL IN PARTIAL FULFILLMENT
OF THE REQUIREMENTS FOR THE MASTER OF SCIENCE
IN CHEMISTRY AT SRINAKHARINWIROT UNIVERSITY

(Assoc. Prof. Dr. Chatchai Ekpanyaskul, MD.)
Dean of Graduate School

ORAL DEFENSE COMMITTEE

..... Major-advisor
(Assoc. Prof.Apinya Chaivisuthangkura)

..... Chair
(Assoc. Prof.Patchareenart Saparpakorn)

..... Co-advisor
(Arthit Makarasen)

..... Committee
(Pornthip Boonsri)

Title	BINDING INTERACTION OF QUINOLINE DERIVATIVES TO SERUM ALBUMIN USING MULTISPECTROSCOPY, MOLECULAR DOCKING AND MOLECULAR DYNAMICS SIMULATIONS
Author	NATCHAPHON NGUEANNGAM
Degree	MASTER OF SCIENCE
Academic Year	2023
Thesis Advisor	Associate Professor Apinya Chaivisuthangkura
Co Advisor	Arthit Makarasen

The interaction between plasma proteins and drugs is crucial for understanding the pharmacodynamics and pharmacokinetics of therapeutic agents. This study examined the intermolecular interactions of both bovine serum albumin (BSA) and human serum albumin (HSA) with two newly synthesized 2,4-disubstituted quinoline derivatives under physiological conditions. Multiple spectroscopic and computational methods were employed to evaluate the binding interaction. The study found that both the quinoline derivatives bound with both BSA and HSA at site III (sub-domain IB) and quenched the fluorescence of the protein through a static quenching mechanism. The binding constant (K_b) at the level of 10^4 L mol^{-1} and the number of binding site was determined to be approximately: (1) the binding mode based on thermodynamic parameters (298,308, and 318 K) suggested a spontaneous process, indicating that the interaction could be hydrogen bonding and van der Waals force. Additionally, the molecular docking and molecular dynamics (MD) simulations corresponded with the spectroscopic results, confirming the binding interactions between the quinoline derivatives and both BSA and HSA. This research provides valuable insights for designing and developing quinoline derivatives to enhance their potency against HIV-1 RT inhibitors.

Keyword : Bovine serum albumin (BSA), Human serum albumin (HSA), Quinoline, Molecular docking, Molecular dynamics simulations (MD)

ACKNOWLEDGEMENTS

My master's dissertation was successfully completed thanks to the invaluable assistance and attention of numerous individuals. Their advice and feedback greatly contributed to the improvement and finalization of this work, and I would like to express my heartfelt gratitude. First and foremost, I extend my deep and sincere gratitude to my advisor, Assoc. Prof. Dr. Apinya Chaivisuthangkura, for her continuous support of my graduate studies and research. Her invaluable guidance, patience, and support throughout my studies at Srinakharinwirot University have significantly enhanced my graduate experience. I am extremely thankful for her willingness to listen to my problems and for giving freedom to work on research. Being a member of her research group has been an invaluable experience. In addition, I would like to thank my co-advisor, Dr. Arthit Makarasen, senior researcher at the Chulabhorn Research Institute, for his generous contribution of time and resources to support this research.

A special thanks to the chair of the committee, Assoc. Prof. Dr. Patchreenart Saparpakorn, for dedicating valuable time to chair my dissertation examination committee. Furthermore, her insightful feedback and suggestions were instrumental in enhancing my research. I am also grateful to Dr. Pornthip Boonsri for her encouragement and assistance in various fields, particularly as a computational chemistry consultant, and for her willingness to listen to students' problems.

Finally, I would like to thank my parents for their unwavering support throughout my education. I also want to honor the memory of my late grandmother, who inspired and encouraged me to pursue a master's degree. Additionally, I am grateful to my seniors, friends, and juniors for their companionship and assistance throughout this research period.

NATCHAPHON NGUEANNGAM

TABLE OF CONTENTS

Page

LIST OF TABLES

Page

LIST OF FIGURES

Page

CHAPTER 1
INTRODUCTION

Background

Quinoline derivatives currently play a pivotal role in drug development, and find widespread applications across various fields including chemistry, medicine, and pharmacology. These compounds exhibit significant pharmacological properties such as anti-inflammatory, anticonvulsant, antimalarial, antibacterial, and anticancer effects, due to their unique chemical structures. Quinoline derivatives serve as foundational structures in the synthesis of pharmacologically active substances and other intriguing chemicals. Currently, drugs within the quinoline derivative group are utilized in medical treatments, particularly in combating bacterial infections with antibiotics like fluoroquinolones, including norfloxacin, ciprofloxacin, and ofloxacin. Additionally, medications such as tafenoquine are prescribed for preventing the recurrence of *Plasmodium vivax* malaria and have gained approval from the United States Food and Drug Administration (US-FDA) in 2018 for treating P. *vivax* malaria infections. Moreover, cancer drugs like neratinib, pelitinib, dovitinib, tipifarnib, and quarfloxin belong to this group and are employed in breast cancer treatment. Studies have also indicated the transportation of quinoline derivative drugs via albumin transport proteins in the bloodstream. Previous research has delved into the use of the cancer drug neratinib in conjunction with the transport protein bovine serum albumin (Wani, Bakheit, Abounassif, & Zargar, 2018). Serum albumin, a globular protein predominantly present in plasma, constitutes roughly 60% of the protein content in plasma (Tao, Wang, Sheng, & Zhen, 2021). Its significance lies in its pivotal role in transporting diverse substances and molecules through the bloodstream, thereby enhancing the distribution of nutrients, hormones, vitamins, drugs, and other compounds to various tissues. This function of serum albumin holds utmost importance in pharmacokinetic studies of drugs. Therefore, investigating the interaction between small biomolecules and serum albumin is immensely valuable for comprehending the mechanism of action of drugs.

Bovine serum albumin (BSA) and human serum albumin (HSA) are both transport proteins found in plasma, sharing approximately 76% similarity in their physical characteristics (Huang, Kim, & Dass, 2004; Majorek et al., 2012; Mishra & Heath, 2021). They are characterized by an α-helix structure with three domains, each containing subdomains A and B. BSA consists of a sequence of 582 amino acids, while HSA has a sequence of 585 amino acids. Both proteins possess binding sites capable of interacting with drugs such as warfarin and ibuprofen, and they exhibit a well-defined amino acid sequence structure. Furthermore, BSA and HSA are readily available at low cost, making them easily accessible for research purposes. They are widely utilized in studying drug interactions with serum albumin due to their similarities and practicality.

Therefore, this research aims to investigate the interaction mechanisms between two quinoline derivatives, 4-(2′,6′-dimethyl-4′-formylphenoxy)-2-(5′-cyanopyridin-2′ylamino) quinoline (C) and 4-(2′,6′-dimethyl-4′-cyanophenoxy)-2-(5′-cyanopyridin-2′ylamino) quinoline (J), with bovine serum albumin (BSA) and human serum albumin (HSA), as depicted in Figures 1 and 2. These derivatives were designed and synthesized due to their observed inhibition of HIV-1 reverse transcriptase (RT) and to assess their cytotoxicity. Compounds C and J were synthesized through molecular hybridization of nevirapine (NVP), efavirenz (EFV), and rilpivirine (RPV), which are common inhibitors of HIV-1 RT. The derivatives exhibited inhibitory effects against HIV-1 RT with IC_{50} values of 1.93 μM and 1.22 μM, respectively, comparable to NVP (IC_{50} = 1.05 μM). Additionally, compound J showed no cytotoxicity against normal embryonic lung (MRC-5) cells, while compound C exhibited very low cytotoxicity compared to EFV and RPV. This study utilized multi-spectroscopic and multi-molecular modeling approaches to elucidate the interaction mechanisms between quinoline derivatives and serum albumins. The findings provide valuable information for the design and development of quinoline derivatives to enhance their efficacy as HIV-1 RT inhibitors in the future.

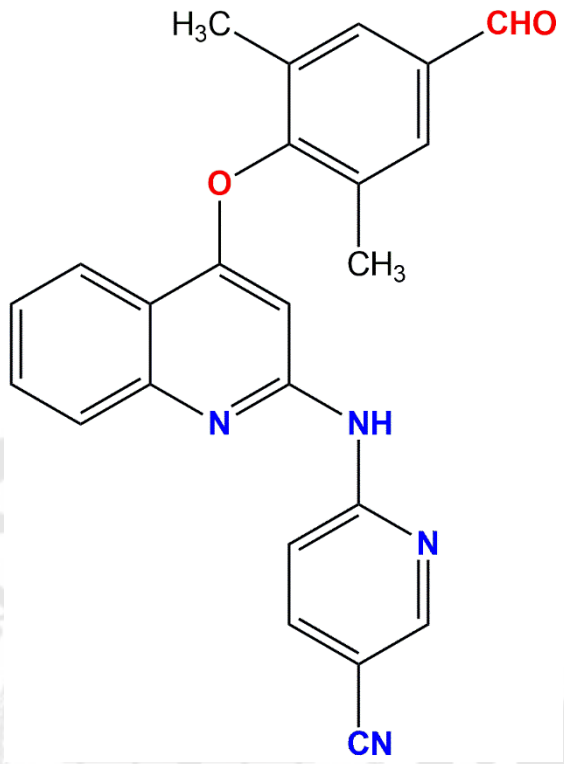

Figure 1 The structure of 4-(2′,6′-dimethyl-4′-formylphenoxy)-2-(5′-cyanopyridin-2′ylamino) quinoline, (C)

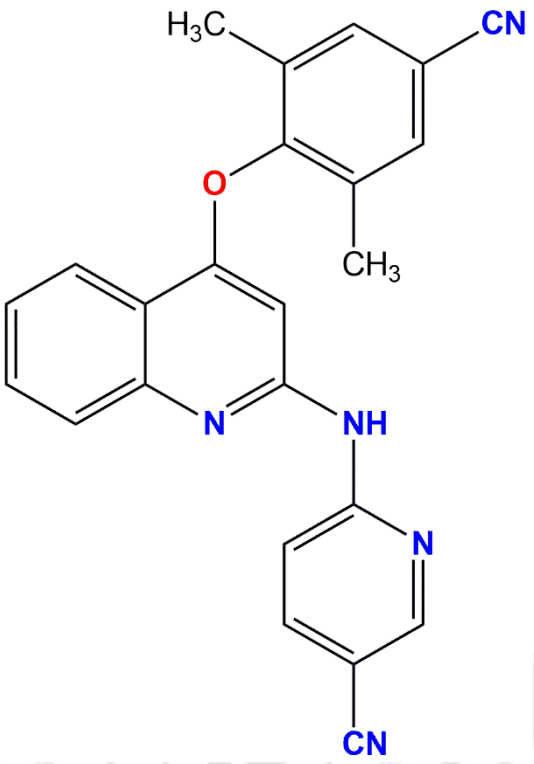

Figure 2 The structure of 4-(2′,6′-dimethyl-4′-cyanophenoxy)-2-(5′-cyanopyridin-2′ylamino) quinoline, **(J)**.

Objectives of the research

1. To study the intermolecular interactions between serum albumins and quinoline derivatives, identifying binding energy, binding sites, and the stability of each ligand on the proteins using multi-spectroscopic and molecular modeling techniques.

2. To determine the thermodynamic parameters associated with the binding forces and processes of serum albumin interactions with both quinoline derivatives.

3. To compare the binding efficiency of compound (C) and compound (J) with proteins.

Scope of the research

1. Investigate the binding mechanism interactions between quinoline derivatives and proteins using spectroscopic techniques.

2. Analyze the thermodynamic parameters of these interactions through spectroscopic methods.

3. Investigate the binding free energy, binding sites, and interaction mechanisms between quinoline derivatives and BSA and HSA using multi-spectroscopic and computational methods.

CHAPTER 2
THEORY AND LITERATURE REVIEWS

This research delves into the mechanism of binding interactions between quinoline derivatives and serum albumin, which is crucial for comprehending the pharmacokinetics of drugs. This investigation holds significant implications for guiding the design and development of quinoline derivatives with the potential to inhibit HIV-1 RT. To understand these interactions, researchers can develop more effective therapeutic agents that optimize drug efficacy and minimize adverse effects. This chapter provides a comprehensive description of the mechanism of binding interaction of quinoline derivatives with serum albumin, along with pertinent general information and related research on the topic, ensuring a thorough understanding of the current state of knowledge.

Proteins

Proteins are essential organic compounds ubiquitous in all living organisms, composed of carbon, hydrogen, oxygen, nitrogen, and sulfur. They consist of amino acid subunits, each comprising functional groups: an amino group, a carboxyl group, and a distinct R group. Amino acids link together via peptide bonds to form peptide chains. For instance, the peptide bond formation in glycine alanine (glycyl alanine, Gly-Ala) involves the amino acids glycine and alanine, resulting in the loss of one water molecule as depicted in Figure 3. Proteins play a vital role in virtually all biological processes, acting as enzymes, structural components, signaling molecules, and transporters. Understanding the structure and function of proteins is fundamental to biochemistry and molecular biology, insights into the proteins perform their diverse functions at the molecular level (Lever, 2014).

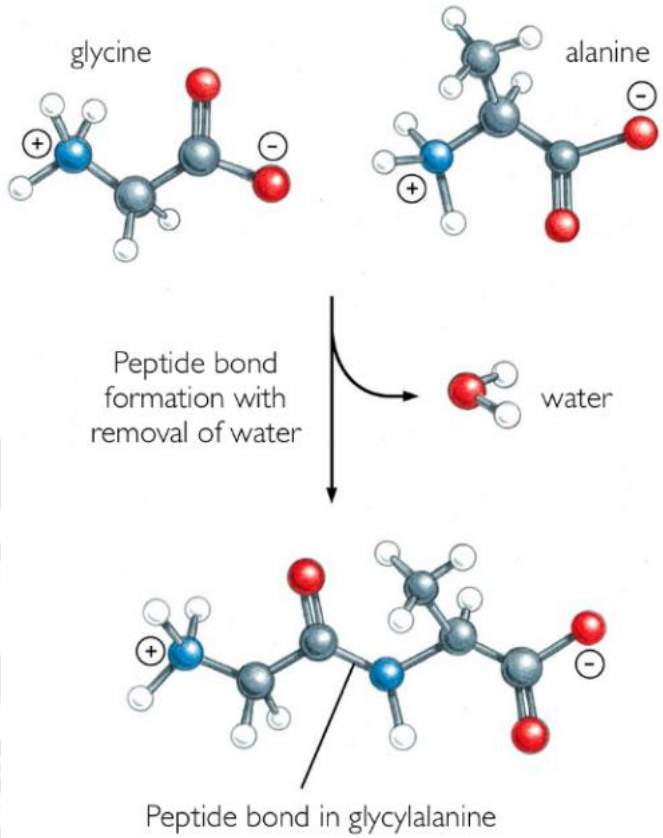

Figure 3 The process of peptide bond formation in glycine alanine (glycylalanine, Gly-Ala)

Source: Lever, G. (2014). Large Scale Quantum Mechanical Enzymology. (Doctoral dissertation. University of Cambridge, Magdalene College, Cambridge, United Kingdom.

Protein Structure

Proteins, when linked together into long chains, have the ability to fold into specific structures, often forming spirals or coils due to interactions such as hydrogen bonding or disulfide linkages. These interactions contribute to the stabilization of the protein's structure. The structure of a protein can be categorized into four levels.

Primary structure

The primary structure of a protein refers to the linear arrangement of amino acids linked together to form a polypeptide chain. At one end of the polypeptide chain, there is a free amino group known as the N-terminal amino acid, while at the other end, there is a free carboxyl group referred to as the C-terminal amino acid. This linear sequence of amino acids is determined during the protein synthesis or translation process (Elansary, 2012). The precise sequence of amino acids in a protein determines its unique characteristics and functions, as even a single change in the sequence can lead to significant alterations in protein function and stability.

Secondary structure

The structure of proteins involves the coiling or folding of the polypeptide chain. Polypeptides form hydrogen bonds between the carbonyl group (C= O) and the amino group (N-H) in the peptide backbone, resulting in the appearance of two main structural motifs: the alpha helix (α-helix) and the beta pleated sheet (β-pleated sheet) (Figure 4). The α-helix structure resembles a spiral rod, formed by the coiling or twisting of the polypeptide chain. In this structure, the carbonyl group (C=O) of one amino acid forms a hydrogen bond with the amino group (N-H) of an amino acid located four positions away along the chain. This repetitive hydrogen bonding pattern creates a uniform spiral structure. On the other hand, the β-pleated sheet structure appears as sheets overlapping each other. This structure is formed by hydrogen bonds between the carbonyl groups of one polypeptide chain and the amino groups of another polypeptide chain that are parallel to each other, resulting in the formation of overlapping sheets. Many globular proteins exhibit both α-helix and β-pleated sheet structures within the same protein molecule (Mishra & Heath, 2021).

Tertiary structure

The tertiary structure of a protein refers to its three-dimensional arrangement, which is formed by the folding and twisting of the secondary structures such as alpha helices and beta sheets. Weak binding forces, including hydrogen bonds, hydrophobic interactions, van der Waals forces, and disulfide bonds, contribute to the stabilization of

this structure. The specific three-dimensional shape of a protein is critical for its function, as it determines how the protein interacts with other molecules, including substrates, inhibitors, and other proteins. Misfolding or alterations in the tertiary structure can lead to loss of function or diseases such as Alzheimer's and cystic fibrosis (Elansary, 2012).

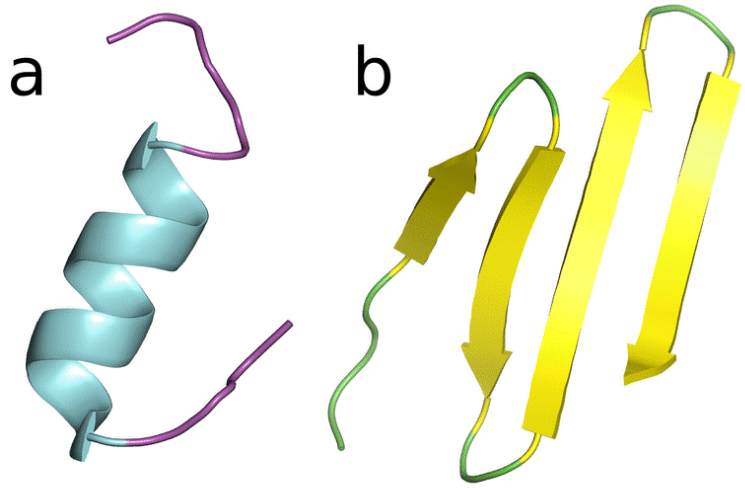

Figure 4 Structures of α-helix (a) and β-pleated sheet (b)

Source: Lever, G. (2014). Large Scale Quantum Mechanical Enzymology. (Doctoral dissertation. University of Cambridge, Magdalene College, Cambridge, United Kingdom.

Quaternary Structure

The quaternary structure forms through the assembly of subunits, either identical or diverse from the tertiary structure. It involves multiple polypeptide chains bound by weak interactions (salt bridges, hydrogen bonds, van der Waals forces, hydrophobic forces), enhancing protein stability and functionality. This level of structure is essential for the activity of many proteins, such as hemoglobin, which requires the interaction of multiple subunits to efficiently transport oxygen in the blood (Lever, 2014).

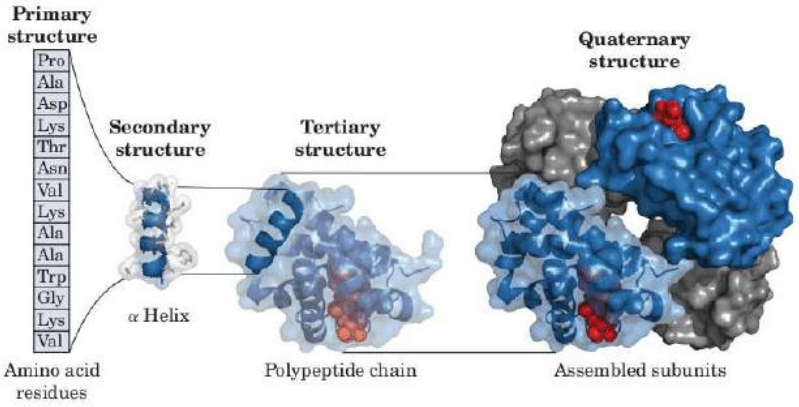

Figure 5 The four levels of protein structure

Source: Elansary, M. (2012). Prediction of protein aggregation inducing mutations.

Plasma protein

Plasma protein, integral to the circulatory system, encompasses various types with distinct roles. These proteins help regulate osmotic pressure, act as buffers, and facilitate the transport of diverse substances or molecules. Among them, serum albumin serves as the principal transport protein within plasma, playing a crucial role in carrying various compounds throughout the bloodstream.

Human Serum Albumin (HSA) and Bovine Serum Albumin (BSA)

Human serum albumin (HSA) predominates in plasma, constituting about 60% of its protein content (Mishra & Heath, 2021). It facilitates the transportation of various substances, including nutrients, hormones, vitamins, and medications, throughout the bloodstream to different tissues. Comprising 585 amino acids and weighing 66.5 kDa, HSA is structured into three domains (I, II, and III), each further divided into sub-domains A and B, characterized by **α**-helices (Belinskaia et al., 2020; Evoli, Mobley, Guzzi, & Rizzuti, 2016; Rabbani & Ahn, 2019)

Bovine serum albumin (BSA), sharing 76% similarity with HSA, serves as a valuable model for studying drug-protein interactions. BSA consists of 582 amino acids and a molecular weight of 66.4 kDa, BSA features three drug binding sites: site I in sub-domain IIA, site II in sub-domain IIIA, and site III in sub-domain IB (Ghuman et al., 2005; Z. M. Wang et al., 2013; Yamasaki, Chuang, Maruyama, & Otagiri, 2013)

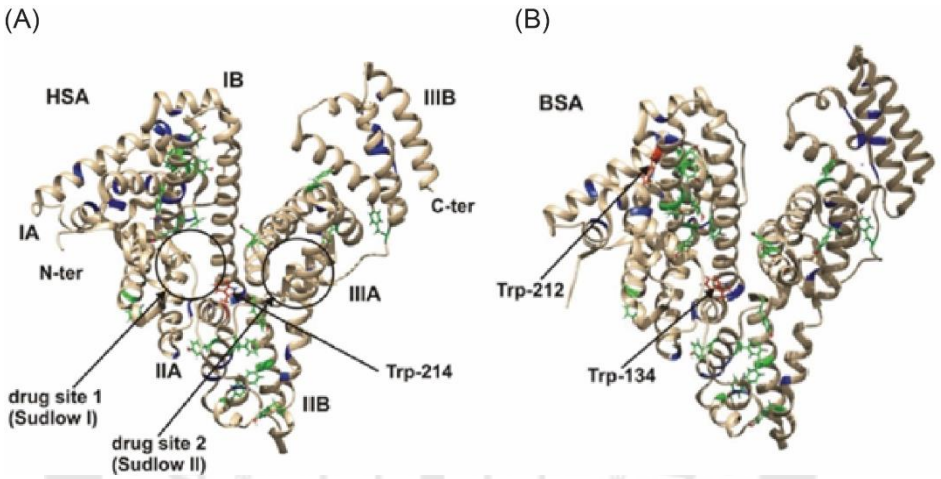

Figure 6 Structural locations of domain-binding sites in (A) HSA and (B) BSA.

Source: Starosta, R., Santos, F. C., & de Almeida, R. F. M. (2020). Human and bovine serum albumin time-resolved fluorescence: Tryptophan and tyrosine contributions, effect of DMSO and rotational diffusion. *Journal of Molecular Structure, 1221*.

Previous research has explored the binding of clonazepam with BSA (Lou, Zhou, Pan, Shen, & Shi, 2017). Spectroscopy and molecular docking studies revealed that clonazepam interacts with site II of BSA. BSA exhibits absorption peaks in the 190-230 nm and 280 nm wavelength range, indicative of ligand-protein binding interactions

involving aromatic amino acids like tyrosine, tryptophan, and phenylalanine (as depicted in Figure 7).

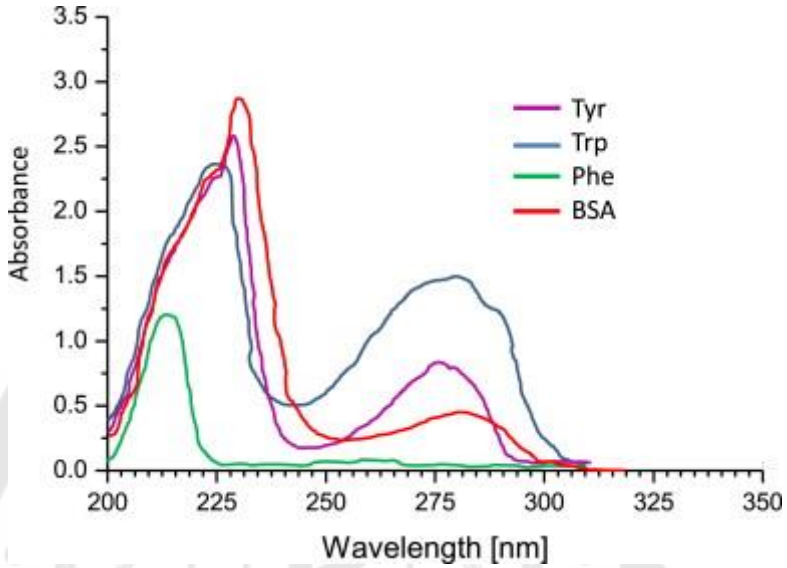

Figure 7 Absorption spectrum for aromatic amino acids as trypotophan (Trp), tyrosine (Tyr), phenylalanine (Phe) and albumin derived from bovine serum (BSA).

Source: Hammond, B. R., Johnson, B. A., & George, E. R. (2014). Oxidative photodegradation of ocular tissues: beneficial effects of filtering and exogenous antioxidants. *Exp Eye Res, 129*, 135-150.

UV-Vis Spectroscopy

UV-VIS radiation encompasses electromagnetic waves resulting from electron energy level transitions associated with rotation and vibration, occurring within the wavelength range of 380–700 nm (Peter Atkins, 2006). This radiation, depicted in Figure 8, plays a crucial role in spectroscopic analyses, enabling the investigation of molecular structures and interactions through the absorption and scattering of light.

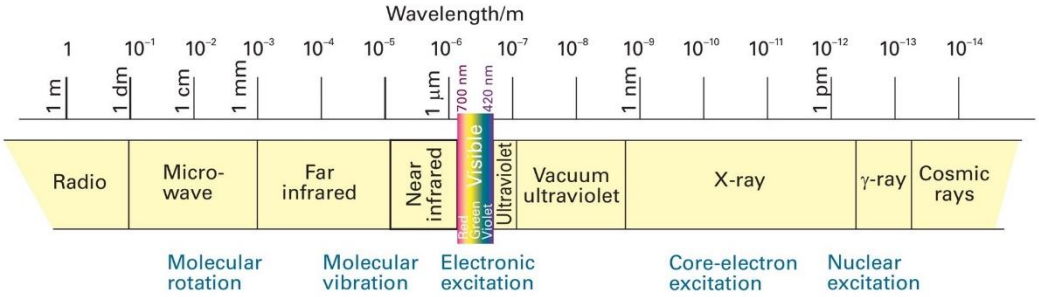

Figure 8 Electromagnetic Spectrum Diagram

Source: Peter Atkins, J. d. P. (2006). *Atkins' Physical Chemistry* (8th ed.). Oxford: Oxford University Press.

When sample molecules encounter UV-Visible light with adequate energy, their electrons absorb the light, transitioning to higher energy states. According to the Beer-Lambert law, substance absorbance correlates with the number of light-absorbing molecules. By assessing light transmission through a sample versus a source with varying wavelengths, absorbance quantifies light absorption, as depicted in Figure 9.

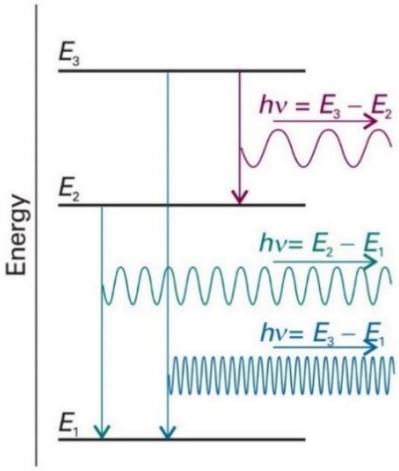

Figure 9 Changing the electronic state of a molecule

Source: Peter Atkins, J. d. P. (2006). *Atkins' Physical Chemistry* (8th ed.). Oxford: Oxford University Press.

Fluorescence Spectroscopy

Under typical circumstances, electrons reside in the ground state (S_0) . When energized by short-wavelength light, electrons transition to an excited state (S_1) in a higher energy orbital, rendering them unstable. Some energy dissipates due to atom collisions and vibrations, causing a return to the ground state and emitting photons, resulting in light emission fluorescence, as illustrated in Figure 10.

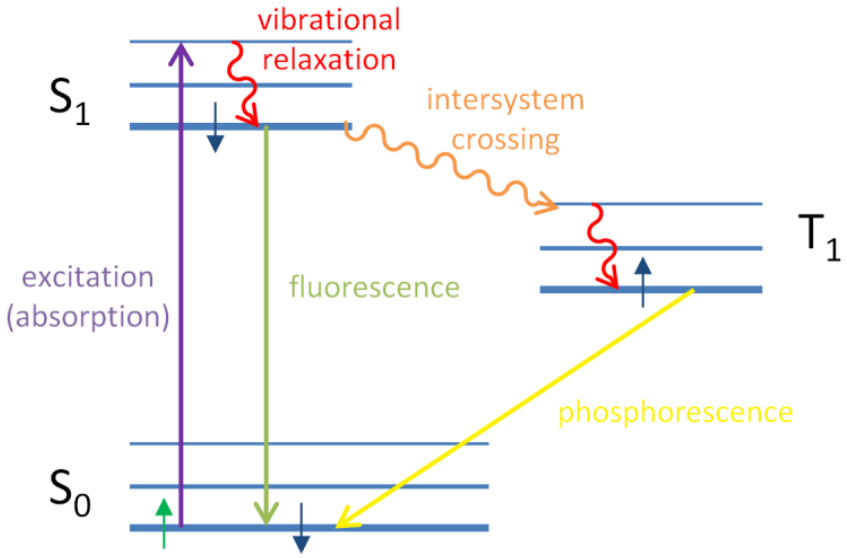

Figure 10 Jablonski diagram

Source: Eck, M. (2014). Performance enhancement of hybrid nanocrystal-polymer bulk heterojunction solar cells: aspects of device efficiency, reproducibility, and stability.

Fluorescence quenching mechanisms

The fluorescence spectroscopic technique was employed to measure the emission spectra, observing a reduction in fluorescence intensity. When molecules in the excited state (S1) interact with other substances, they are prevented from emitting fluorescent light, leading to energy loss. This energy loss can occur through various mechanisms, including complex formation (static quenching) or collisions (dynamic quenching), ultimately reducing fluorescence. Quenching mechanisms can generally be categorized into two types: static quenching, where a non-fluorescent complex is formed between the fluorophore and the quencher, and dynamic quenching, where collisional interactions between the excited fluorophore and the quencher lead to non-radiative energy transfer.

Static quenching

Static quenching occurs when a fluorophore in the ground state (S0) is excited by light energy, transitioning to the excited state (S1) and forming a complex compound with the quencher. This complex formation transfers energy to the quencher, reducing light emission. Figure 11(A) illustrates this process.

Dynamic quenching

Dynamic quenching involves a fluorophore in the excited state (S1) transferring kinetic energy to two molecules, causing them to diffuse towards each other and collide with the quencher. This collision results in the loss of energy and a reduction in fluorescence intensity, leading to less emitted light. Figure 11(B) illustrates this process.

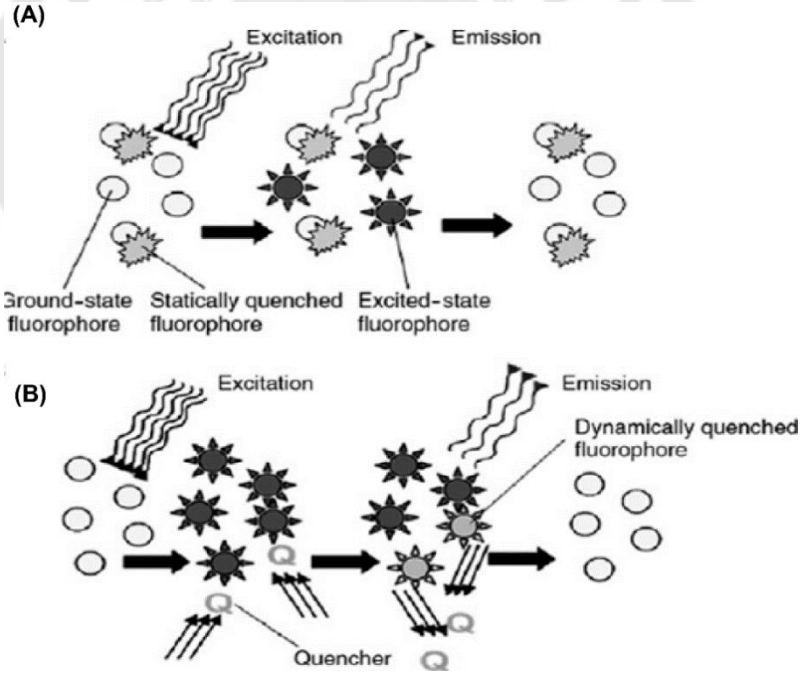

Figure 11 Fluorescence quenching mechanisms. (A) Static quenching, and (B) Dynamic quenching mechanisms

Source: Lakowicz, J. R. (2006). Principles of Fluorescence Spectroscopy (3rd ed). New York: Springer.

The static quenching mechanism, identified in Lou et al. (2017), highlights the interaction between clonazepam and BSA, leading to the formation of complex compounds. This interaction blocks the emission of fluorescent light, shedding light on ligand-protein binding through fluorescence techniques.

In this study, fluorescence quenching can classify static or dynamic mechanisms of quinoline derivatives with serum albumin. This is achieved by experimentally blocking fluorescence emission and analyzing thermodynamic parameters at varying temperatures. Stern-Volmer equation [1] allows calculating the constant value, shedding light on the quenching mechanism.

$$\frac{F_0}{F} = 1 + K_{SV}[Q] = 1 + K_q \tau_0 [Q] \qquad [1]$$

The Stern-Volmer equation, which relates the fluorescence intensity in the presence (F) and absence (F_0) of the quencher, involves the quenching constant (K_q), the lifetime of the fluorophore without the quencher (τ_0), the quencher concentration ([Q]), and the Stern-Volmer constant (K_{SV}). The change in light output with temperature control can reveal the mechanism of fluorescence emission quenching. In Figure 12 (A), with rising temperature, if the slope of the graph increases, indicating an increase in the K_{SV} value, it suggests a dynamic quenching mechanism. On the other hand, in Figure 12(B), if the slope of the F0/F plot decreases with increasing temperature, resulting in a decrease in the KSV value, it indicates a static quenching mechanism.

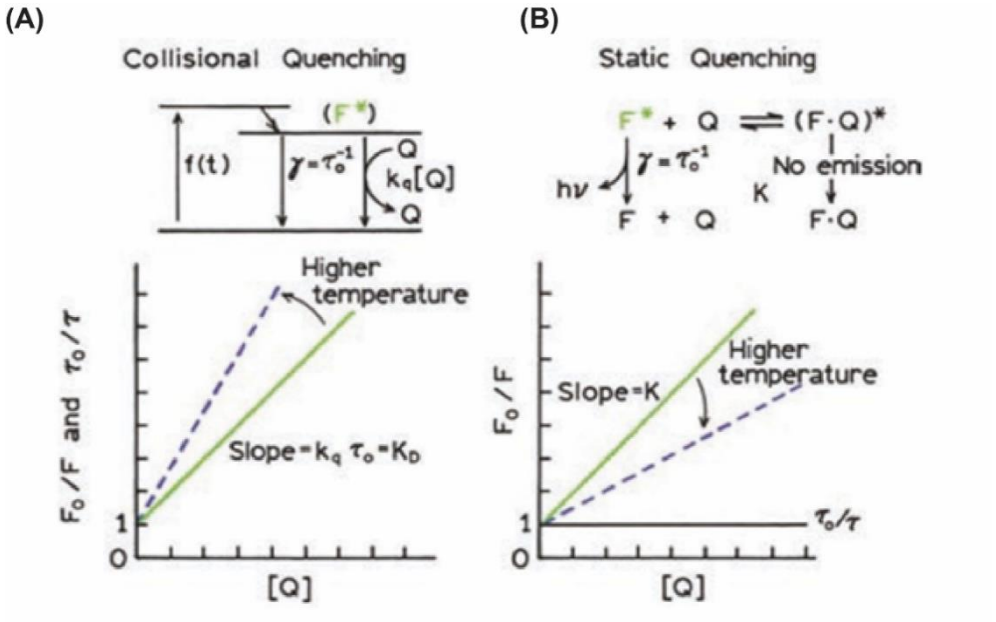

Figure 12 (A) Dynamic quenching (B) Static quenching

Source: Lakowicz, J. R. (2006). *Principles of Fluorescence Spectroscopy*. New York: Springer.

The binding constant (K_b) for the interaction between quinoline derivatives and serum albumin can be determined using equation [2].

$$\log \frac{F_0\text{-}F}{F} = \log K_b + n\log [Q] \qquad [2]$$

$$\ln K_b = - \frac{\Delta H}{RT} + \frac{\Delta S}{R} \qquad [3]$$

$$\Delta G = -RT\ln K_b = \Delta H - T\Delta S \qquad [4]$$

Thermodynamic parameters and binding mode

The binding modes between proteins and non-covalent ligands, such as van der Waals forces, hydrogen bonding interactions, electrostatic interactions, and hydrophobic interactions, can be elucidated through thermodynamic parameters like entropy change (ΔS) , enthalpy change (ΔH) , and Gibbs free energy (ΔG) , as determined by Equations [3] and [4]. Typically, negative values of both ΔS and ΔH suggest van der Waals forces or hydrogen bonding as the main interaction forces, while positive values of ΔS and ΔH indicate predominant hydrophobic interactions. If ΔH is close to zero and ΔS is positive, electrostatic interactions are likely the driving forces. The Van't Hoff equations, shown in equations [3] and [4], are used to determine these thermodynamic parameters in the binding model between proteins and ligands (Philip D. Ross, 1981)

The site marker competition

Studies on the competitive binding of specific sites reveal that small molecules typically bind to serum albumin at sub-domains IIIA, IIA, and IB within the hydrophobic pockets known as sites I, II, and III, respectively. The ligands binding sites on serum albumin can be identified through competitive binding experiments using drugs that bind to known serum albumin sites. For the site marker, warfarin binds to subdomain IIA, whereas ibuprofen binds to subdomain IIIA. Fluorescence competitive binding experiments can accurately pinpoint the binding sites of ligands on serum albumin, as illustrated in Figure 18 (Tan, Zaremska, Lim, Knoll, & Pelosi, 2020) . Additionally, highlighted the importance of this method for understanding drug interactions at the molecular level.

Computational chemistry

Computational chemistry utilizes computer power and mathematical models to simulate chemical structures and reactions, often employing quantum mechanics theory. This approach, demonstrated in Figure 13, aids in understanding molecular properties and interactions, such as protein-ligand binding energies studied through molecular docking techniques.

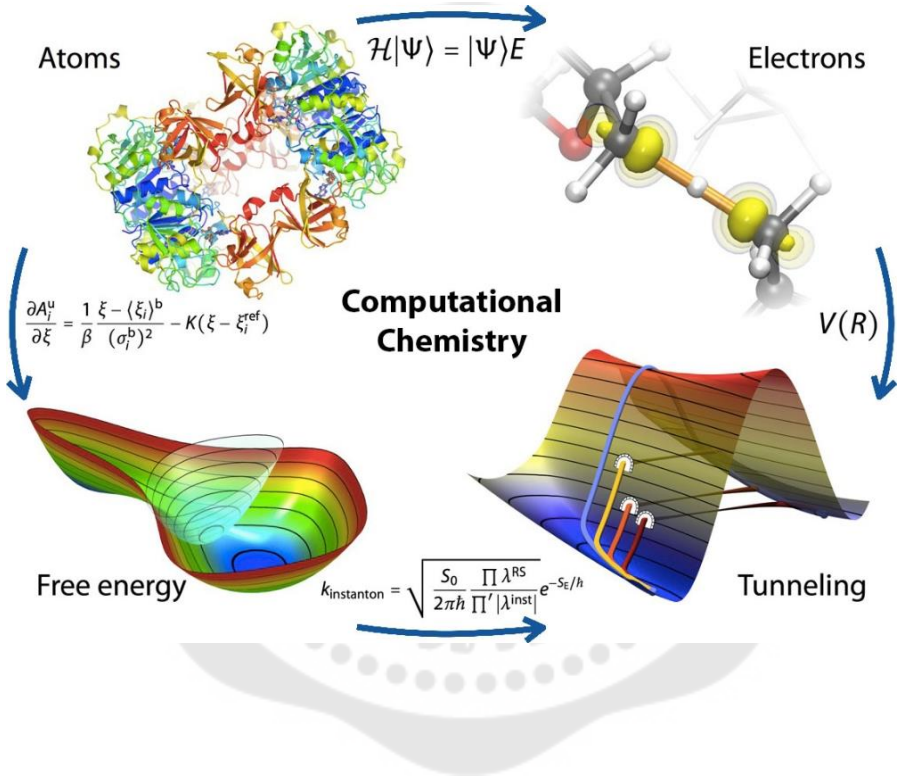

Figure 13 Computational chemistry integrates various techniques to predict and analyze chemical reactions and properties, providing a deeper understanding of chemical processes.

Source: Kästner, J. Computational chemistry. Retrieved from https://www.itheoc.uni-stuttgart.de/research/kaestner/

Molecular docking

Molecular docking predicts molecular interactions, identifying stable complex formations, binding sites, and binding energies. This technique is pivotal in designing and developing drugs with specific effects on biomolecules like enzymes and nucleic acids. Based on the lock-and-key theory, it ensures specificity between ligands and receptors, facilitating binding. Figure 14 illustrates this concept (Garrett M. Morris, 1998).

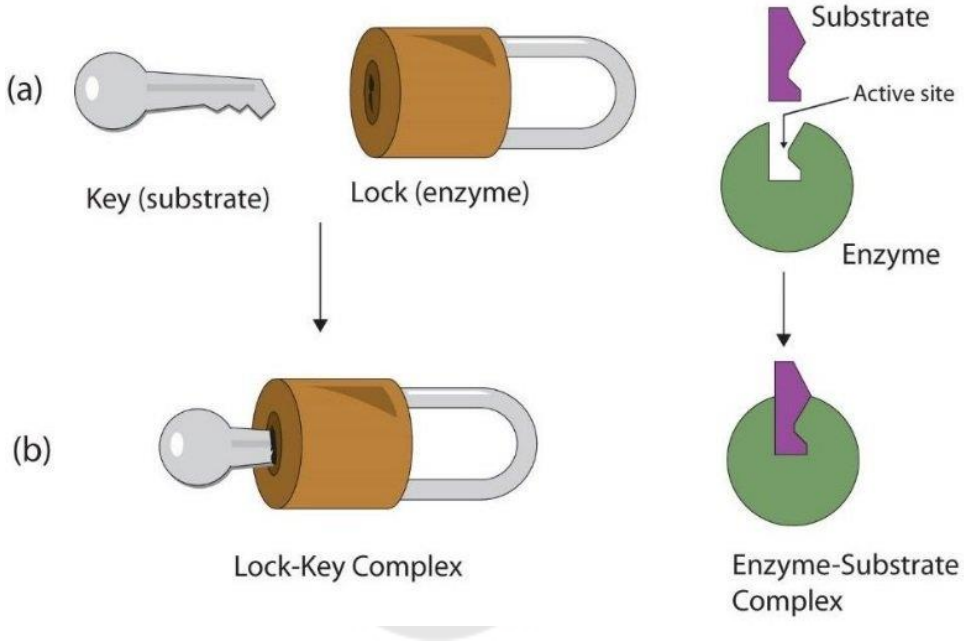

Figure 14 The Lock-and-Key Model of Enzyme-Substrate Interaction

Source: Raval, K., & Ganatra, T. (2022). Basics, types and applications of molecular docking: A review. *IP International Journal of Comprehensive and Advanced Pharmacology, 7*(1), 12-16.

Molecular dynamics (MD) simulations

Molecular dynamics simulations are employed to model the structural movements of biomolecules, offering insights into protein-ligand binding mechanisms and molecular flexibility (Ding & Peng, 2016) . This computational technique is essential in drug development, as it helps to analyze dynamic interactions and understand time-dependent conformational changes that are crucial for protein function (Ali et al., 2021; Van Der Spoel et al., 2005) MD simulations provide a detailed view of how proteins and ligands interact over time, revealing the stability and binding characteristics of potential drug candidates. For example, Figure 15 illustrates the molecular dynamics simulation of Human Hemoglobin, showcasing its movement and interaction dynamics.

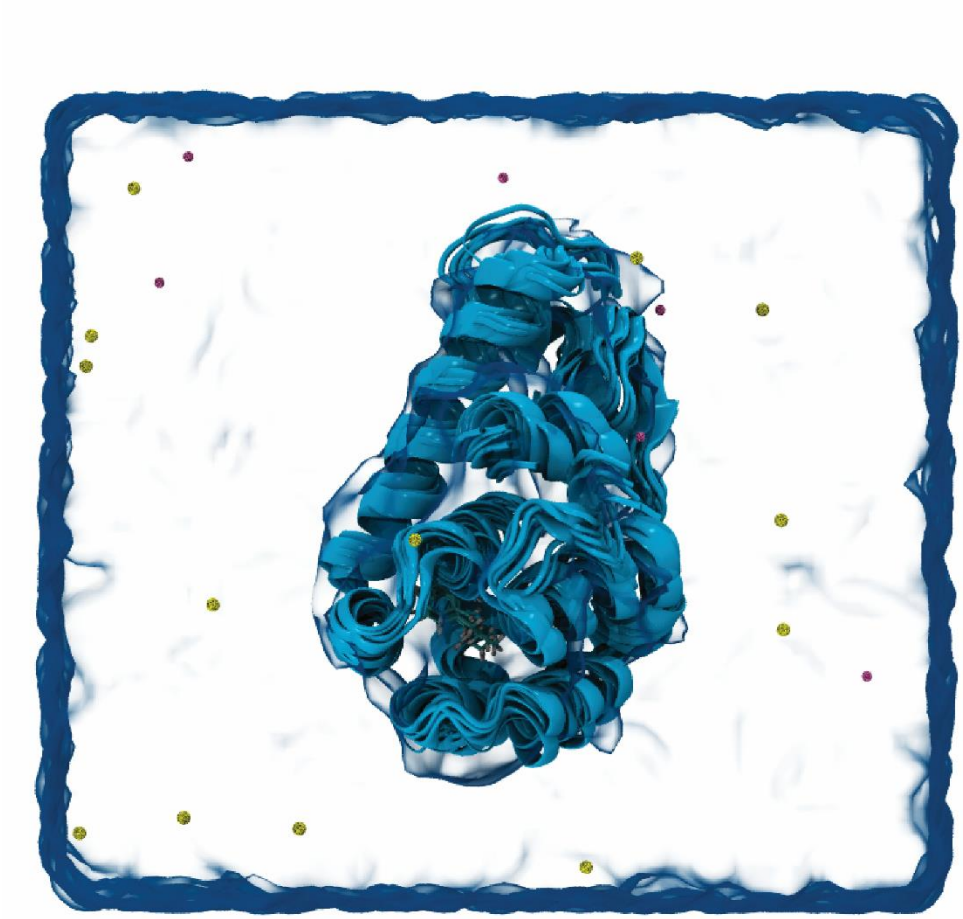

Figure 15 Structural representation of the Lysozyme-ligand complex in aqueous solution with NaCl, illustrating the dynamic movement observed during MD simulations.

Binding free energy calculation using MM-PBSA

The binding free energy was calculated using the Molecular Mechanics/Poisson-Boltzmann Surface Area (MM-PBSA) method, which is widely utilized in computational chemistry to estimate the contributions and interactions within protein-ligand complexes. The MM-PBSA method calculates the free energy difference between two states, typically representing the bound and unbound states of two solvated molecules. It also

compares the free energy of different solvated conformations of the same molecule in a simulation. This approach integrates molecular mechanics energies with solvation-free energies obtained from the Poisson-Boltzmann equation. The method involves considering molecular mechanics energy, solvation-free energy from the Poisson-Boltzmann equation, and the nonpolar contribution estimated using the solvent-accessible surface area (SASA) model. Furthermore, it decomposes the free energy contributions from various interaction forces, such as van der Waals interactions, electrostatic interactions, and solvation effects, into separate components, and then calculates the binding free energies ($\Delta G_{binding}$) according to the following equations.

$$\Delta G_{binding} = \Delta E_{MM} - T\Delta S + \Delta G_{solv} \quad [5]$$

$$\Delta G_{solv} = \Delta G_{polar} + \Delta G_{non-polar} \quad [6]$$

$$\Delta G_{non-polar} = \Delta G_{vdw} + \Delta G_{elec} - G_{vdw} \quad [7]$$

When The total binding free energy (ΔG_{bind}) was calculated as the sum of the changes in molecular mechanical energy in the gas phase (ΔE_{MM}), the conformational entropy after ligand binding ($-T\Delta S$), and the free energy of solvation (ΔG_{sol}). ΔE_{MM}, based on the molecular mechanics force field, includes van der Waals (ΔE_{vdw}) and electrostatic (ΔE_{elec}) energies. ΔG_{solv} comprises polar (ΔG_{polar}) and nonpolar ($\Delta G_{non-polar}$) contributions, computed using the Poisson–Boltzmann (PB) equation and solvent-accessible surface area (SASA), respectively. The entropic component is represented by ($-T\Delta S$) was computed using the interaction entropy (IE) approach.

Related research

Previous research has elucidated the pharmacokinetic and pharmacodynamic properties of diverse quinoline derivatives.

Ghosh et al. (2008). focused on synthesizing a series of 2-(2-methyl-quinoline-4ylamino) -N-(2-chlorophenyl) -acetamide derivatives to assess their potential against Japanese encephalitis (JE), a disease transmitted by *Culex tritaeniorrhynchus* mosquitoes. The objective was to explore the antiviral efficacy of these quinoline core structure compounds. Their research demonstrated that these derivatives possess significant inhibitory effects on the JE virus, both *in vitro* and *in vivo*. This study highlights the importance of quinoline derivatives in developing antiviral agents and underscores the potential of these compounds as therapeutic candidates for JE disease.

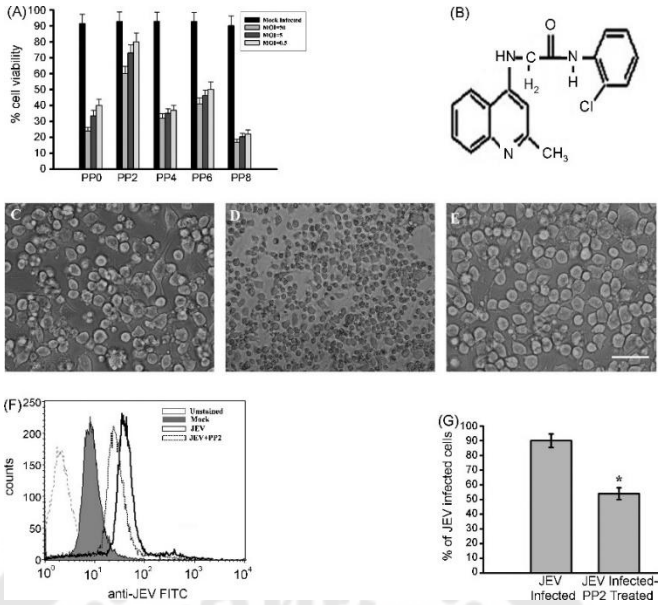

Figure 16 Anilidoquinoline analogue PP2 demonstrated significant inhibition of the virus both *in vivo* and *in vitro*.

Source: Ghosh, J., Swarup, V., et al. (2008). Therapeutic effect of a novel anilidoquinoline derivative, 2-(2-methyl-quinoline-4ylamino) -N-(2-chlorophenyl) -acetamide, in Japanese encephalitis: correlation with in vitro neuroprotection. International Journal of Antimicrobial Agents, 32(4), 349-354.

In their study, Zeng et al. (2010) developed Diarylbenzoprimidine (DABPs) using a hybrid structure combining elements of DPC083 and etravirine to enhance pharmacological properties. Their innovative application of hybrid structures in drug design, particularly for quinoline derivatives, aimed to improve efficacy and interaction with biological targets, as shown in Figure 17. DABPs effectively inhibited HIV-1 in MT-4 cells, with an EC_{50} value of 0.034 μM. This study marks a significant advancement in medicinal chemistry, demonstrating a strategic method for optimizing quinoline-derived drug candidates.

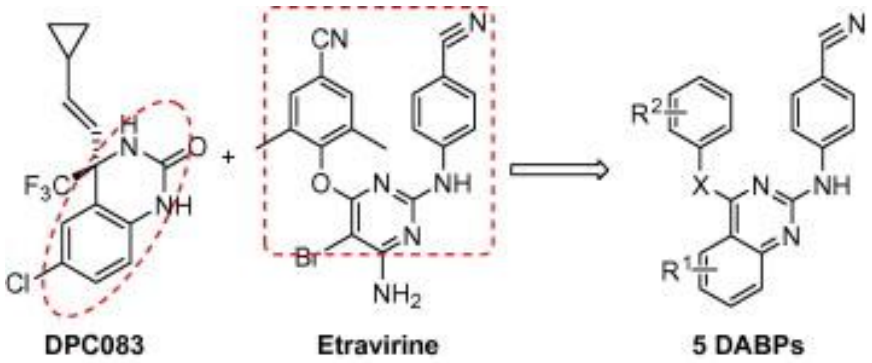

Figure 17 The fusion of DPC083 and etravirine yields a novel derivative known as diarylbenzoprimidine (DABPs).

Source: Zeng, Z.-S., He, Q.-Q., Liang, Y.-H., Feng, X.-Q., Chen, F.-E., Clercq, E. D., Pannecouque, C. (2010) . Hybrid diarylbenzopyrimidine non-nucleoside reverse transcriptase inhibitors as promising new leads for improved anti-HIV-1 chemotherapy. Bioorganic & Medicinal Chemistry, 18(14), 5039-5047.

In their study, Asahchop, Wainberg, Sloan, and Tremblay (2012) conducted research focusing on antiretroviral drug resistance. Their work led to the design and development of new drugs aimed at inhibiting HIV-1 reverse transcriptase (RT) . The results of their study showed that these newly developed drugs were effective in inhibiting the activity of HIV-1 RT, highlighting their potential as therapeutic agents in the fight against HIV.

J. Wang et al. (2014) synthesized diarylpyrimidine-quinolone hybrids by altering the position of substituents to various groups. Their research demonstrated that inhibiting HIV-1 RT is achievable by modifying the position of substituents, as depicted in Figure 18.

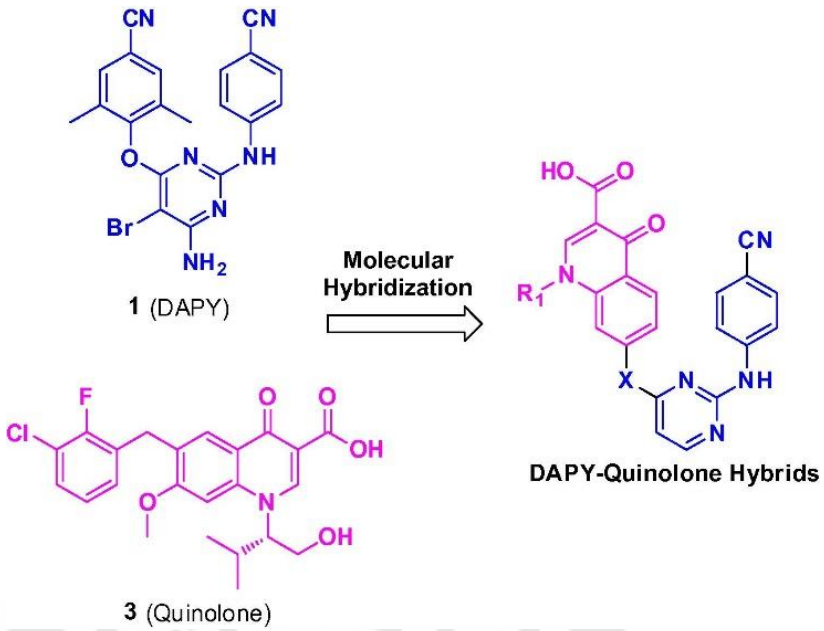

Figure 18 Hybridization alters the positions of substances within the diarylpyrimidine–quinolone group.

Source: Wang, J., Zhan, P., Li, Z., Liu, H., De Clercq, E., Pannecouque, C., & Liu, X. (2014). Discovery of nitropyridine derivatives as potent HIV-1 non-nucleoside reverse transcriptase inhibitors via a structure-based core refining approach. European Journal of Medicinal Chemistry, 76, 531-538.

In their study, Makarasen et al. (2019) conducted a comprehensive study involving the synthesis and molecular docking of amino-oxy-diarylquinoline derivatives, identifying them as potent non-nucleoside inhibitors of HIV-1 reverse transcriptase (RT). Among these derivatives, compounds like 4-Cyanophenoxy (Figure 19) were found to inhibit HIV-1 RT by 39.71%. Additionally, they exhibited significant inhibitory effects on various cancer cells, including liver cancer (HepG2) with an IC_{50} value of 44.80 µg/mL, leukemia (MOLT-3) with an IC_{50} of 6.00 µg/mL, cholangiocarcinoma (HuCCA-1) with an IC_{50} of

23.00 µg/mL, lung cancer (A549) with an IC_{50} of 26.00 µg/mL, and lung cancer (MRC-5) with an IC_{50} of 12.03 µg/mL.

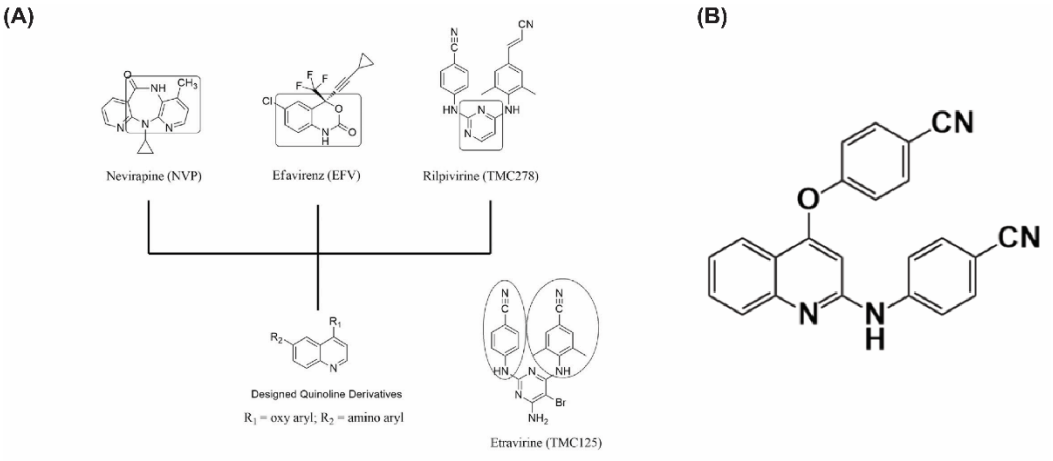

Figure 19 Hybrid design and structure of quinoline derivative. (A) Schematic representation of the design process of quinoline derivatives using hybrid molecular techniques from NVP, EFV, TMC278, and TMC125. (B) Structure of 4-Cyanophenoxy.

Source: Makarasen, A., Kuno, M., Patnin, S., Reukngam, N., Khlaychan, P., Deeyohe, S., Techasakul, S. (2019). Molecular Docking Studies and Synthesis of Amino-oxy-diarylquinoline Derivatives as Potent Non-nucleoside HIV-1 Reverse Transcriptase Inhibitors. Drug Res (Stuttg), 69(12), 671-682.

In their study, Lou et al. (2017) investigated the distribution of clonazepam, a benzodiazepine used for treating seizures and panic disorder, in the bloodstream. They explored its pharmacokinetic and pharmacodynamic mechanisms, focusing on its binding interaction with BSA using spectroscopy and molecular docking. Clonazepam was found to block BSA's intrinsic fluorescence emission via static quenching, involving hydrogen and van der Waals forces. Molecular docking revealed clonazepam's interaction with Site II of BSA, elucidating the experimental findings (Figure 20).

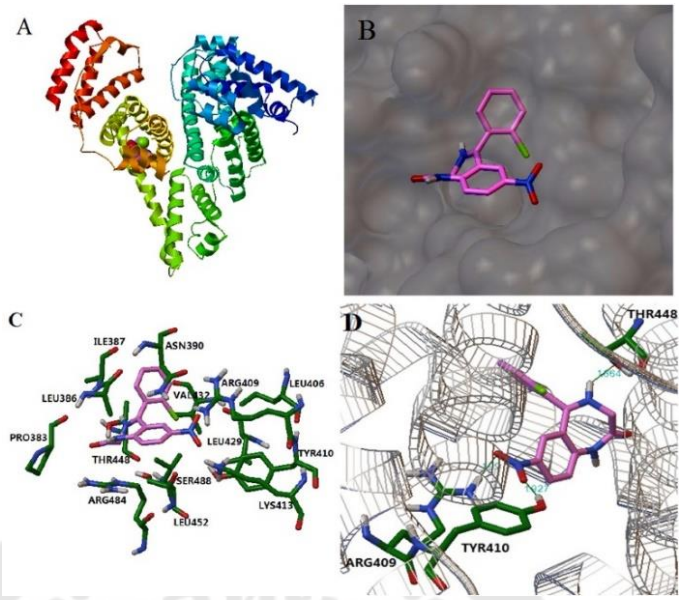

Figure 20 The internal structure of the site II interaction between BSA and clonazepam.

Source: Lou, Y.-Y., Zhou, K.-L., Pan, D.-Q., Shen, J.-L., & Shi, J.-H. (2017). Spectroscopic and molecular docking approaches for investigating conformation and binding characteristics of clonazepam with bovine serum albumin (BSA). Journal of Photochemistry and Photobiology B: Biology, 167, 158-167.

In their study, Patnin et al. (2020) investigated the interaction between amino-oxy-diarylquinoline, known for its HIV-1RT inhibitory effect, and serum albumin transport proteins. Specifically, they observed that 4-(4'-cyanophenoxy)-2-(4"-cyanophenyl)-aminoquinoline interacted with both BSA and HSA at site I. The binding energy values were calculated to be -10.64 kcal/mol for BSA and -10.14 kcal/mol for HSA, indicating a strong affinity. The study revealed a static quenching mechanism, driven by hydrogen bonds and van der Waals forces, suggesting spontaneous interaction (Figure 21).

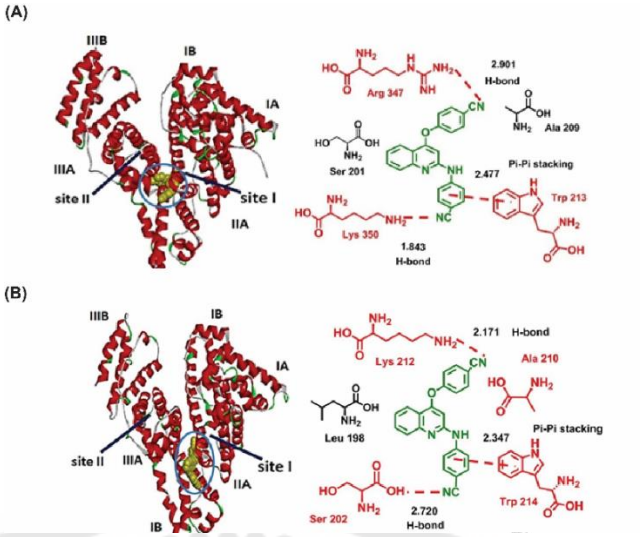

Figure 21 The binding interaction between amino-oxy-diarylquinoline with BSA (a) and HSA (b) at site I

Source: Patnin, S., Makarasen, A., Kuno, M., Deeyohe, S., Techasakul, S., & Chaivisuthangkura, A. (2020). Binding interaction of potent HIV-1 NNRTIs, amino-oxy-diarylquinoline with the transport protein using spectroscopic and molecular docking. Spectrochim Acta A Mol Biomol Spectrosc, 233, 118159.

Makarasen et al. (2022) designed and synthesized 2-Phenylamino-4-phenoxyquinoline derivatives, 4-(2',6'-dimethyl-4'-formylphenoxy)-2-(5"-cycanopyridin-2"ylamino) quinoline (6b) and 4-(2',6'-dimethyl-4'-cyanophenoxy)-2-(5"-cycanopyridin-2" ylamino) quinoline (6d), indicated that the efficactive against HIV-1 reverse transcriptase. The laboratory results demonstrated that these derivatives exhibit significant inhibitory activity against the HIV-1 enzyme, with IC_{50} values of 1.93 μM for compound 6b and 1.22 μM for compound 6d. Additionally, the study confirmed that both compounds were non-toxic to MRC-5 cells, highlighting their potential as effective and safe therapeutic agents for HIV-1 treatment.

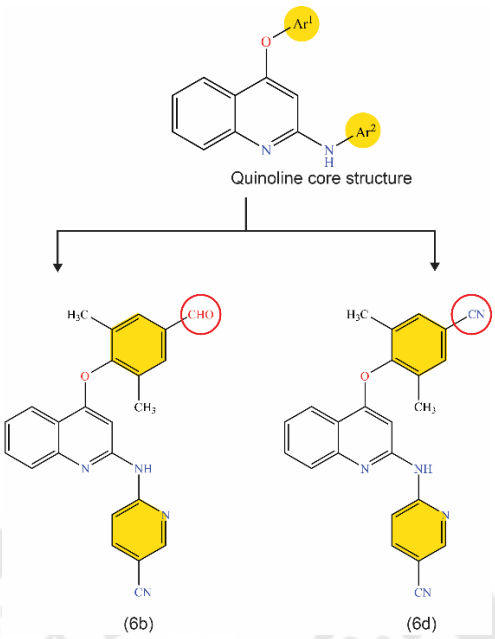

Figure 22 Structural modifications of quinoline derivatives leading to the synthesis of compounds 6b and 6d with distinct functional groups (CHO and CN), enhancing activity against HIV-1 RT.

Shamsi et al. (2020) conducted a comprehensive study on the interaction between Rosmarinic acid and human serum albumin (HSA) using molecular dynamics simulations with the GROMOS 54A7 force field. Their findings revealed that Rosmarinic acid forms a stable complex with HSA without causing significant conformational changes, primarily stabilized by hydrogen bonding and van der Waals forces. This research enhances our understanding of the pharmacokinetic behavior of Rosmarinic acid, emphasizing its potential as a therapeutic agent and improving our knowledge of drug-serum albumin interactions.

Ali et al. (2021) extensively studied the binding interactions between cefoperazone and bovine serum albumin (BSA) using experimental and computational methods. Their molecular dynamics simulations with the GROMOS96 43a1 force field revealed that

cefoperazone binds most stably to site II on BSA. This finding was corroborated by fluorescence quenching and UV-Vis spectroscopy data. The study showed that van der Waals forces and hydrogen bonding significantly contribute to the binding at site II. These insights underscore the importance of understanding drug-serum albumin interactions for drug design and development, aiding in optimizing cefoperazone's therapeutic efficacy.

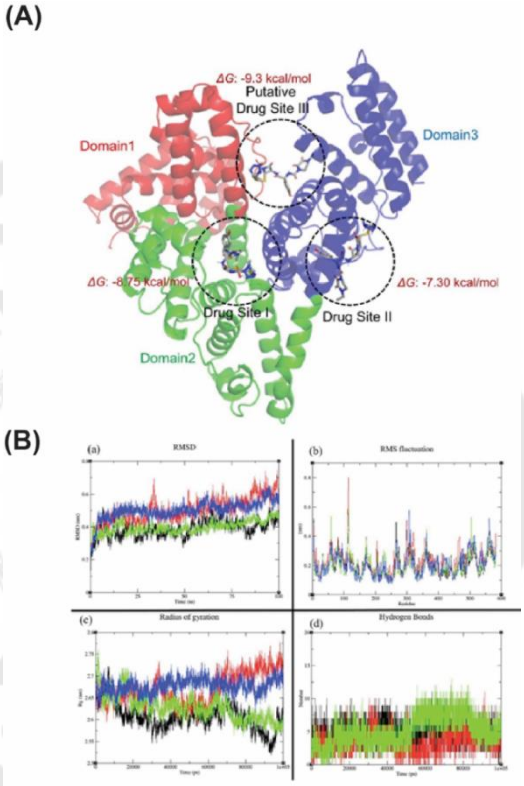

Figure 23 Molecular dynamics simulation analysis of cefoperazone binding with bovine serum albumin (BSA), indicating the most stable binding at site II, supported by van der Waals forces and hydrogen bonding. Data includes RMSD and RMSF fluctuation plots.

Source: Ali, M. S., Muthukumaran, J., Jain, M., Santos-Silva, T., Al-Lohedan, H. A., & Al-Shuail, N. S. (2021). Molecular interactions of cefoperazone with bovine serum albumin: Extensive experimental and computational investigations. Journal of Molecular Liquids, 337.

CHAPTER 3
EXPERIMENTAL

Equipment

- Precision analytical balance digital scale, Mettler Toledo, code AB104-S
- pH meter, Mettler Toledo
- Water baths, Memmert
- UV-VIS spectrophotometer, Jasco, code V-750
- Fluorescence spectrophotometer, Jasco, code FP-8300

Chemical reagents

- 4-(2′,6′-dimethyl-4′-formylphenoxy)-2-(5′-cyanopyridin-2′-ylamino) quinoline, (C)
- 4-(2′,6′-dimethyl-4′-cyanophenoxy)-2-(5′-cyanopyridin-2′-ylamino) quinoline, (J)
- Trizma hydrochloride, Sigma-Aldrich
- Bovine serum albumin (BSA), Sigma-Aldrich
- Human serum albumin (HSA), Sigma-Aldrich
- Warfarin, Tokyo Chemical Industry
- Ibuprofen, Tokyo Chemical Industry
- Digitoxin, Tokyo Chemical Industry

All chemicals were of reagent grade and utilized without additional purification. Protein solutions were freshly prepared using 50 mM Tris-HCl buffer (pH 7.0).

Methods

UV-Vis absorption measurement

The absorption spectra of serum albumin in the presence and absence of newly synthesized compounds were recorded at room temperature using the UV-VIS spectrophotometer (Jasco V-750) equipped with 1. 0 cm quartz cells. The spectrophotometer was blanked with 1000 µL of 50 mM Tris-HCl buffer at pH 7.0 in the quartz cuvette. To measure the absorption titrations of BSA and HSA solutions in 50 mM Tris-HCl buffer at pH 7.0 with compounds (C) and (J), both protein solutions were maintained at a concentration of 5.0 µM. The concentrations of compounds (C) and (J) were increased from 0 to 50 µM, and the spectral data were recorded in the 200-700 nm region.

Fluorescence measurement

Fluorescence spectroscopy was employed to investigate fluorescence quenching mechanisms, with excitation at 280 nm and recording of fluorescence emission spectra from 290 to 700 nm. In the binary systems, serum albumin was maintained at a concentration of 5.0 µM in 50 mM Tris-HCl buffer at pH 7.0, while concentrations of quinoline derivatives (C) and (J) ranged from 0 to 12 µM. Thermodynamic parameters were evaluated at temperatures of 298, 308, and 313 K using the Jasco FP-8300 spectrofluorometer, enabling calculation of the quenching constant via the Stern–Volmer equation and determination of thermodynamic parameters through temperature-dependent measurements.

Site marker competitive experiments

Competitive experiments were conducted using site markers warfarin, ibuprofen, and digitoxin to determine the binding positions of compounds (C) and (J) at sites I, II, and III of BSA and HSA structures. In the ternary systems at room temperature, both

protein solutions and site markers were maintained at 6 μM, while the concentration of (C) or (J) ranged from 0 to 12 μM, and all systems were stabilized during a 6-minute incubation. The excitation wavelength was set to 280 nm, and emission was recorded from 290 to 700 nm.

Molecular docking

Molecular docking was employed to predict the interactions and binding energy between small molecules and the binding site of serum albumin. The binding interactions of the new compounds with both BSA and HSA structures, acquired from the Protein Data Bank (PDB) under the identification codes 4F5S and 1AO6, respectively, were assessed using AutoDock 4.2 software. The compounds underwent geometry optimizations using density functional theory (DFT) with the B3LYP/6-31G (d, p) basis set within the Gaussian09 package. For the docking analysis, a three-dimensional grid box measuring 60 Å x 60 Å x 60 Å, with a grid spacing of 0.375 Å along the X, Y, and Z axes, was employed. The central grid sites I, II, and III for BSA and HSA were located at (-4.795, 30.487, 101.007), (10.906, 16.276, 119.720), and (19.857, 33.531, 97.915) for BSA, and (34.720, 31.631, 33.029), (13.616, 35.053, 19.672), and (43.486, 22.726, 15.244) for HSA, respectively. Autodocking parameters consisted of a population size of 150 for the Genetic Algorithm (GA) and a maximum of 2,500,000 energy evaluations. The docked conformations' interactions were visualized and residue interactions were analyzed using the Biovia Discovery Studio 2020 program.

Molecular dynamics simulations (MD)

All molecular dynamics simulations (MD) were performed using GROMACS 2022.3 on GPU. The simulations were accelerated by NVIDIA GeForce RTX 4090, operating within an AMD Ryzen 9 7950X processor-based system environment (Chulabhorn Research Institute). Therefore, simulations were conducted to understand the stability and conformational changes, and they have been applied to investigate and screen the three different binding sites (I, II, and III) of both BSA and HSA, comparing their

unbound and bound with each newly synthesized quinoline (C) and (J), respectively. The topologies of proteins and ligands were prepared using the AMBER package, with the proteins employing the AMBER 99SB force field. The ligands were parameterized with corresponding the restrained electrostatic potential atomic partial (RESP) charges at the HF/6-31G(d) level using the Antechamber module. These complexes were centered within a periodic cubic box filled using the TIP3P water model, while maintaining a 10 Å distance from the box edges. The protonation state of ionizable residues was evaluated at pH 7.0 using the software tool PDB2PQR implemented by the ProPka server. Additionally, sodium ions were added to the solvent to neutralize the system. The energy minimization process employed the steepest descent algorithm, with a tolerance value of 10 kJ/mol/nm applied to the protein-ligand complexes. Subsequently, equilibration was performed using position restraints in the canonical ensemble (NVT) followed by the isothermal–isobaric ensemble (NPT) for a duration of 1000 ps. Additionally, the velocity of atoms was initialized at 300 K according to the Maxwell distribution with a random seed. The LINCS algorithm was employed to restrict bonds involving hydrogen atoms. Long-range electrostatic interactions were calculated using the particle mesh Ewald (PME) method, applying a cutoff of 12 Å. Temperature and pressure coupling were managed using the Berendsen thermostat and Parrinello–Rahman barostat, respectively. The MD simulation was performed for a duration of 30 ns, maintaining a temperature of 300 K and a pressure of 1 bar. Additionally, the MD simulation results were analyzed and visualization of the trajectory using the Visual Molecular Dynamics (VMD) program.

The Gibbs free energy landscape (FEL) obtained from principal component analysis (PCA) confirms the structural stability of the complexes. This was achieved by calculating eigenvectors from the covariance matrix using the gmx_covar and gmx_anaeig commands, focusing on the protein backbone. Simulation trajectories were then used to identify the structural energy minimum state of the complexes through FEL analysis. The 3D FEL plots were created using the Python script xpm2txt, which converts xpm files to dat format. These files were generated using the xpm2ps module

implemented in the GROMACS package. The JupyterLab interface in the Anaconda Navigator program was used to analyze the time period of the global energy minimum state from the MD trajectory. Subsequently, the binding free energy of the complexes was calculated for the period corresponding to the global energy minimum state.

Binding Free Energy Calculation using MM-PBSA

The binding free energy of both the BSA and HSA complexes was assessed using the widely employed Molecular Mechanics/Poisson-Boltzmann Surface Area (MM-PBSA) method, commonly utilized in studies related to protein-ligand interactions and drug design. The binding free energy and per-residue decomposition free energy were calculated from 500 frames extracted from the Gibbs free energy landscape to select the region corresponding to the global energy minimum state. These calculations were performed at a temperature of 300 K. Additionally, the solvation energy of complexes was computed using PB models (ipb= 2), with an implicit solvent dielectric constant of 80. The dielectric constant parameters for the solute were set to 4, and the ionic strength was adjusted to 0.15 M to replicate physiological conditions. These calculations utilized appropriate algorithms, with a solvent probe radius of 1.4 Å, and incorporated the Interaction Entropy (IE) method. The binding free energy results were analyzed using the gmx_MMPBSA_ana program, a component of the gmx_MMPBSA package.

CHAPTER 4
RESULTS

UV-Vis absorption studies

UV-Vis spectroscopy is a widely used technique for investigating the binding interactions and complex formation of serum albumin with small molecules. The absorption spectrum of serum albumin exhibits two significant peaks at approximately 210 nm and 280 nm. The absorption peak at 210 nm corresponds to the polypeptide backbone of the serum albumin structure, while the peak around 280 nm is associated with the π-π^* electronic transitions characteristic of the aromatic residues tryptophan (Trp), tyrosine (Tyr), and phenylalanine (Phe). Furthermore, this peak was utilized to monitor changes in the absorption spectrum, thus enabling the study of interactions between both BSA and HSA with newly synthesized compounds. The absorption spectra of BSA from 240 to 650 nm in the absence and presence of various concentrations of compounds (C) and (J) are displayed in Figures 24A and 24B, respectively. The spectra for HSA are shown in Figures 25A and 25B, corresponding to the titration with increasing concentrations of compounds (C) and (J), respectively. As seen in Figures 24 and 25, increasing the concentration of compounds (C) and (J) enhanced the absorbance at 280 nm for both BSA and HSA, with no shifts in the spectral peaks. Therefore, significant changes in the absorption peak intensities of both serum albumins in the presence of compounds (C) and (J) indicate the formation of conformational complexes.

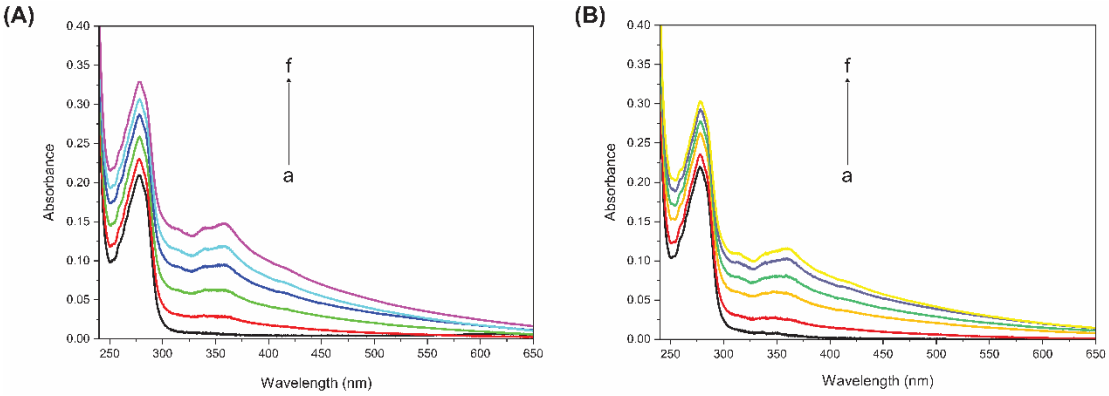

Figure 24 Absorption spectra of BSA (5 μM) in the absence and presence of increasing concentrations (a-f) of compounds (C) and (J), shown as BSA-(C) (A) and BSA-(J) (B), respectively. The concentrations of quinoline derivatives were increased to 0, 10, 20, 30, 40, and 50 μM.

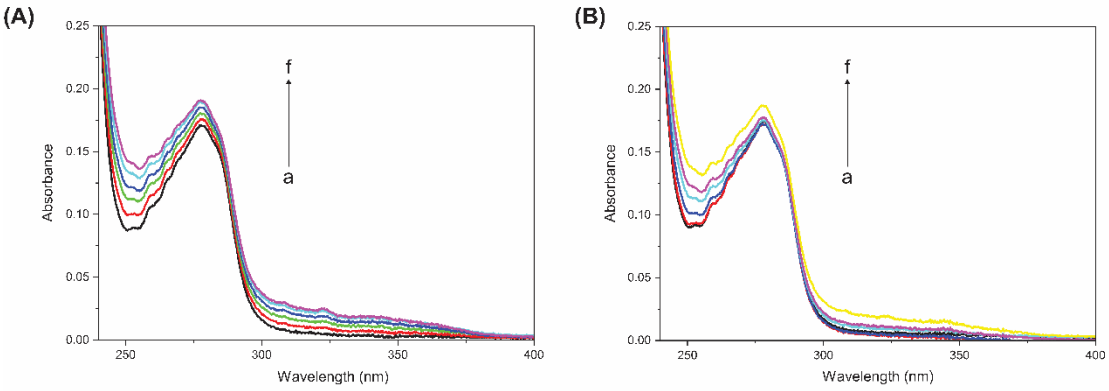

Figure 25 Absorption spectra of HSA (5 μM) in the absence and presence of increasing concentrations (a-f) of compounds (C) and (J), shown as HSA-(C) (A) and HSA-(J) (B), respectively. The concentrations of quinoline derivatives were increased to 0, 10, 20, 30, 40, and 50 μM.

Fluorescence quenching measurements

To elucidate the binding interactions of both BSA and HSA with compounds (C) and (J), fluorescence spectroscopy was employed. The emission spectra of BSA at different concentrations of these compounds were analyzed, revealing a strong fluorescence emission peak at 340 nm upon excitation at 280 nm. Similarly, when excited at 280 nm, the HSA displayed a strong fluorescence emission peak around 335 nm. Increasing the concentration of the (C) compound decreases the fluorescence intensity of both BSA and HSA at 280 and 335 nm and without significant changes in the emission peak position. In contrast, the titrations of both BSA and HSA with the (J) compound caused a slight red shift and hypochromism in the fluorescence spectra, along with a new emission peak around 450 nm. Therefore, these changes indicate an altered environment surrounding the chromophores, such as tryptophan (Trp) and phenylalanine (Phe), with tryptophan having the highest fluorescence intensity among these residues, affecting the protein structure of serum albumin upon binding to each compound. The decrease in fluorescence emission is shown in Figures 26 and 27 for BSA and HSA, respectively.

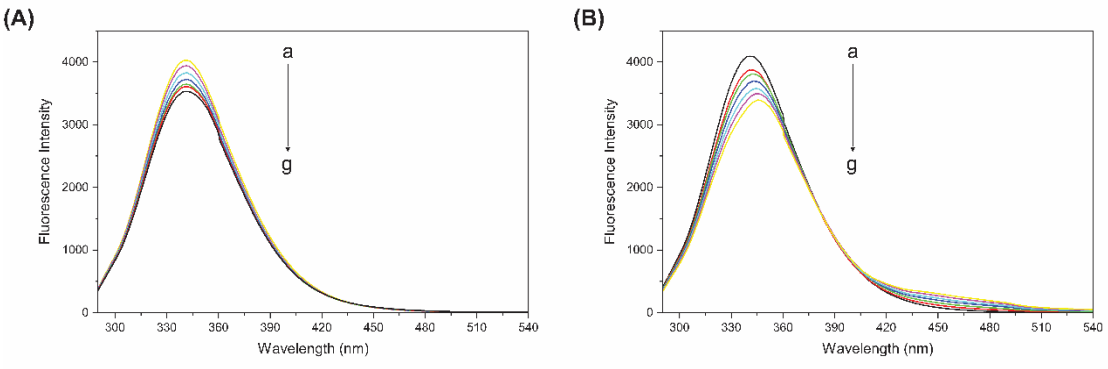

Figure 26 Fluorescence quenching spectra of BSA with compound (C) (Figure 26A) and compound (J) (Figure 26B) at various increasing concentrations (a-g) with an excitation wavelength of 280 nm.

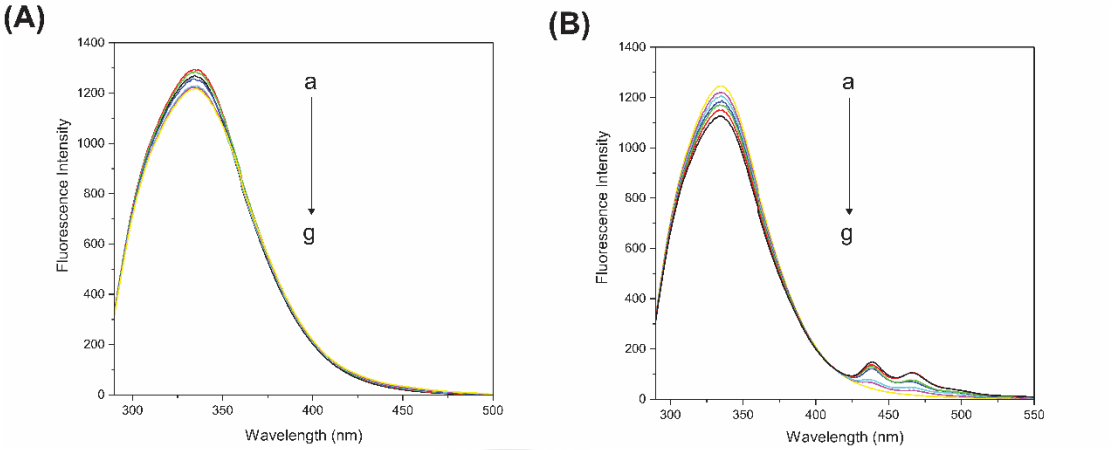

Figure 27 Fluorescence quenching spectra of HSA with compound (C) (Figure 27A) and compound (J) (Figure 27B) at various increasing concentrations (a-g) with an excitation wavelength of 280 nm.

Fluorescence quenching mechanisms can be clearly differentiated by temperature differences and classified as either dynamic (collisional) or static (complex formation) quenching. The fluorescence quenching mechanism was determined by analyzing the quenching constant (K_{sv}) from the fluorescence intensity data using the Stern-Volmer equation (equation [1]). In dynamic quenching, the quenching constant (K_{sv}) increases with rising temperature due to enhanced diffusion and collision of the fluorophore and quencher. Conversely, in static quenching, the stability of the fluorophore-quencher complex decreases with increasing temperature, resulting in a lower quenching constant (Liu, Chen, Luo, Lin, & Song, 2013; Phopin, Ruankham, Prachayasittikul, Prachayasittikul, & Tantimongcolwat, 2019; Y. Zhang, Cao, Li, & Zhang, 2022).

The fluorescence intensity data were analyzed using the Stern-Volmer equation (Equation 1) to determine the type of fluorescence quenching mechanism.

$$F_0/F = 1 + K_{SV}[Q] \quad [1]$$

The K_{sv} value was determined from the slope of the plot of F_0 / F versus [Q] and used to analyze the fluorescence intensity data. Where F_0 and F represent the fluorescence intensities of both BSA and HSA in the absence and presence of the quencher (compounds (C) or (J)), respectively. The concentration of the quencher is denoted as [Q]. The Stern-Volmer quenching plots at three different temperatures, along with the corresponding fitted data, are shown in Figures 28A for BSA bound with (C) and in Figure 28B for BSA bound with (J). Similarly, Figures 29A and 29B show the fitted Stern-Volmer quenching plots for HSA bound with (C) and (J), respectively. The K_{sv} values were determined and are presented in Tables 1 and 2 for BSA and HSA, respectively. The results showed that the K_{sv} values decreased as the temperature increased. This behavior suggests that the interaction between serum albumin and both compounds is likely due to static quenching, where the formation of a stable complex becomes less stable at higher temperatures.

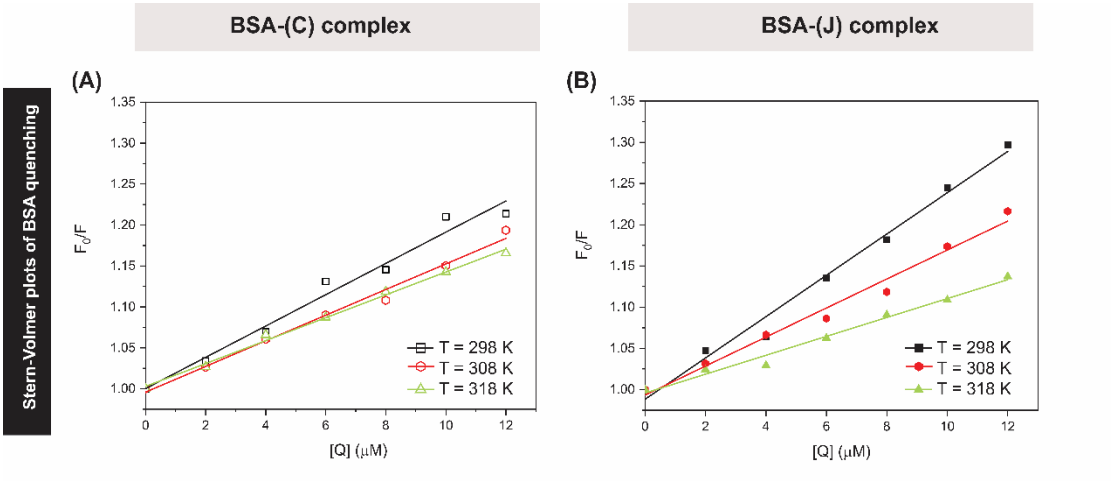

Figure 28 The Stern-Volmer quenching plots of BSA with compound (C) (Figure 28A) and compound (J) (Figure 28B) at different temperatures (298 K, 308 K, and 318 K).

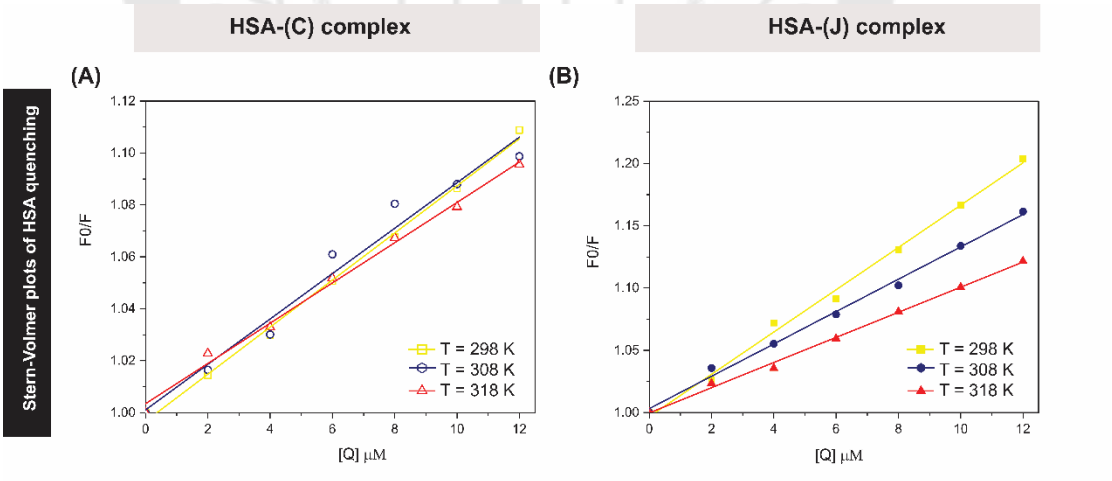

Figure 29 The Stern-Volmer quenching plots of HSA with compound (C) (Figure 29A) and compound (J) (Figure 29B) at different temperatures (298 K, 308 K, and 318 K).

Table 1 Stern–Volmer quenching constant (K_{sv}), the binding constant (K_b), and the number of binding sites (n) for the interaction of (C) and (J) with BSA at 298, 308 and 318 K.

Systems	T (K)	K_{sv} ($x10^4$ $Lmol^{-1}$)	K_b ($x10^4$ $Lmol^{-1}$)	n
BSA-(C)	298	1.91	4.31	1.07
	308	1.56	3.48	1.07
	318	1.40	1.44	1.00
BSA-(J)	298	2.50	6.31	1.09
	308	1.76	2.75	1.04
	318	1.15	1.69	1.04

Table 2 Stern–Volmer quenching constant (K_{sv}), the binding constant (K_b), and the number of binding sites (n) for the interaction of (C) and (J) with HSA at 298, 308 and 318 K.

Systems	T (K)	K_{sv} ($Lmol^{-1}$)	K_b ($Lmol^{-1}$)	n
HSA-(C)	298	9.07×10^3	3.86×10^4	1.13
	308	8.75×10^3	1.75×10^4	1.06
	318	7.75×10^3	1.01×10^3	1.02
HSA-(J)	298	1.70×10^4	6.17×10^4	1.07
	308	1.30×10^4	2.16×10^4	1.02
	318	1.25×10^4	5.52×10^3	1.02

Determination of binding constants and the number of binding site

To estimate the binding affinity of the newly synthesized compounds (C and J) with serum albumin, the binding constant (K_b) and the number of binding site (n) were determined using equation [2]. The K_b values were derived from the intercept and slope of the double logarithmic regression curve of log $(F_0\text{-}F)/F$ versus log [Q].

$$\log \frac{F_0\text{-}F}{F} = \log K_b + n\log [Q] \qquad [2]$$

In Equation [2], n represents the number of binding sites per molecule of serum albumin, and K_b is the binding constant for the interaction of both BSA and HSA bound with either compound (C) or (J). The K_b values, calculated at three different temperatures, are listed in Tables 1 and 2 for the BSA and HSA systems, respectively. Additionally, the fitted data corresponding to the double logarithm plots of both BSA and HSA with compounds (C) and (J) are illustrated in Figures 30(A and B) and 31(A and B). Therefore, the binding constants (K_b) and the number of binding sites (n) obtained from the results indicated that the K_b values ranged from 10^3 to 10^4 $L{\cdot}mol^{-1}$ for both BSA and HSA bound to compounds (C) and (J), respectively, indicating strong binding interactions. Moreover, the number of binding sites for the serum albumin-ligand complex was approximately 1, indicating a 1:1 binding ratio between serum albumin and the compounds.

The thermodynamic parameters and binding mode

The binding modes for intermolecular interactions between ligands and proteins can be categorized into four types: electrostatic interactions, hydrogen bonding, hydrophobic interactions, and van der Waals forces. To investigate the binding forces between serum albumin and compounds (C) and (J), thermodynamic parameters such as Gibbs free energy (ΔG), enthalpy change (ΔH), and entropy change (ΔS) were calculated using equations [3] and [4]. These parameters were determined using the Van't Hoff equation and the Gibbs function. Additionally, the binding process of protein and ligand interactions was evaluated to establish the binding mode.

$$\ln K_b = -\frac{\Delta H}{RT} + \frac{\Delta S}{R} \quad [3]$$

$$\Delta G = -RT\ln K_b = \Delta H - T\Delta S \quad [4]$$

In the equations, R denotes the universal gas constant, T represents the temperature in Kelvin, and K_b is the binding constant. The values of ΔH and ΔS for the binding reaction provide crucial information for elucidating the main binding forces. Positive values of both enthalpy change (ΔH) and entropy change (ΔS) indicate hydrophobic interactions. On the other hand, negative values of both ΔH and ΔS suggest interactions dominated by van der Waals forces or hydrogen bonding. Additionally, when ΔH is close to zero and ΔS is positive, electrostatic interactions are considered the main binding force (Philip D. Ross, 1981; X. Zhang, Lin, Liu, & Lin, 2015). According to the Van't Hoff equations, the thermodynamic parameters for both BSA and HSA binding with compounds (C) and (J) were obtained from the slope and intercept of the plots of K_b versus 1/T, shown in Figure 30(C and D) and 31(C and D), respectively. Tables 3 and 4 show that the values of ΔH and ΔS for both BSA and HSA binding with compounds (C) and (J) were negative indicating that hydrogen bonding and van der Waals forces play a major role importance in this binding process. The negative ΔG

values observed at different temperatures confirm that the binding processes of compounds (C) and (J) with both BSA and HSA are spontaneous processes.

Table 3 Thermodynamic parameters for the interaction of BSA with compounds (C) and (J) at different temperatures.

Temperature	ΔH (kJ·mol^{-1})		ΔS (kJ·mol^{-1})		ΔG (kJ·mol^{-1})	
(K)	(C)	(J)	(C)	(J)	(C)	(J)
298	-42.65	-52.08	-53.48	-83.29	-26.43	-27.38
308					-26.78	-26.18
318					-25.32	-25.74

Table 4 Thermodynamic parameters for the interaction of HSA with compounds (C) and (J) at different temperatures.

Temperature	ΔH (kJ·mol^{-1})		ΔS (kJ·mol^{-1})		ΔG (kJ·mol^{-1})	
(K)	(C)	(J)	(C)	(J)	(C)	(J)
298	-142.55	-95.49	-387.62	-229.97	-26.16	-27.33
308					-25.02	-23.87
318					-18.29	-22.78

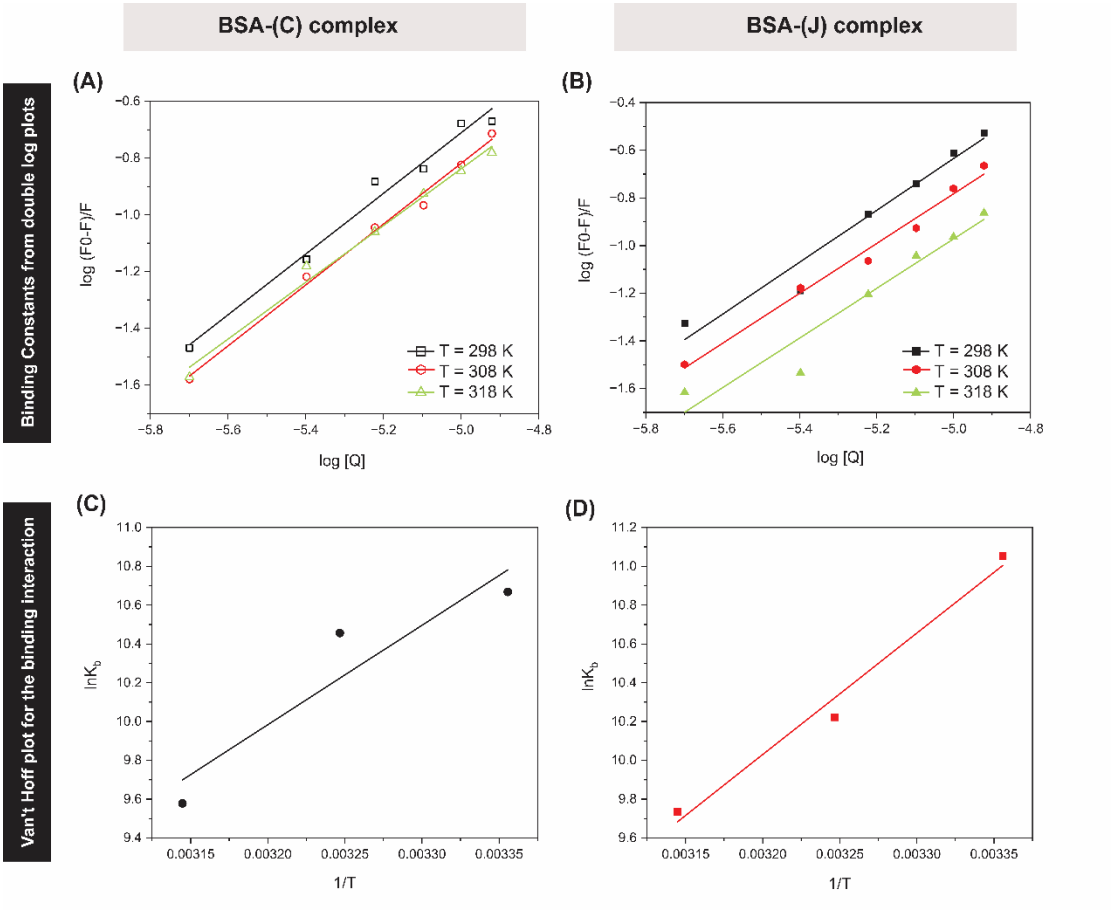

Figure 30 The double logarithmic plots of $(F_0\text{-}F)/F$ versus log [Q] for BSA-(C) and BSA-(J) complexes in Figures 30(A) and 30(B), respectively, at 298, 308 and 318 K. Van't Hoff plots of In K_b versus 1/T for the binding interactions of BSA-(C) and BSA-(J) are shown in Figures 30(C) and 30(D), respectively.

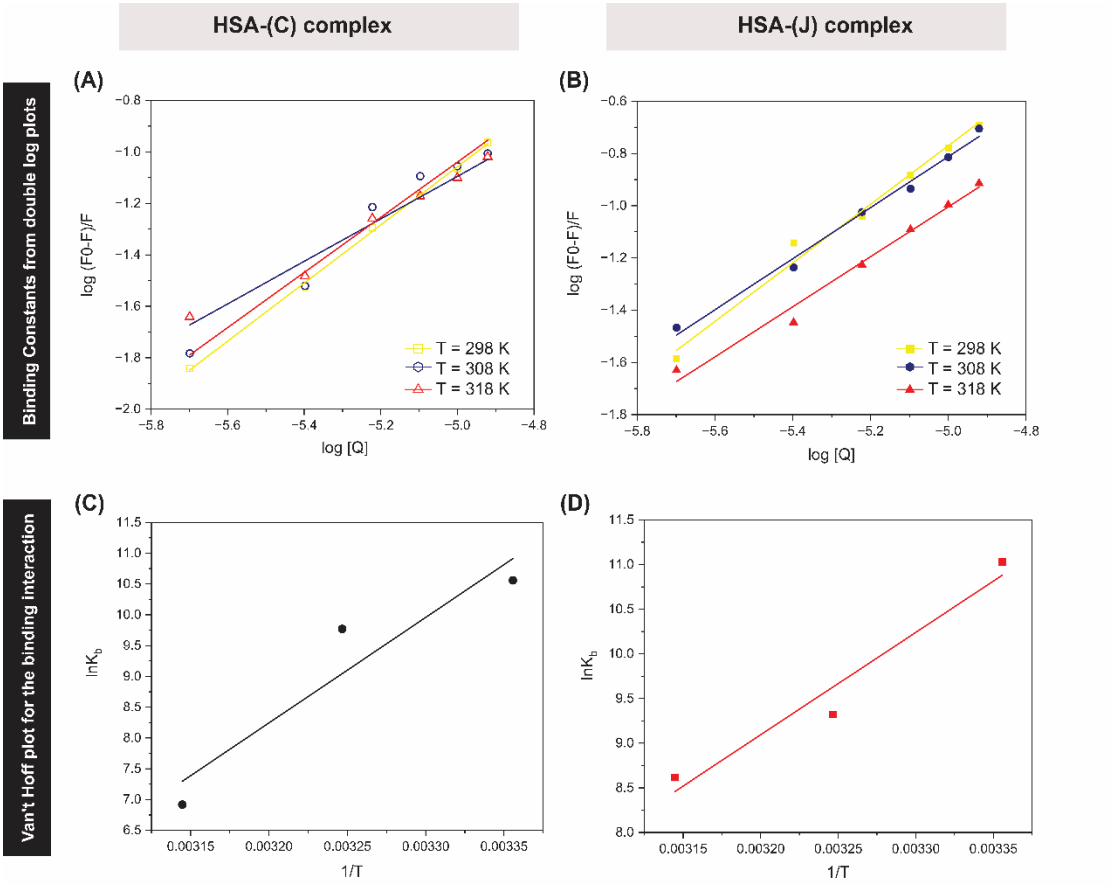

Figure 31 The double logarithmic plots of $(F_0\text{-}F)/F$ versus log [Q] for HSA-(C) and HSA-(J) complexes in Figures 31(A) and 31(B), respectively, at 298, 308 and 318 K. Van't Hoff plots of ln K_b versus 1/T for the binding interactions of HSA-(C) and HSA-(J) are shown in Figures 31(C) and 31(D), respectively.

Identification of the binding site

The ligand binding sites on the structure of serum albumins are located within the hydrophobic pockets of subdomains IIA (site I), IIIA (site II), and IB (site III). The specific binding site of each ligand on the protein can be determined through competitive binding experiments using warfarin, ibuprofen, and digitoxin as site probes. These site markers, with known binding sites on both BSA and HSA, indicate that warfarin binds at site I, ibuprofen at site II, and digitoxin at site III (Ha & Bhagavan, 2013; Phopin et al., 2019). Therefore, to investigate the binding sites of compounds (C) and (J) on the structures of both BSA and HSA, competitive binding experiments were performed using fluorescence measurements (Wu et al., 2011). To evaluate the binding constants (K_b) at the competitive binding sites, compounds (C) or (J) were gradually added to systems where BSA and HSA were each bound with their respective site markers. The binding constants (K_b) of compounds (C) and (J) with both BSA and HSA, in the absence and presence of the site markers, were determined by analyzing the fluorescence intensity using equation [2]. The results for the BSA system are presented in Table 5, and the results for the HSA system are presented in Table 6. According to the data in Table 5, the binding constants of BSA with compounds (C) and (J) significantly decreased from 2.743 and 2.699 to 1.767 and 1.523, respectively, in the presence of digitoxin. According to the data in Table 4, the binding constants (K_b) of BSA with compounds (C) and (J) significantly decreased from 2.743 and 2.699 to 1.767 and 1.523, respectively, in the presence of digitoxin. Similarly, Table 5 shows the K_b values of HSA with compounds (C) and (J) were 3.286 and 3.226, respectively, in the absence of the site marker. When digitoxin was present as a site marker, the K_b values for HSA with compounds (C) and (J) decreased to 2.390 and 2.198, respectively. Conversely, the binding constants remained largely unchanged in the presence of warfarin and ibuprofen. The decrease in K_b values for competitive interactions in the absence of the site marker was less significant than in its presence, indicating the major binding site for the ligand (Li et al., 2022). Thus, the binding sites for compounds (C) and (J) on both BSA and HSA are located at site III in subdomain IB.

Table 5 Binding constants of BSA with compounds (C) and (J) in both the absence and presence of site markers.

System	Without the site marker		Site I marker (Warfarin)		Site II marker (Ibuprofen)		Site III marker (Digitoxin)	
	$\log K_b$	R^2	$\log K_b$	R^2	$\log K_b$	R^2	$\log K_b$	R^2
BSA – (C)	2.743	0.9880	2.665	0.9809	2.851	0.9806	1.767	0.9779
BSA – (J)	2.699	0.9836	2.584	0.9868	2.616	0.9817	1.523	0.9881

Table 6 Binding constants of HSA with compounds (C) and (J) in both the absence and presence of site markers.

System	Without the site marker		Site I marker (Warfarin)		Site II marker (Ibuprofen)		Site III marker (Digitoxin)	
	$\log K_b$	R^2	$\log K_b$	R^2	$\log K_b$	R^2	$\log K_b$	R^2
HSA – (C)	3.286	0.9727	3.4013	0.9868	3.212	0.9941	2.390	0.9842
HSA – (J)	3.226	0.9929	3.098	0.9913	3.128	0.9817	2.198	0.9867

Molecular docking studies

Molecular docking, a widely used and efficient technique, has been employed to investigate the binding interactions between a protein and small molecules. It illustrates the types of amino acids surrounding the ligand and the formation of hydrogen bonds (Abdullah, Fatma, Rabbani, & Ashraf, 2017; Zargar & Wani, 2021). To support the results from the competitive experiment, a molecular docking technique was employed to investigate the binding mechanism between newly synthesized compounds and serum albumin. This approach aimed to enhance the understanding of the potential efficacy of quinoline derivatives as candidate drugs. The amino acid sequences of BSA share approximately 76% similarity with those of HSA. This docking method aids in predicting the binding locations and affinities of compounds (C) and (J) on the structures of BSA and HSA. The optimized structures of compounds (C) and (J) were docked to BSA (PDB ID: 4F5S) and HSA (PDB ID: 1AO6) using the AutoDock program (version 4.2). The docking results with the lowest binding free energies and the interactions with amino acids within 5 Å of both compounds are presented in Table 7 for BSA and Table 8 for HSA. Docking studies revealed that the estimated binding free energies of both compounds in subdomain IB (site III) of BSA and HSA were lower than those in subdomains IIA (site I) and IIIA (site II). This indicates that compounds (C) and (J) bind to both BSA and HSA at site III in subdomain IB (Figures 32A and 33A for BSA-(C) and BSA-(J); Figure 34A and 35A for HSA-(C) and HSA-(J)), consistent with the experimental data obtained from the competitive experiment.

As shown in Figure 32A, compound (C) exhibited the lowest binding energy of -10.48 kcal/mol at site III of BSA. Within 5 Å, this binding pose was surrounded by the amino acids Lys114, Leu115, Lys116, Pro117, Asp118, Thr121, Leu122, Glu125, Phe133, Lys136, Tyr137, Glu140, Ile141, Tyr160, Ile181, Met184, Arg185, and Val188. Hydrogen bonding interactions were observed between the aldehyde group of compound (C) and the nitrogen atom on the Lys116 residue, as well as between the cyanide group (CN) of compound (C) and the oxygen atom on the Tyr137 residue in BSA. For compound (J), Figure 33B shows the lowest binding energy of -10.53 kcal/mol

at site III of BSA. The amino acids encircling compound (J) within 5 Å included Leu115, Lys116, Pro117, Asp118, Leu122, Glu125, Phe126, Asp129, Lys132, Phe133, Lys136, Tyr137, Glu140, Ile141, Tyr160, Ile181, Met184, Arg185, and Val188. In the BSA structure, the cyanide group of compound (J) formed hydrogen bonds with the oxygen atom on the Tyr137 residue. Additionally, the oxygen atom of the Tyr137 residue formed hydrogen bonds with the cyanide group (CN) of compound (J). The hydrogen bonding interactions of the newly synthesized compounds to BSA indicate that the binding mode aligned with the thermodynamic parameter analysis results. Furthermore, compound (C) exhibited **π-π** stacking interactions with residues Phe133 and Tyr160 in site III of BSA, while compound (J) also bound to the same domain through **π-π** stacking interactions with Tyr160.

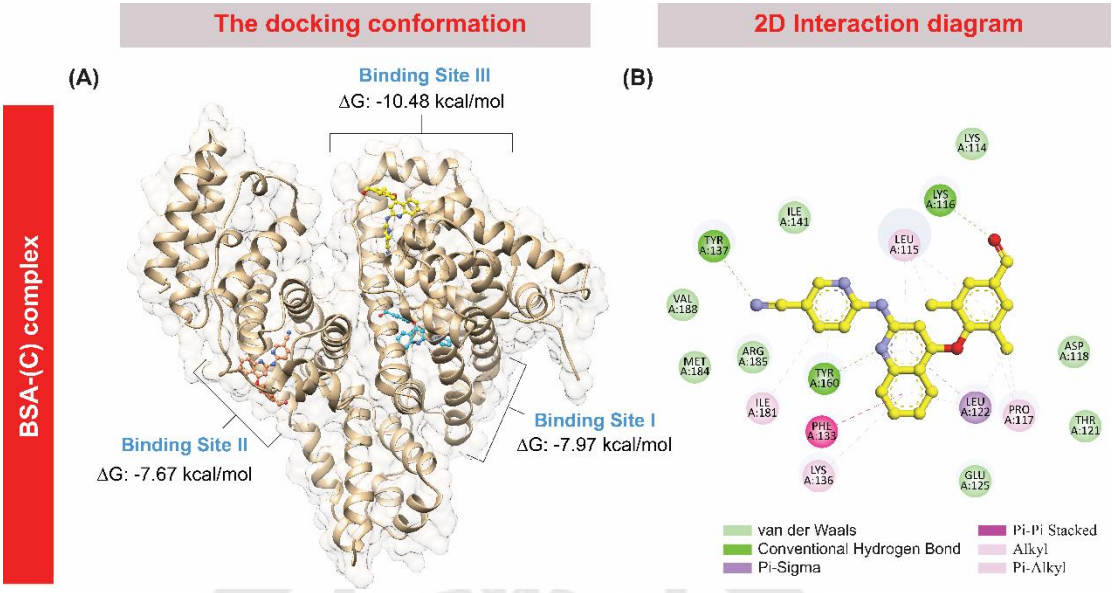

Figure 32 Conformation and interaction of compound (C) with BSA, conformation at three sites (A), 2D interaction at site III (B).

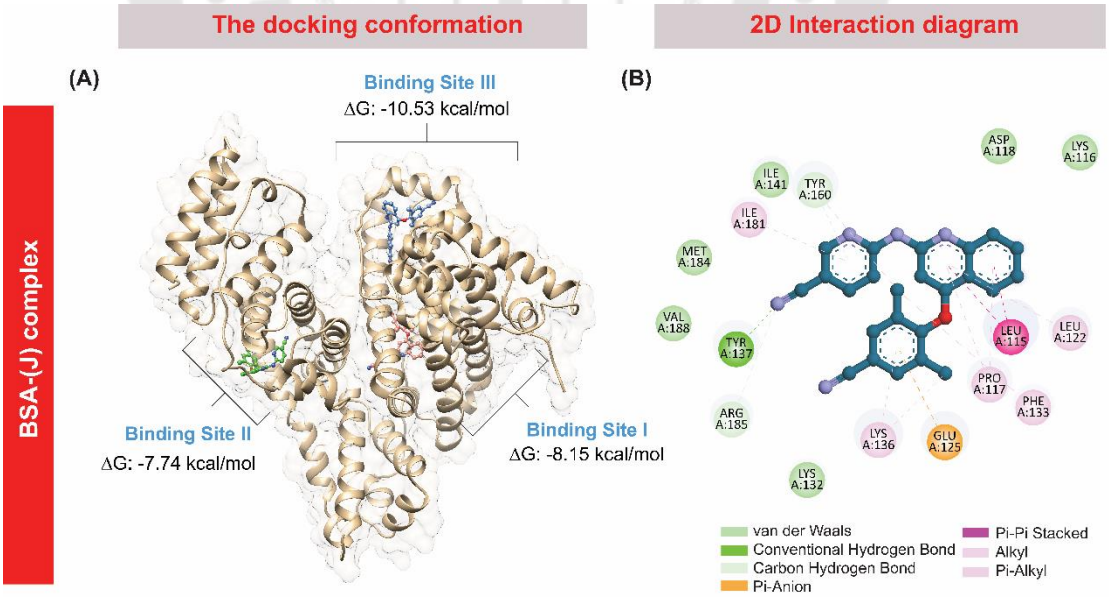

Figure 33 Conformation and interaction of compound (J) with BSA, conformation at three sites (A), 2D interaction at site III (B).

Figure 34A illustrates that compound (C) binding at site III of HSA exhibited a binding free energy of -10.15 kcal/mol, without forming hydrogen bonds in this region. The amino acids within 5 Å of this binding pose included Leu115, Val116, Arg117, Pro118, Met123, Thr133, Phe134, Lys135, Lys136, Lys137, Tyr138, Ile142, Phe149, Phe157, Tyr161, Phe165, Lys181, Lys182, Asp183, Lys185, Arg186, Gly189, and Lys190. For compound (J), Figure 35A shows a binding free energy of -10.50 kcal/mol at site III of HSA. The amino acids surrounding this binding pose within 5 Å included Leu115, Val116, Arg117, Pro118, Met123, Thr133, Phe134, Lys135, Lys136, Lys137, Tyr138, Ile142, Phe149, Phe157, Tyr161, Lys181, Lys182, Asp183, Lys185, Arg186, Glu188, Gly189, and Lys190. Additionally, the NH group in the linker region of compound (J) formed hydrogen bonds with the oxygen atom of Tyr161. Furthermore, the results of the binding interactions of HSA with both compounds indicate that the binding mode aligns with the thermodynamic parameter analysis. Compound (C) exhibited **π-π** stacking interactions with residues Phe134 and Tyr161 at site III of HSA, while compound (J) also bound to the same domain through **π-π** stacking interactions with Tyr161. Therefore, the result of docking interaction exhibited the **π-π** stacking interactions align with the UV-Vis absorption study results, where the absorption intensities of both BSA and HSA increased with rising concentrations of compounds (C) and (J).

Comparisons of the binding energies in subdomain IB (site III) of compounds (C) and (J) bound to both BSA and HSA showed that serum albumin bound to (J) with lower binding free energy than to (C). These results indicate that (J) bound to both BSA and HSA is more stable than (C). To determine the greater stability of compound (J) binding with the proteins, further studies were conducted using molecular dynamics simulations.

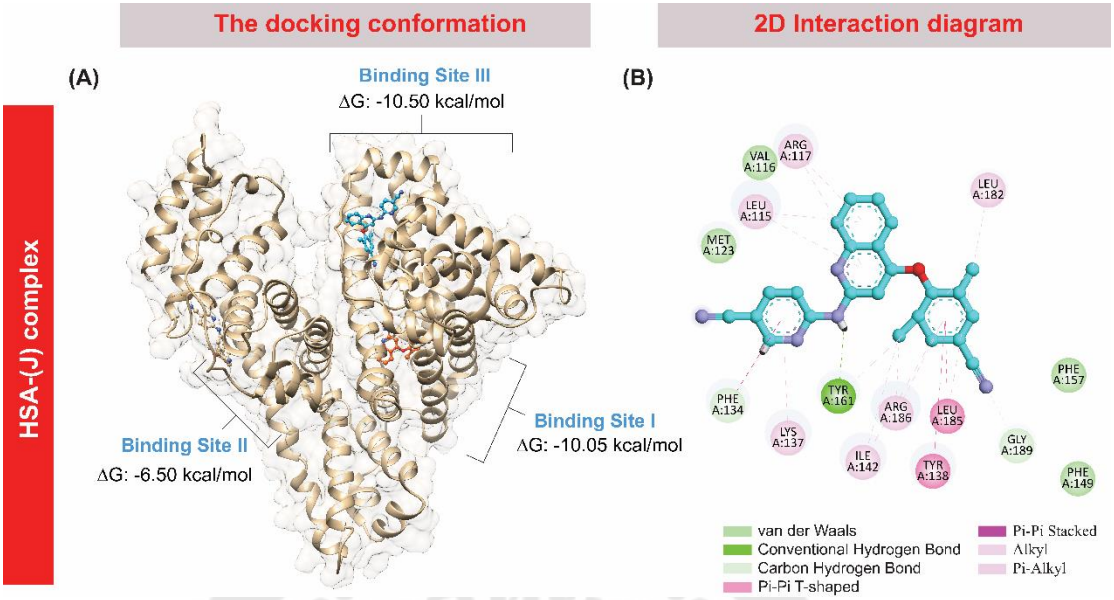

Figure 34 Conformation and interaction of compound (C) with HSA. Conformation at three sites (A). 2D interaction at site III (B).

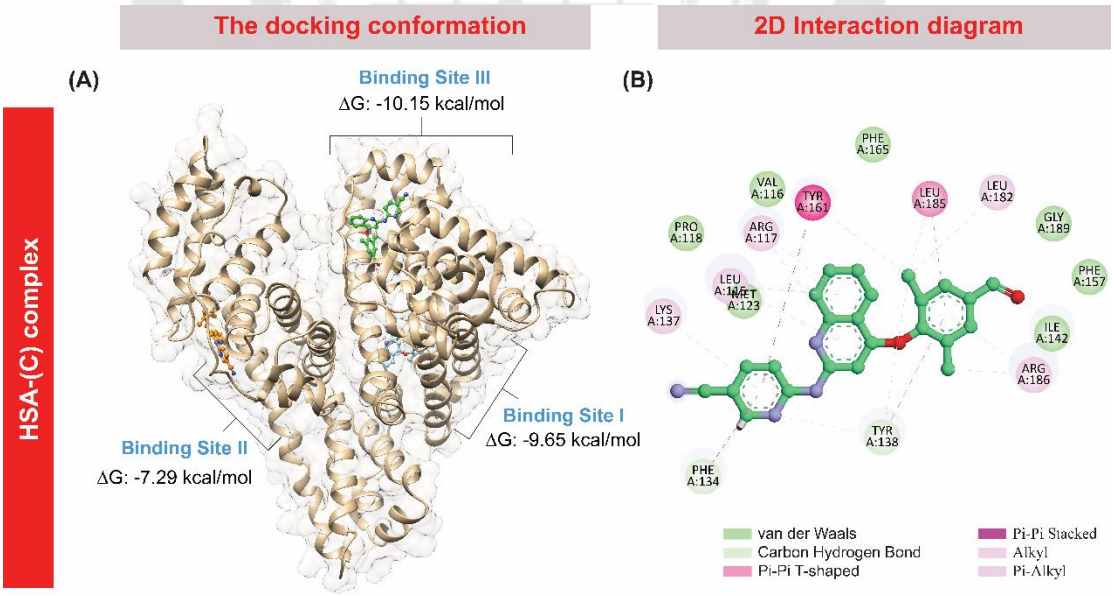

Figure 35 Conformation and interaction of compound (J) with HSA. Conformation at three sites (A). 2D interaction at site III (B).

Table 7 Binding energies and interacting amino acids of compounds (C) and (J) with BSA at three sites.

System	Binding site on BSA	Binding energy (kcal/mol)	Surrounding amino acid within 5 Å	
			H-bond	**π-π** stacking
BSA – (C)	Site I	-7.97	Arg194, Arg256	His287
	Site II	-7.67	Arg409, Arg484	-
	Site III	-10.48	Lys116, Tyr137	Phe133, Tyr160
BSA – (J)	Site I	-8.15	Arg198, Arg217	Trp213
	Site II	-7.74	Arg409, Lys413	-
	Site III	-10.53	Tyr137	Tyr160

Table 8 Binding energies and interacting amino acids of compounds (C) and (J) with HSA at three sites.

System	Binding site on HSA	Binding energy (kcal/mol)	Surrounding amino acid within 5 Å	
			H-bond	**π-π** stacking
HSA – (C)	Site I	-9.65	Tyr150, Lys195, Glu292, Ser287	-
	Site II	-7.29	Lys414	-
	Site III	-10.15	-	Phe134, Tyr161
HSA – (J)	Site I	-10.05	Tyr150, Lys195, Glu292	-
	Site II	-6.50	Lys545, Ala406	-
	Site III	-10.50	Tyr161	Phe134

Molecular dynamics (MD) simulations

Molecular dynamics (MD) simulations were performed to assess the binding stability between ligands and the target protein, along with conformational changes, ligand-binding, and protein folding within the surrounding solvent environment. MD simulations treat each protein, ligand, and solvent atom dynamically and flexibly (Ding & Peng, 2016). In contrast, molecular docking assumes a rigid macromolecule with a flexible ligand in the protein binding site (Ali et al., 2021). Therefore, MD simulations were conducted to investigate the structural stability of both BSA and HSA bound with newly synthesized compounds (C) and (J) at three different binding sites (site I, II, and III), compared to unbound proteins. These simulations were analyzed using several parameters, including root mean square deviations (RMSD), root mean square fluctuations (RMSF), and radius of gyration (Rg).

Root Mean Square Deviation (RMSD) is a key parameter used to measure the stability of proteins in the presence of ligands over time, indicating the binding stability and equilibrium of protein-ligand complexes by determining fluctuations in the protein backbone within the simulated system (Al-Khafaji & Taskin Tok, 2020; Li et al., 2022). RMSD calculations were performed using three replicate simulations to reduce bias in classical MD simulations for compounds (C) and (J) bound to both BSA and HSA at the three binding sites, as shown in Figures 36 and 37, respectively. Interestingly, site III of both BSA and HSA bound with compounds (C) and (J) exhibited slightly fluctuations compared to protein-free systems, indicating that both complexes had reached an equilibrium state. The average of three replicate simulations indicated that the stability of both compounds (C) and (J) bound to the BSA and HSA structures at site III was greater than at sites I and II, supporting the results from competitive experiments and docking studies. The RMSD of BSA-(C) at site III showed similar fluctuations and a slight increase compared to unbound BSA, beginning to equilibrate after about 15 ns, as illustrated in Figure 36A. For BSA-(J) at site III (Figure 36B), the dynamic equilibrium of the backbone indicated a stable state from 10 ns onwards. When comparing fluctuations at the three binding sites, (J) exhibited the most structural stability when

bound to BSA at site III. From Figure 37A, HSA bound with compounds (C) and (J) at site III had slight fluctuations compared to HSA-free. Additionally, Figure 37B indicates that the RMSD of HSA-(J) exhibited the most stability when bound to HSA at site III. The RMSD plots of HSA-(C) and HSA-(J) at site II showed similar fluctuations and a slight increase compared to HSA-free because both compounds (C) and (J) were located on the outside of the binding pocket at site II.

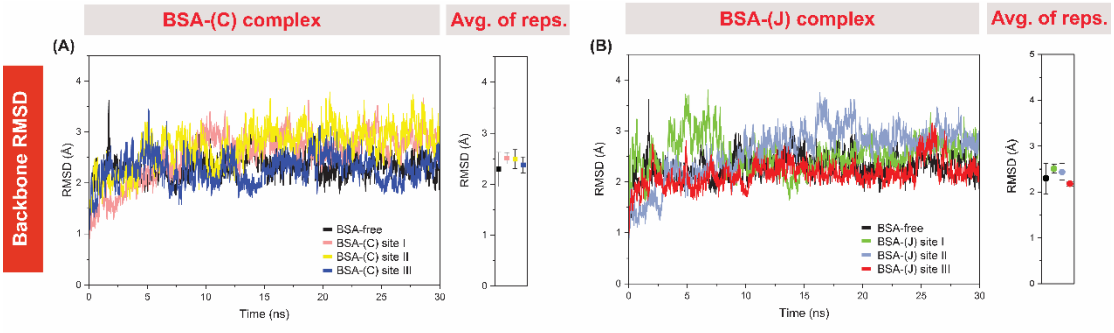

Figure 36 The RMSD backbone plots for BSA-(C) and BSA-(J) at three different binding sites, including the average of replicates, RMSD plot for BSA-(C) complex (A), RMSD plot for BSA-(J) complex (B).

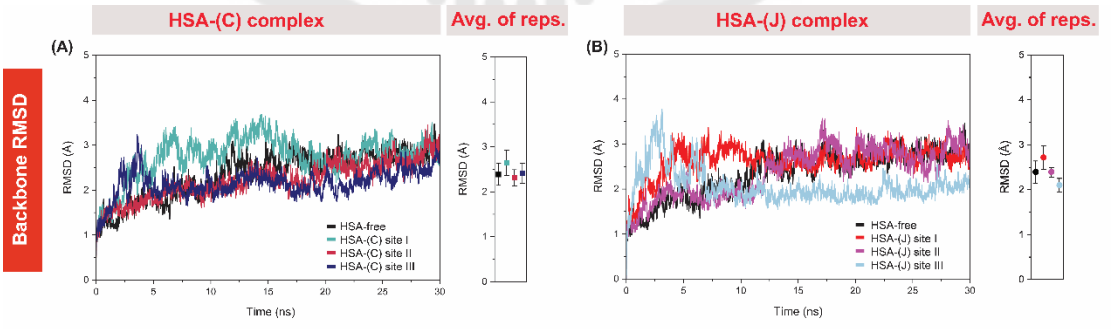

Figure 37 The RMSD backbone plots for HSA-(C) and HSA-(J) at three different binding sites, including the average of replicates, RMSD plot for HSA-(C) complex (A), RMSD plot for HSA-(J) complex (B).

The RMSF plots indicate that reduced fluctuations of residues in the backbone atoms exhibit stable interactions between the protein and ligand. Conversely, higher fluctuations imply greater flexibility in the protein structure, which may suggest conformational changes (Ding & Peng, 2016; Kooravand, Asadpour, Haddadi, & Farhadian, 2021). The structural flexibility derived from ligand binding results in residue fluctuations, indicating conformational changes. Figures 38 and 39 present the RMSF calculations for both BSA and HSA complexes with compounds (C) and (J), compared to changes in the free and bound forms of the proteins at different binding sites. Figure 38A shows that the RMSF of BSA-(C) at site III (navy blue) had reduced fluctuations compared to pure BSA (black), indicating increased stability in sub-domain IB. Similarly, the reduced fluctuation of the BSA-(J) complex at site III (red) compared to pure BSA (black) showed stability at binding site III (sub-domain IB). Increased RMSF fluctuations in certain regions indicated conformational changes upon ligand binding. For the RMSF plot for HSA at site III (Figures 39A and 39B, respectively), the decreased fluctuation of the HSA-(C) complex (royal blue) and the HSA-(J) complex (light blue) compared with unbound HSA indicates that the binding interactions at sub-domain IB.

The radius of gyration (Rg) is a key parameter for assessing the compactness and stability of protein-ligand complexes, indicating fluctuations in the protein backbone within the simulated system. Fluctuations in the Rg plot for the complex being higher than that of the unbound protein indicate conformational changes aimed at stabilizing the complex (Lobanov, Bogatyreva, & Galzitskaya, 2008). The Rg plots for BSA-(C) and BSA-(J) complexes at all three binding sites, compared to unbound BSA, are shown in Figure 38C and 38D, respectively. The Rg plot in Figure 38C demonstrates that BSA-(C) at site III exhibits reduced fluctuations, indicating enhanced stability compared to sites I and II. Similarly, the Rg plot for BSA-(J) at site III (Figure 38D) shows decreased fluctuations, almost coinciding with unbound BSA, suggesting greater compactness and structural stability. Additionally, the Rg plots for HSA bound with both (C) and (J) compounds are shown in Figures 39C and 39D, respectively. Interestingly, site III of HSA binding with both (C) and (J) exhibited lower Rg fluctuations compared to unbound

HSA, indicating compactness of the complexes. These results suggest that conformational changes lead to the stability of the complex. Therefore, the MD simulation results showed that both BSA and HSA bound with (C) and (J) form more stable complexes at site III compared to sites I and II, consistent with the competitive experiment and docking study results.

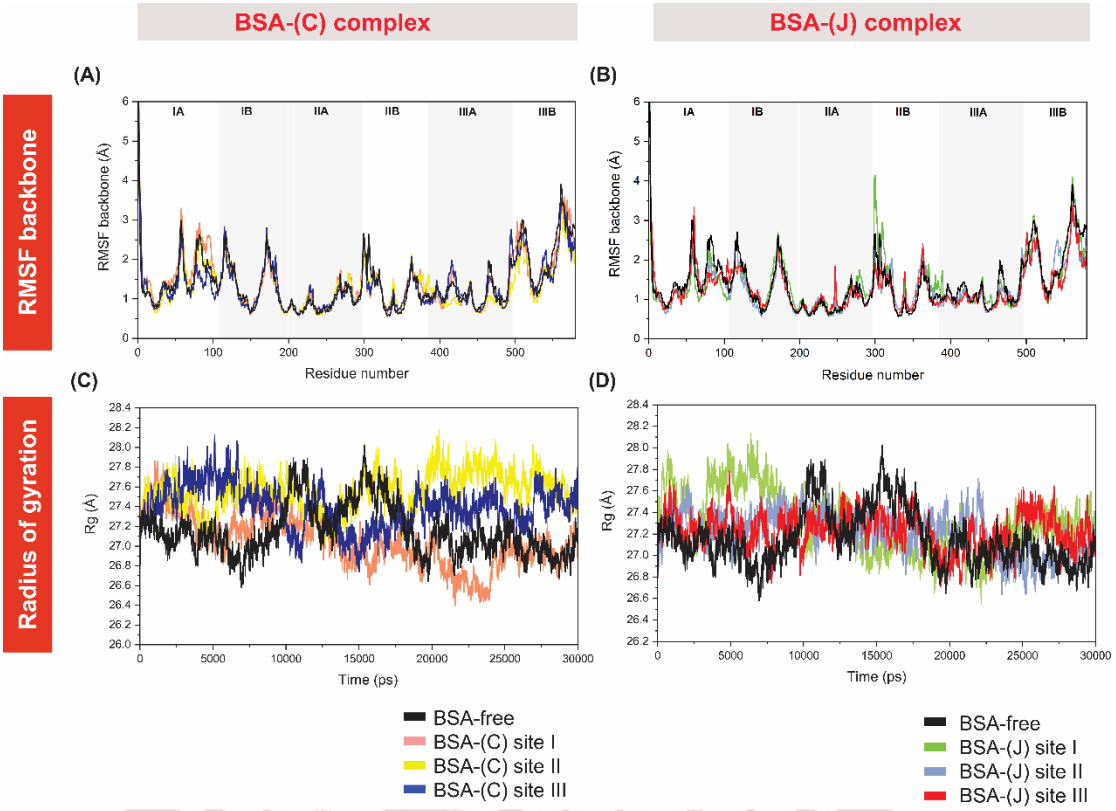

Figure 38 Analysis of MD simulation plots for BSA-(C) and BSA-(J) at three different binding sites, (A) RMSF plots of the protein backbone for BSA-(C), (B) RMSF plots of the protein backbone for BSA-(J), (C) Radius of gyration (Rg) plots for BSA-(C), (D) Radius of gyration (Rg) plots for BSA-(J).

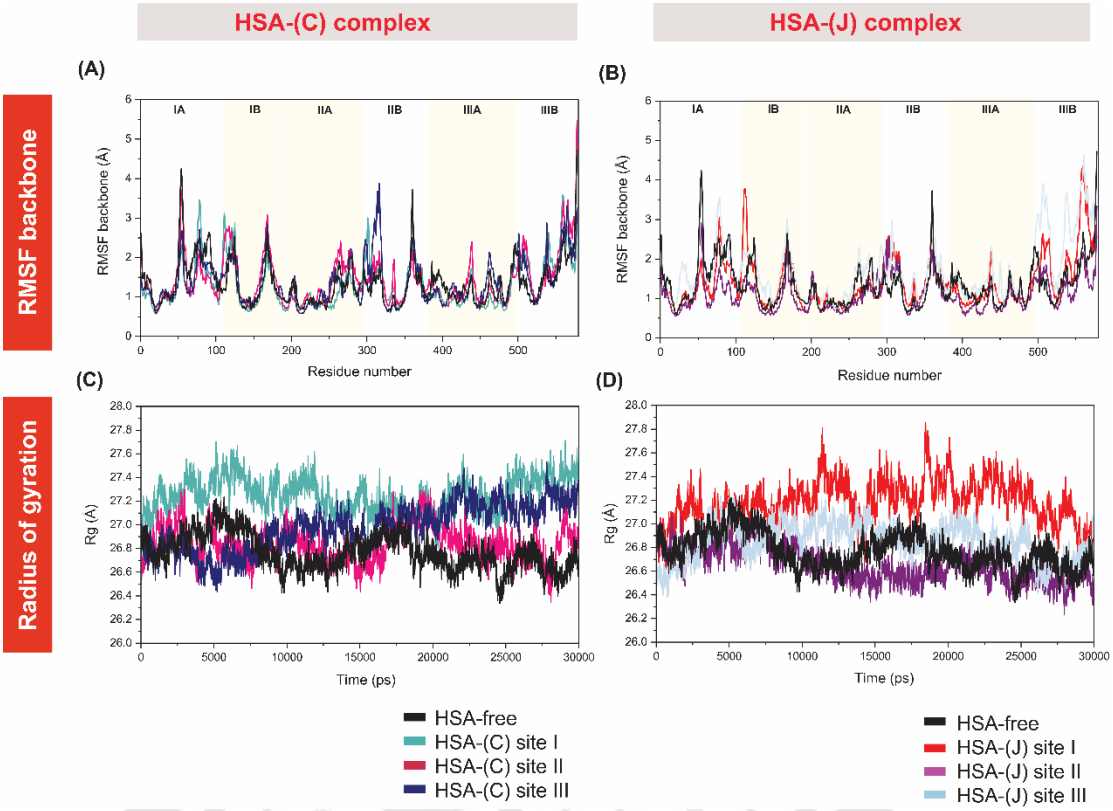

Figure 39 Analysis of MD simulation plots for HSA-(C) and HSA-(J) at three different binding sites, (A) RMSF plots of the protein backbone for HSA-(C), (B) RMSF plots of the protein backbone for HSA-(J), (C) Radius of gyration (Rg) plots for HSA-(C), (D) Radius of gyration (Rg) plots for HSA-(J).

Since the results for both BSA and HSA are consistent, particularly in terms of stability when binding with compounds (C) and (J) at site III, and in accordance with spectroscopic data, we chosed to use BSA for further calculations. Additionally, running simulations and binding free energy calculations for both BSA and HSA would require extensive computational resources. Therefore, we selected BSA for the calculation of binding free energy using the MM-PBSA method.

Binding free energy calculation

The Gibbs free energy landscape (FEL) indicates the global minimum of protein-ligand complex states in relation to energy function and time (Al-Khafaji & Taskin Tok, 2020; Khan et al., 2020). To ensure the structural stability of the complexes throughout the simulation, we examined the structural minimum state. Therefore, we extended the period of the three replicated MD simulations to 100 ns. The average of replicates from the RMSD plots is shown in Figure 40 for BSA-(C) and BSA-(J) at site III, illustrating similar fluctuations for both complexes. The average RMSD replicates indicated that BSA-(J) at site III was more stable than BSA-(C).(Al-Khafaji & Taskin Tok, 2020; Ding & Peng, 2016; Miller et al., 2012)

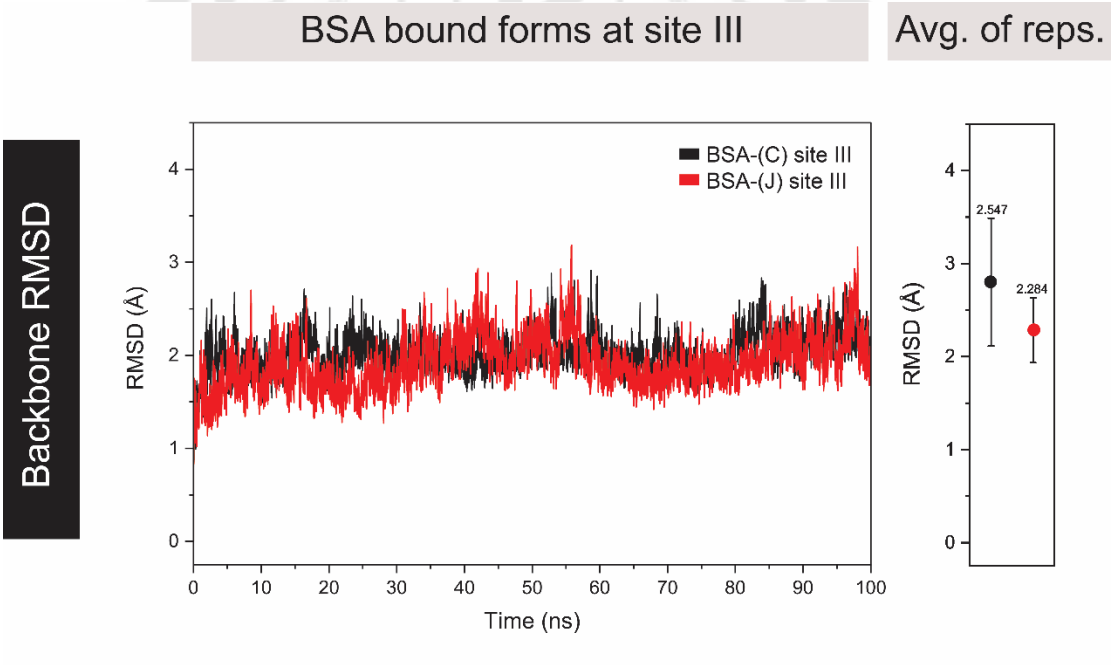

Figure 40 RMSD backbone plots for BSA bound forms at site III, (A) RMSD plots for BSA-(C) and BSA-(J) complexes, (B) Average RMSD values for the replicates of BSA-(C) and BSA-(J) complexes at site III (Avg. of reps. stands for the Average of replicates).

The structural stability of the complexes, represented by the purple color in the FEL, indicates the lowest energy minimum state, signifying the stability of the protein-ligand complex. The FEL for BSA-(C) and BSA-(J) at site III, illustrated using 2D and 3D color maps in Figures 41A and 41B, showed global minimal stability during the intervals of 70-80 ns and 81-90 ns for BSA-(C) and BSA-(J), respectively. These intervals were used for binding free energy calculations using the MM-PBSA methods.

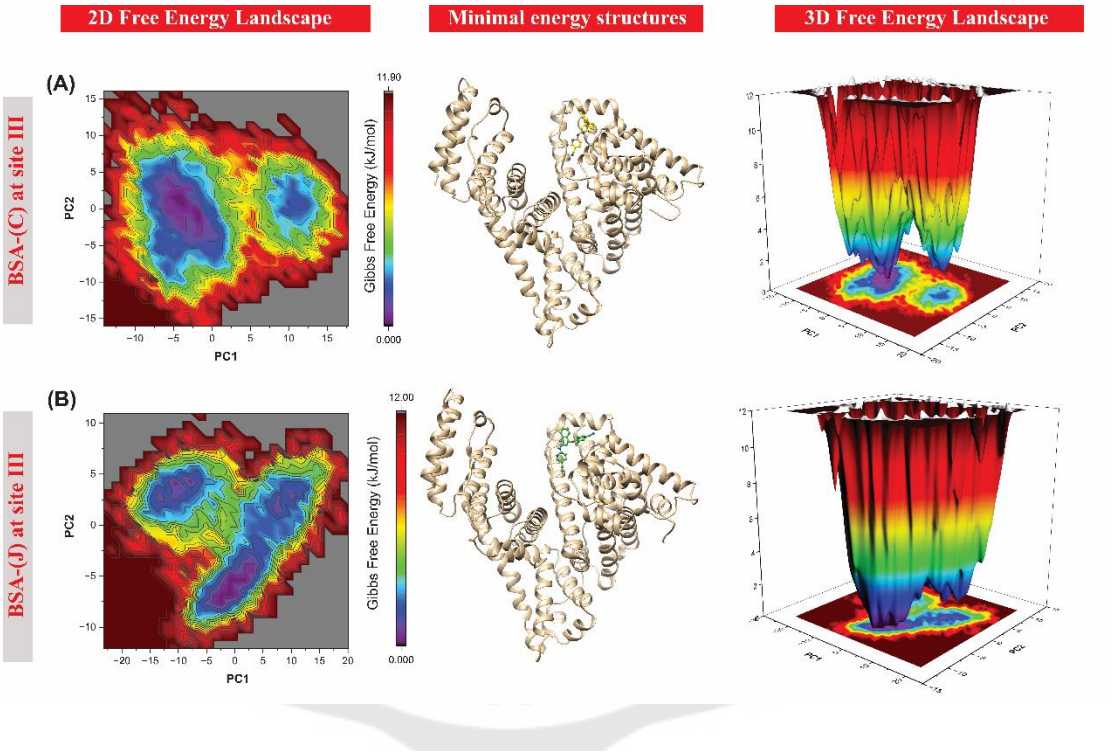

Figure 41 Gibbs free energy landscapes and minimal energy structures for BSA complexes at site III, BSA-(C) complex (A) and BSA-(J) complex (B), illustrated using 2D and 3D color maps during a 100 ns MD simulation.

The binding free energies of compounds (C) and (J) with BSA were calculated using the Molecular Mechanics/ Poisson-Boltzmann Surface Area (MMPBSA) method. This approach evaluates various energy components, including van der Waals forces, electrostatic interactions, solvation energies, and entropy contributions. The binding free

energies of compounds (C) and (J) with BSA were calculated using the Molecular Mechanics/ Poisson-Boltzmann Surface Area (MM-PBSA) method. This approach evaluates various energy components, including van der Waals forces, electrostatic interactions, solvation energies, and entropy contributions. To analyze the binding energies of the BSA-(C) and BSA-(J) complexes, 500 frames from the global energy minimum state were extracted based on MD trajectories, and the MM-PBSA method was utilized for calculation. This approach is commonly employed to compute binding free energy and per-residue free energy decomposition, providing deeper insights into molecular interactions and mechanisms. The individual component free energies for both complexes are summarized in Table 9. According to Table 9, compounds (C) and (J) bound to BSA exhibited binding energies of -34.89 ± 2.64 kcal/mol and -40.44 ± 3.62 kcal/mol, respectively. These binding energies indicated that the BSA-(J) complex was more stable than BSA-(C), consistent with the binding constants (Kb) obtained from fluorescence studies (Table 1). The van der Waals interaction energies for BSA-(C) and BSA-(J) were -42.87 ± 2.62 kcal/mol and -47.38 ± 2.89 kcal/mol, respectively. The contributions of the van der Waals energy were a driving force for the binding interaction, suggesting strong hydrophobic interactions within the complexes. The van der Waals energy component was predominant for both systems, indicating that van der Waals forces were the primary driving force for the interaction between BSA and the newly synthesized compounds. As for the electrostatic interaction energies, the BSA-(C) and BSA-(J) complexes exhibited -3.82 ± 0.95 kcal/mol and -2.82 ± 1.66 kcal/mol, respectively, highlighting the significant role of electrostatic interactions in their binding process. The results revealed strong hydrogen bonds and van der Waals interactions in BSA binding with compounds (C) and (J), aligning with the binding mode data from the thermodynamic parameter analysis.

Table 9 Binding energies and individual component energies from the MMPBSA calculation of BSA-(C) and BSA-(J) complexes.

Energetic terms (kcal/mol)	BSA-(C)	BSA-(J)
ΔE_{vdw}	-42.87 ± 2.62	-47.38 ± 2.89
ΔE_{ele}	-3.82 ± 0.95	-2.82 ± 1.66
ΔE_{MM}	-46.69 ± 2.52	-50.19 ± 3.20
$\Delta G_{polar/PB}$	10.76 ± 1.52	9.72 ± 1.70
$\Delta G_{non-polar/PB}$	-4.20 ± 0.10	-4.58 ± 0.11
$\Delta G_{solv/PB}$	6.56 ± 1.48	5.14 ± 1.66
ΔG_{IE}	5.25 ± 0.21	4.62 ± 1.79
$\Delta G_{binding}$	-34.89 ± 2.64	-40.44 ± 3.62

ΔE_{vdw} represents van der Waals energy, ΔE_{elec} represents electrostatic energy, ΔGpolar/ PB represents the polar solvation free energy obtained from the Poisson-Boltzmann method, $\Delta_{Gnon-polar/PB}$ represents the nonpolar solvation energy obtained from the Poisson-Boltzmann method, ΔG_{IE} represents interaction entropy, and $\Delta G_{Binding}$ represents the binding free energy (kcal/ mol) obtained from the Poisson-Boltzmann method.

Furthermore, the energy decomposition contributions between the new quinoline derivatives and BSA are illustrated in Figure 42. Residues exhibiting energies equal to or greater than 1.0 kcal/mol were subjected to energy decomposition analysis, highlighting their essential role in facilitating the binding of compounds (C) and (J) to site III on BSA. The results suggested that the binding ability of these compounds was primarily driven by hydrophobic and hydrogen bonding interactions. The van der Waals energy component for both systems was higher than other components, indicating that van der Waals forces were the primary driving force for the binding interaction between BSA and the newly synthesized compounds. To gain deeper insights into the interactions of

individual residues for both complexes, MD trajectory data were used to extract structures. These findings revealed strong hydrogen bonds and van der Waals interactions involved in BSA binding with (C) and (J), which corresponded with the binding mode data obtained from the thermodynamic parameters.

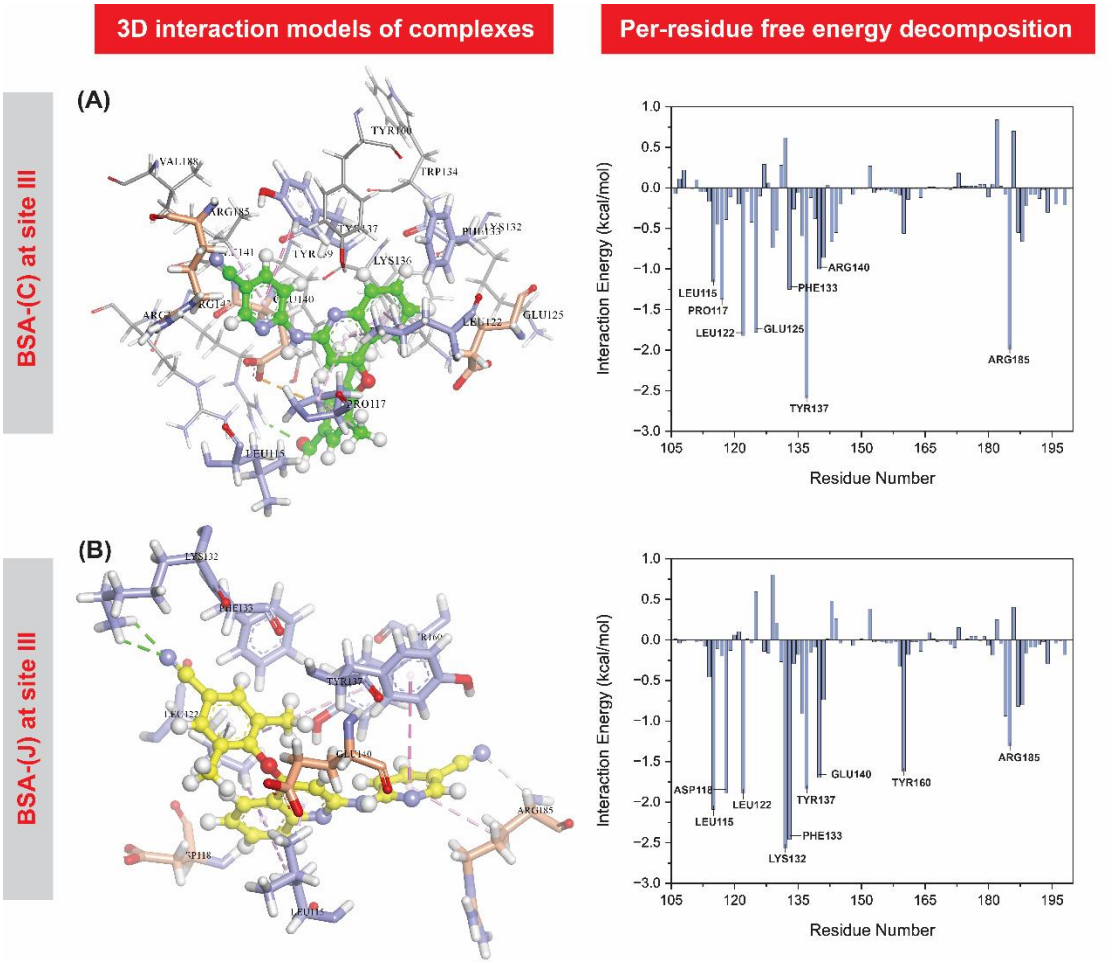

Figure 42 The energy decomposition and interactions at site III on the BSA structure, for both the BSA-(C) complex (A) and BSA-(J) complex (B), show contributions to binding stability. These interactions were extracted from MD simulations at the global minimum state.

CHAPTER 5
CONCLUSIONS

In this study, we employed a combination of spectroscopic techniques and computational methods to investigate the binding interactions of newly synthesized quinoline derivatives, specifically compounds (C) and (J), with BSA and HSA under physiological conditions. The results indicated that both compounds bind to site III (subdomain IB) of BSA and HSA, quenching the fluorescence intensity of both serum albumins through a static quenching mechanism. The binding interactions exhibited binding constants (K_b) of 4.31 x 10^{-4} L/mol for BSA-(C) and 6.31 x 10^{-4} L/mol for BSA-(J), while for HSA, the binding constants were 3.86 x 10^{-4} L/mol for HSA-(C) and 6.17 x 10^{-4} L/mol for HSA-(J). The main interaction forces in the binding process of compounds (C) and (J) with both BSA and HSA were van der Waals forces and hydrogen bonding, indicating a spontaneous binding process. Furthermore, molecular docking and molecular dynamics simulations confirmed that both compounds bind at site III on the structures of BSA and HSA, with the BSA-(J) and HSA-(J) complexes exhibiting greater stability compared to the BSA-(C) and HSA-(C) complexes. MMPBSA calculations provided detailed insights into the binding free energies and per-residue energy contributions, highlighting that van der Waals interactions were the predominant driving force. These computational results were consistent with the experimental binding constants and provided a comprehensive understanding of the molecular interactions at play. Overall, this study enhances our understanding of the binding mechanisms of drug-ligand interactions with serum albumins and could inform the design and development of novel therapeutic agents based on quinoline derivatives in the future.

REFERENCES

Abdullah, S. M. S., Fatma, S., Rabbani, G., & Ashraf, J. M. (2017). A spectroscopic and molecular docking approach on the binding of tinzaparin sodium with human serum albumin. *Journal of Molecular Structure, 1127*, 283-288.

Al-Khafaji, K., & Taskin Tok, T. (2020). Molecular dynamics simulation, free energy landscape and binding free energy computations in exploration the anti-invasive activity of amygdalin against metastasis. *Comput Methods Programs Biomed, 195*, 105660.

Ali, M. S., Muthukumaran, J., Jain, M., Santos-Silva, T., Al-Lohedan, H. A., & Al-Shuail, N. S. (2021). Molecular interactions of cefoperazone with bovine serum albumin: Extensive experimental and computational investigations. *Journal of Molecular Liquids, 337*.

Asahchop, E. L., Wainberg, M. A., Sloan, R. D., & Tremblay, C. L. (2012). Antiviral drug resistance and the need for development of new HIV-1 reverse transcriptase inhibitors. *Antimicrob Agents Chemother, 56*(10), 5000-5008.

Belinskaia, D. A., Voronina, P. A., Shmurak, V. I., Vovk, M. A., Batalova, A. A., Jenkins, R. O., & Goncharov, N. V. (2020). The Universal Soldier: Enzymatic and Non-Enzymatic Antioxidant Functions of Serum Albumin. *Antioxidants (Basel), 9*(10).

Ding, F., & Peng, W. (2016). Biophysical evaluation of protein structural flexibility for ligand biorecognition in solid solution. *Phys Chem Chem Phys, 18*(9), 6595-6606.

Elansary, M. (2012). *Prediction of protein aggregation inducing mutations.* (Master's thesis). Katholieke Universiteit Leuven, Leuven, Belgium.

Evoli, S., Mobley, D. L., Guzzi, R., & Rizzuti, B. (2016). Multiple binding modes of ibuprofen in human serum albumin identified by absolute binding free energy calculations. *Phys Chem Chem Phys, 18*(47), 32358-32368.

Garrett M. Morris, D. S. G., Robert S. Halliday, Ruth Huey, William E. Hart, Richard K. Belew, Arthur J. Olson. (1998). Automated Docking Using a Lamarckian Genetic Algorithm and an Empirical Binding Free Energy Function. *Journal of*

Computational Chemistry, 19(14), 1639-1662.

Ghosh, J., Swarup, V., Saxena, A., Das, S., Hazra, A., Paira, P., . . . Basu, A. (2008). Therapeutic effect of a novel anilidoquinoline derivative, 2-(2-methyl-quinoline-4ylamino)-N-(2-chlorophenyl)-acetamide, in Japanese encephalitis: correlation with in vitro neuroprotection. *Int J Antimicrob Agents, 32*(4), 349-354.

Ghuman, J., Zunszain, P. A., Petitpas, I., Bhattacharya, A. A., Otagiri, M., & Curry, S. (2005). Structural basis of the drug-binding specificity of human serum albumin. *J Mol Biol, 353*(1), 38-52.

Ha, C. E., & Bhagavan, N. V. (2013). Novel insights into the pleiotropic effects of human serum albumin in health and disease. *Biochim Biophys Acta, 1830*(12), 5486-5493.

Huang, B. X., Kim, H. Y., & Dass, C. (2004). Probing three-dimensional structure of bovine serum albumin by chemical cross-linking and mass spectrometry. *J Am Soc Mass Spectrom, 15*(8), 1237-1247.

Khan, M. T., Ali, S., Zeb, M. T., Kaushik, A. C., Malik, S. I., & Wei, D. Q. (2020). Gibbs Free Energy Calculation of Mutation in PncA and RpsA Associated With Pyrazinamide Resistance. *Front Mol Biosci, 7*, 52.

Kooravand, M., Asadpour, S., Haddadi, H., & Farhadian, S. (2021). An insight into the interaction between malachite green oxalate with human serum albumin: Molecular dynamic simulation and spectroscopic approaches. *J Hazard Mater, 407*, 124878.

Lever, G. (2014). *Large Scale Quantum Mechanical*

Enzymology. (Doctoral dissertation). University of Cambridge, Magdalene College, Cambridge, United Kingdom.

Li, W., Fan, Y., Yan, C., Du, Y., Liang, T., Wang, C., . . . Liang, T. (2022). Triptolide and methotrexate binding competitively to bovine serum albumin: A study of spectroscopic experiments, molecular docking, and molecular dynamic simulation. *Journal of Molecular Liquids, 367*.

Liu, Y., Chen, M., Luo, Z., Lin, J., & Song, L. (2013). Investigation on the site-selective binding of bovine serum albumin by erlotinib hydrochloride. *J Biomol Struct Dyn, 31*(10), 1160-1174.

Lobanov, M. Y., Bogatyreva, N. S., & Galzitskaya, O. V. (2008). Radius of gyration as an indicator of protein structure compactness. *Molecular Biology, 42*(4), 623-628.

Lou, Y. Y., Zhou, K. L., Pan, D. Q., Shen, J. L., & Shi, J. H. (2017). Spectroscopic and molecular docking approaches for investigating conformation and binding characteristics of clonazepam with bovine serum albumin (BSA). *J Photochem Photobiol B, 167*, 158-167.

Majorek, K. A., Porebski, P. J., Dayal, A., Zimmerman, M. D., Jablonska, K., Stewart, A. J., . . . Minor, W. (2012). Structural and immunologic characterization of bovine, horse, and rabbit serum albumins. *Mol Immunol, 52*(3-4), 174-182.

Makarasen, A., Kuno, M., Patnin, S., Reukngam, N., Khlaychan, P., Deeyohe, S., . . . Techasakul, S. (2019). Molecular Docking Studies and Synthesis of Amino-oxy-diarylquinoline Derivatives as Potent Non-nucleoside HIV-1 Reverse Transcriptase Inhibitors. *Drug Res (Stuttg), 69*(12), 671-682.

Makarasen, A., Patnin, S., Vijitphan, P., Reukngam, N., Khlaychan, P., Kuno, M., . . . Techasakul, S. (2022). Structural Basis of 2-Phenylamino-4-phenoxyquinoline Derivatives as Potent HIV-1 Non-Nucleoside Reverse Transcriptase Inhibitors. *Molecules, 27*(2).

Miller, B. R., 3rd, McGee, T. D., Jr., Swails, J. M., Homeyer, N., Gohlke, H., & Roitberg, A. E. (2012). MMPBSA.py: An Efficient Program for End-State Free Energy Calculations. *J Chem Theory Comput, 8*(9), 3314-3321.

Mishra, V., & Heath, R. J. (2021). Structural and Biochemical Features of Human Serum Albumin Essential for Eukaryotic Cell Culture. *Int J Mol Sci, 22*(16).

Patnin, S., Makarasen, A., Kuno, M., Deeyohe, S., Techasakul, S., & Chaivisuthangkura, A. (2020). Binding interaction of potent HIV-1 NNRTIs, amino-oxy-diarylquinoline with the transport protein using spectroscopic and molecular docking. *Spectrochim Acta A Mol Biomol Spectrosc, 233*, 118159.

Peter Atkins, J. d. P. (2006). *Atkins' Physical Chemistry* (8th ed.). Oxford: Oxford University Press.

Philip D. Ross, S. S. (1981). Thermodynamics of Protein Association Reactions: Forces

Contributing to Stability. *Biochemistry, 20*(11), 3096-3102.

Phopin, K., Ruankham, W., Prachayasittikul, S., Prachayasittikul, V., & Tantimongcolwat, T. (2019). Insight into the Molecular Interaction of Cloxyquin (5-chloro-8-hydroxyquinoline) with Bovine Serum Albumin: Biophysical Analysis and Computational Simulation. *Int J Mol Sci, 21*(1).

Rabbani, G., & Ahn, S. N. (2019). Structure, enzymatic activities, glycation and therapeutic potential of human serum albumin: A natural cargo. *International Journal of Biological Macromolecules, 123*, 979-990.

Shamsi, A., Ahmed, A., Khan, M. S., Al Shahwan, M., Husain, F. M., & Bano, B. (2020). Understanding the binding between Rosmarinic acid and serum albumin: In vitro and in silico insight. *Journal of Molecular Liquids, 311*.

Tan, J., Zaremska, V., Lim, S., Knoll, W., & Pelosi, P. (2020). Probe-dependence of competitive fluorescent ligand binding assays to odorant-binding proteins. *Anal Bioanal Chem, 412*(3), 547-554.

Tao, H. Y., Wang, R. Q., Sheng, W. J., & Zhen, Y. S. (2021). The development of human serum albumin-based drugs and relevant fusion proteins for cancer therapy. *Int J Biol Macromol, 187*, 24-34.

Van Der Spoel, D., Lindahl, E., Hess, B., Groenhof, G., Mark, A. E., & Berendsen, H. J. (2005). GROMACS: fast, flexible, and free. *J Comput Chem, 26*(16), 1701-1718.

Wang, J., Zhan, P., Li, Z., Liu, H., De Clercq, E., Pannecouque, C., & Liu, X. (2014). Discovery of nitropyridine derivatives as potent HIV-1 non-nucleoside reverse transcriptase inhibitors via a structure-based core refining approach. *Eur J Med Chem, 76*, 531-538.

Wang, Z. M., Ho, J. X., Ruble, J. R., Rose, J., Ruker, F., Ellenburg, M., . . . Carter, D. C. (2013). Structural studies of several clinically important oncology drugs in complex with human serum albumin. *Biochim Biophys Acta, 1830*(12), 5356-5374.

Wani, T. A., Bakheit, A. H., Abounassif, M. A., & Zargar, S. (2018). Study of Interactions of an Anticancer Drug Neratinib With Bovine Serum Albumin: Spectroscopic and Molecular Docking Approach. *Front Chem, 6*, 47.

Wu, X., Liu, J., Wang, Q., Xue, W., Yao, X., Zhang, Y., & Jin, J. (2011). Spectroscopic and molecular modeling evidence of clozapine binding to human serum albumin at subdomain IIA. *Spectrochim Acta A Mol Biomol Spectrosc, 79*(5), 1202-1209.

Yamasaki, K., Chuang, V. T., Maruyama, T., & Otagiri, M. (2013). Albumin-drug interaction and its clinical implication. *Biochim Biophys Acta, 1830*(12), 5435-5443.

Zargar, S., & Wani, T. A. (2021). Protective Role of Quercetin in Carbon Tetrachloride Induced Toxicity in Rat Brain: Biochemical, Spectrophotometric Assays and Computational Approach. *Molecules, 26*(24).

Zeng, Z. S., He, Q. Q., Liang, Y. H., Feng, X. Q., Chen, F. E., De Clercq, E., . . . Pannecouque, C. (2010). Hybrid diarylbenzopyrimidine non-nucleoside reverse transcriptase inhibitors as promising new leads for improved anti-HIV-1 chemotherapy. *Bioorg Med Chem, 18*(14), 5039-5047.

Zhang, X., Lin, Y., Liu, L., & Lin, C. (2015). Study on the synthesis of sulfonamide derivatives and their interaction with bovine serum albumin. *Luminescence, 30*(3), 269-279.

Zhang, Y., Cao, Y., Li, Y., & Zhang, X. (2022). Interactions between Human Serum Albumin and Sulfadimethoxine Determined Using Spectroscopy and Molecular Docking. *Molecules, 27*(5).

Appendix

Spectrochimica Acta Part A: Molecular and Biomolecular Spectroscopy 310 (2024) 123948

Contents lists available at ScienceDirect

Spectrochimica Acta Part A:
Molecular and Biomolecular Spectroscopy

journal homepage: www.journals.elsevier.com/spectrochimica-acta-part-a-molecular-and-biomolecular-spectroscopy

Multiple spectroscopic and computational studies on binding interaction of 2-phenylamino-4-phenoxyquinoline derivatives with bovine serum albumin

Natchaphon Ngueanngam [a], Benchawan Jityuti [a], Suwicha Patnin [b], Pornthip Boonsri [a], Arthit Makarasen [b], Apinya Buranaprapuk [a,*]

[a] Department of Chemistry, Faculty of Science, Srinakharinwirot University, Sukhumvit 23, Bangkok 10110, Thailand
[b] Department of Chemistry, Laboratory of Organic Synthesis, Chulabhorn Research Institute, Laksi, Bangkok 10210, Thailand

HIGHLIGHTS

- New synthesized quinoline derivatives bound to BSA at site III (subdomain IB).
- These compounds quenched BSA fluorescence through static quenching process.
- Strong hydrogen bonds and van der Waals force are involved in binding interactions.
- BSA structure conformation was changed upon interaction with these compounds.
- Ligand-BSA complex has a greater stability compared to free BSA.

GRAPHICAL ABSTRACT

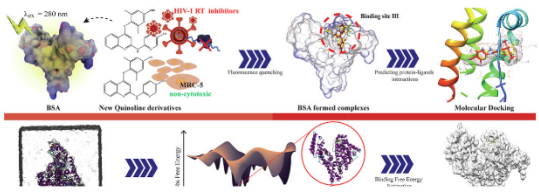

ARTICLE INFO

Keywords:
Molecular dynamics simulation
Quinoline
Bovine serum albumin
Molecular docking

ABSTRACT

Binding characteristics of potent non-nucleoside HIV-1 reverse transcriptase inhibitors, 4-(2′,6′-dimethyl-4′-formylphenoxy)-2-(5″-cyanopyridin-2″ylamino) quinoline **(1)** and 4-(2′,6′-dimethyl-4′-cyanophenoxy)-2-(5″-cyanopyridin-2″ylamino) quinoline **(2)**, to bovine serum albumin (BSA) under simulative physiological conditions were investigated by multiple spectroscopic and computational methods. The experimental results demonstrated that **(1)** and **(2)** bound to BSA at site III (subdomain IB), and quenched BSA fluorescence through a static quenching process. The binding interaction of **(1)** or **(2)** to BSA forms stable complexes with the binding constants (K_b) at the level of 10^4 L/mol and the number of binding site was determined to be 1 for both systems, indicating that new synthesized compounds occupied one site in BSA with moderate binding affinities. Based on the analysis of the thermodynamic parameters, it can be indicated that the main binding forces for interaction between BSA and both compounds were hydrogen bonding and van der Waals force. Synchronous fluorescence results revealed that the interaction of two compounds with BSA led to modifications in the microenvironment surrounding tryptophan residue of BSA. Circular dichroism spectra demonstrated alterations in the secondary structure of BSA induced by **(1)** and **(2)**. Moreover, the experimental data of molecular docking and molecular dynamics (MD) simulations supported the results obtained from multiple spectroscopic techniques, confirming the binding interactions between both compounds and BSA.

* Corresponding author.
E-mail address: apinyac@g.swu.ac.th (A. Buranaprapuk).

https://doi.org/10.1016/j.saa.2024.123948
Received 13 September 2023; Received in revised form 15 January 2024; Accepted 21 January 2024
Available online 23 January 2024

1. Introduction

Serum albumin is the most abundant multifunctional proteins in the circulatory system, and has physiological functions as carriers transporting a variety of endogenous and exogenous compounds in blood [1–4]. Studies on the binding interaction of various compounds such as drugs, dyes and metals, with serum albumin can provide important information about the metabolism, transport and excretion process of these chemical compounds in body [5]. In particular, studies of drug-serum albumin interaction have long been of interest in the pharmaceutical industry because this interaction plays a dominant role in drug pharmacokinetics and pharmacodynamics, and has a strong effect on the absorption, distribution, metabolism and excretion properties of drugs in the blood circulation [6–8]. The information of these interactions can modify a number of properties of drugs, such as enhancing the solubility in plasma, reducing toxicity, increasing drug's *in vivo* half life, and hence, being essential for drug development and discovery [9,10].

Bovine serum albumin (BSA) is most widely studied for the interaction with chemical compounds because of its availability, low cost, stability and high structure homology when compared with human serum albumin (HSA) [11,12]. The structure of BSA is a heart-shaped monomer, composed of three helical domains (I, II and III), and each domain consists of two subdomains (A and B) [9,13,14]. There are three main binding sites of various compounds on BSA structure which are commonly known as sites I, II and III, positioned in subdomains IIA, IIIA and IB, respectively [15,16]. In addition, fatty acid and other ligands bind to serum albumin at seven binding sites, which are located in subdomains IB, IIIA, IIIB and subdomain interfaces [16,17].

Quinoline and its derivatives are important heterocyclic compounds because they exhibit a broad range of pharmacological properties, such as anticancer, antimycobacterial, antimicrobial, anticonvulsant, anti-inflammatory and cardiovascular activities [18,19]. In previous research, derivatives of quinoline have been developed and reported for the inhibition of HIV-1 reverse transcriptase and their cytotoxicity [20]. The synthesized compounds were developed using molecular hybridization of nevirapine (NVP), efavirenz (EFV) and rilpivirine (RPV), to generate novel series of quinoline derivatives. NVP, EFV and RPV are common drugs used as inhibitors against HIV-1 RT. According to the previous results, the substituents of quinoline at 2- and 4-positions play an important role in their inhibitory activity against HIV-1 RT. 4-(2′,6′-dimethyl-4′-formylphenoxy)-2-(5″-cyanopyridin-2″ylamino) quinoline **(1)** and 4-(2′,6′-dimethyl-4′-cyanophenoxy)-2-(5″-cyanopyridin-2″ylamino) quinoline **(2)**, as shown in Fig. 1, exhibited high inhibitory activity against HIV-1 RT with IC_{50} values of 1.93 and 1.22 μM, respectively, which are similar to that of NVP (IC_{50} = 1.05 μM). Additionally, **(2)** had no cytotoxic against normal embryonic lung (MRC-5) cells compared with the common drugs, including EFV and RPV, whereas **(1)** had very low cytotoxicity against normal embryonic lung (MRC-5) cells.

Understanding of the binding processes between quinoline derivatives and serum albumin is essential to determine pharmacokinetics and pharmacodynamics that significantly influence on pharmacological properties of quinoline derivatives. This knowledge is also valuable for design and improvement of potential quinoline derivatives in the future. Therefore, the molecular interactions between quinoline derivatives and serum albumin have been investigated in this research. Multi-spectroscopic methods have been employed to determine the binding interactions and thermodynamic parameters of BSA and new quinoline derivatives, (**1** and **2**) under physiological conditions. Furthermore, their binding location and structural stability have been examined with molecular docking and molecular dynamics (MD) simulations. The results from this study were expected to provide useful information in explaining the physicochemical properties of new quinoline derivatives – albumin binding process *in vivo*.

2. Materials and methods

Bovine serum albumin (BSA) and digitoxin were purchased from Sigma-Aldrich Company (USA). Warfarin and Ibuprofen were purchased from Tokyo Chemical Industry. New synthesized compounds (**1** and **2**) were prepared according to the method in reported literature [20]. All other chemicals were reagent grade and used without further purification. Protein solutions were freshly prepared in 50 mM Tris-HCl buffer (pH 7.0).

2.1. Spectral measurement

The absorption spectra of BSA in the absence and presence of new synthesized compounds were recorded using UV–VIS spectrophotometer (Jasco V-750). The experiments were carried out in 50 mM Tris-HCl buffer pH 7.0 at room temperature. The absorption titrations of BSA with **(1)** or **(2)** were performed by keeping the concentration of BSA constant (5 μM), while changing the concentration of **(1)** or **(2)** (0–50 μM), and the spectral data were recorded in 200–700 nm region. In fluorescence titration experiments, fluorescence emission spectra were recorded by using Jasco FP-8300 spectrofluorometer. The fluorescence measurements were monitored in the range of 290–700 nm upon excitation at 280 nm. The experiments were performed by titrating BSA solution (5 μM) with various concentrations of **(1)** or **(2)** (0–12 μM) at three different temperatures (298, 308 and 318 K). Synchronous fluorescence spectra were also recorded, in the range of 300–400 nm, by using Jasco FP-8300 spectrofluorometer. Circular dichroism (CD) spectra were performed using Jasco J-815CD spectrometer to determine circular dichroism spectra of BSA in the absence and presence of **(1)** or **(2)** at 293 K, under constant nitrogen flush. The BSA concentration was set at 1 μM, and the molar ratio of **(1)** or **(2)** to BSA was varied as 0:1 and 1:1. Spectral measurements were conducted after a 6 min incubation period for all samples, and the CD spectra were recorded in the wavelength range of 200–260 nm.

2.2. Site marker competitive experiments

Site marker competitive experiments were carried out by using warfarin, ibuprofen and digitoxin as the site makers for investigating the possibility of **(1)** and **(2)** binding into site I, site II and site III of BSA structure, respectively [16]. During the spectral measurement, the concentration of BSA and the site markers were all stabilized at 6 μM, and the concentration of **(1)** or **(2)** was varied (0–12 μM). The fluorescence emission spectra were recorded in the range of 290–700 nm upon excitation the reaction mixture at 280 nm.

2.3. Molecular docking studies

The known crystal structure of BSA was taken from the Protein Data Bank (PDB) with the identification code as 4F5S since this structure of BSA contains an analogous amino acid sequence with HSA with the same number of amino acids (583 residues) and high homology of the primary sequence (83.1 %), and the resolution is adequate. All water molecules and heteroatoms were eliminated, and the hydrogen atoms were added at the beginning of docking study. The stable conformations of new compounds were prepared and optimized by using Gaussian 09 package on DFT/B3LYP/6-31G (d, p) level of calculation. Molecular docking using Autodock 4.2 software [21] was applied to evaluate the possible binding interaction of new compounds on BSA structure. For the docking analysis, the size of three-dimensional grid box for calculation was set to 60, 60 and 60 along X, Y and Z axis with 0.375 Å grid spacing. The center of grid for sites I, II and III, was set at (-4.795, 30.487, 101.007), (10.906, 16.276, 119.720) and (19.857, 33.531, 97.915), respectively [22]. The autodocking parameters were used with 150 as population size for the Genetic Algorithm (GA) and 2,500,000 as maximum number of energy evolutions. Biovia Discovery Studio 2020 program was used to

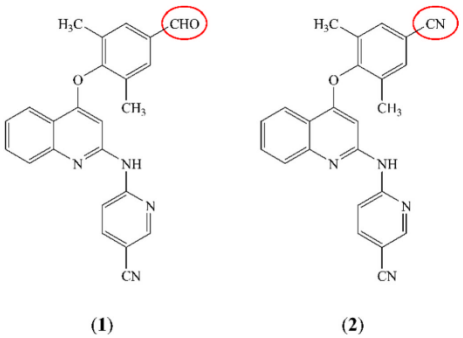

Fig. 1. The structures of 4-(2′,6′-dimethyl-4′-formylphenoxy)-2-(5″-cyanopyridin-2″ylamino) quinoline **(1)**, and 4-(2′,6′-dimethyl-4′-cyanophenoxy)-2-(5″-cyanopyridin-2″ylamino) quinoline **(2)**.

visualize the docked conformation and to analyze the residues involved in the binding process [23].

2.4. Molecular dynamics (MD) simulation

To understand the stability and conformational change, molecular dynamics simulation has been applied to investigate the ligand-binding and protein folding in the surrounding solvent environment. The MD simulation treats every atom in protein, ligand, and solvent to dynamic and flexible [24]. Therefore, three different binding sites (I, II, and III) of BSA bound to each new synthesized compound (**1** and **2**) have been investigated by using MD simulations in comparison to unbound BSA.

All MD simulations were performed under periodic boundary conditions using the GROMACS 2022.3 software package [25]. AMBER99SB [26] and AMBER [27] force fields were used separately for protein and ligands, respectively. The complexes of BSA-**(1)** and BSA-**(2)** were solvated in a cubic box with SPC216 water model [28]. The energy minimization was carried out using steepest descent algorithm (50,000 steps). Subsequently, an equilibration of 1000 ps was performed for the whole system. Finally, production simulation was run for 30 ns at a temperature of 300 K and 1 bar of pressure. The GROMACS and Visual Molecular Dynamics (VMD) [29] programs were exploited for analysis and visualization of the trajectory. Comparative MD analysis was achieved between BSA-**(1)** and BSA-**(2)** complexes in three different binding sites based on root mean square deviation (RMSD), radius of gyration (Rg), and root mean square fluctuation (RMSF). Furthermore, the global minimum structures for BSA-**(1)** and BSA-**(2)** were calculated from Gibbs free energy landscape. Subsequently, the Molecular Mechanics/Poisson-Boltzmann surface area (MM/PBSA) method was taken to compute the binding free energy for BSA-**(1)** and BSA-**(2)** complexes based on gmx_MMPBSA tool [30].

3. Results and discussion

3.1. UV–Vis absorption studies

UV–Vis absorption measurement is a simple method for exploring the binding interaction between BSA and small molecules. The absorption peak of BSA at around 280 nm represented π-π^* transition caused by absorption characteristic of aromatic amino acid residues (Trp, Tyr and Phe). This peak was used for monitoring the interaction between BSA and new synthesized compounds. The absorbance of compounds **(1)** and **(2)** (12 μM) at 280 nm is very low (OD < 0.0415 and 0.0331, respectively), compared to the absorbance of BSA (5 μM) at the same wavelength. Therefore, the absorbance of **(1)** and **(2)** is considered to be significantly less than that of BSA. The inner filter effects should not have a significant effect on the studies.

The absorption spectra of BSA in the presence of various concentrations of **(1)** and **(2)** are shown in Fig. 2A and B, respectively. Upon increasing concentration of **(1)** or **(2)**, the absorbance at 280 nm of BSA was enhanced and no spectral shifts were noted. The significant changes of the absorption peak intensities of BSA in the presence of both compounds were evidence for the formation of BSA-**(1)** and BSA-**(2)** complexes.

3.2. Fluorescence quenching of BSA by new synthesized compounds

In order to elucidate the binding interaction of BSA with **(1)** and **(2)**, the fluorescence spectroscopic technique was also used. The emission spectra of BSA with different concentrations of **(1)** or **(2)** are shown in Fig. 3A and B, respectively. At the excitation wavelength of 280 nm, BSA displayed a strong fluorescence emission peak at 340 nm. The fluorescence spectra of **(1)** or **(2)** alone showed low intensity when excited at 280 nm. Therefore, the fluorescence signal of BSA should not be interfered. The fluorescence intensity of BSA at 340 nm reduced with increasing concentration of **(1)**, and no significant changes in emission peak position were observed. In contrast, when titration of BSA with **(2)**, a small red shift with hypochromism of the fluorescence spectra was observed, and a new small emission peak centered at around 450 nm was detected. The distinction of fluorescence emission changes of BSA after addition of two new synthesized compounds indicated the differences environment surrounding BSA upon binding to each compound. Therefore, the functional group at the 4-position of both compounds has shown an important role on the binding interaction with the protein.

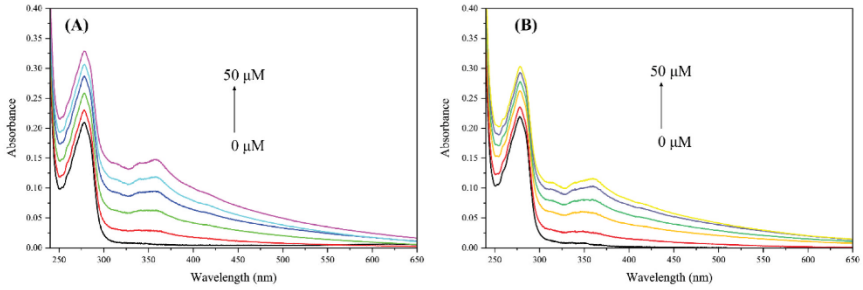

Fig. 2. Absorption spectra of BSA (5 μM) in the presence of various concentrations (0–50 μM) of compound **1** (A) and compound **2** (B).

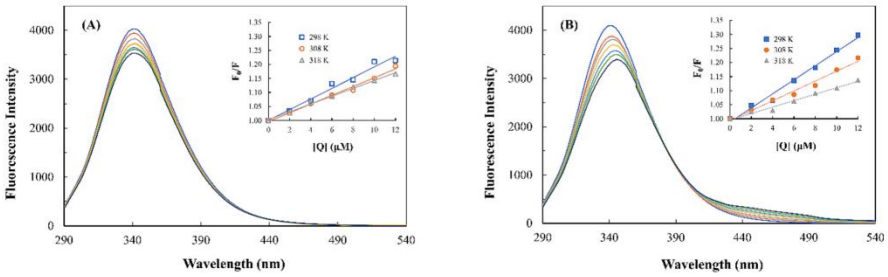

Fig. 3. Fluorescence emission spectra of BSA (5 μM) upon increasing concentration (0–12 μM) of compound **1** (A) and compound **2** (B) at the excitation wavelength of 280 nm. Inset: The Stern-Volmer quenching plots of BSA by **(1)** and **(2)** at different temperatures (298, 308 and 318 K).

Table 1
Quenching constant (K_{sv}), binding constant (K_b) and number of binding site (n) for the interaction of **(1)** and **(2)** with BSA at 298, 308 and 318 K.

Compound	T (K)	K_{sv} ($\times 10^4$ $Lmol^{-1}$)	K_b ($\times 10^4$ $Lmol^{-1}$)	n
(1)	298	2.03 ± 0.13	4.43 ± 0.13	1.07
	308	1.69 ± 0.14	3.61 ± 0.15	1.07
	318	1.55 ± 0.13	1.59 ± 0.13	1.00
(2)	298	2.64 ± 0.13	6.45 ± 0.13	1.09
	308	1.88 ± 0.13	2.87 ± 0.13	1.04
	318	1.30 ± 0.14	1.84 ± 0.14	1.04

The fluorescence quenching mechanism are usually categorized as dynamic quenching (molecular collision) and static quenching (complex formation), which can be differentiated by temperature dependence. For the dynamic quenching, the quenching constant is expected to increase with rising temperature due to the greater diffusion and collision of the fluorophore and quencher. In contrast, for the static quenching, rising temperature reduces the stability of fluorophore-quencher complex, resulting in a lower quenching constant [9,16,31].

The type of fluorescence quenching mechanism was determined by analyzing the fluorescence intensity data using the Stern-Volmer equation (Eq. (1)) [5,11,32].

$$F_0/F = 1 + K_{SV}[Q] \quad (1)$$

Where F_0 and F are the fluorescence intensities of BSA in the absence and presence of the quencher (**1** or **2**), respectively. K_{sv} is the Stern-Volmer quenching constant, which demonstrates the fluorescence quenching efficiency upon addition of **(1)** or **(2)**, and [Q] is the quencher concentration. The Stern-Volmer plot of F_0/F as a function of quencher concentration can be constructed to determine the K_{sv} from the slope of the plot. Fig. 3 (inset) shows Stern-Volmer quenching plot of BSA with **(1)** (Fig. 3A) and **(2)** (Fig. 3B) at three different temperatures. The K_{sv} values obtained from these data were determined and listed in Table 1. The results showed that the values of K_{sv} decreased with increase of temperature, which indicated that the fluorescence quenching mechanism between BSA and both compounds could be static quenching.

3.3. Determination of binding constants and the number of binding sites

To estimate the binding affinity between new synthesized compounds and BSA, the binding constant (K_b) and the number of binding site (n) can be calculated according to the Eq (2) [5,32,33].

$$\log\frac{F_0 - F}{F} = \log K_b + n\log[Q] \quad (2)$$

where n is the number of binding site per one molecule of BSA and K_b is the binding constant for the interaction of BSA with **(1)** or **(2)**. According to equation (2), the values of n and K_b (shown in Table 1) can be determined from the intercept and the slope of the double logarithm regression curve of log (F_0-F)/F versus log [Q], respectively, and the plots are shown in Fig. 4. The results illustrated that the binding interaction between BSA and both compounds was moderate with the number of binding site approximately 1, indicating that there was one binding site in BSA for both new synthesized compounds. Since the number of binding sites is 1. Therefore, the concentration ratio between BSA and **(1)** or **(2)** was kept to 1:1 ratio for the studies. This concentration was chosen due to the solubility of the compounds and also the absorbance/fluorescence intensity of BSA.

3.4. Circular dichroism (CD) studies

Circular dichroism (CD) spectroscopy is commonly used to investigate the conformational changes of protein upon binding with ligands.

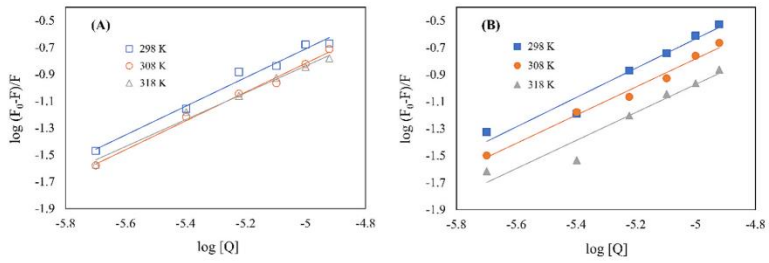

Fig. 4. The plots of log (F_0-F)/F versus log [Q] from the interaction of compound **1** (A) and compodund **2** (B) with BSA at 298, 308 and 318 K.

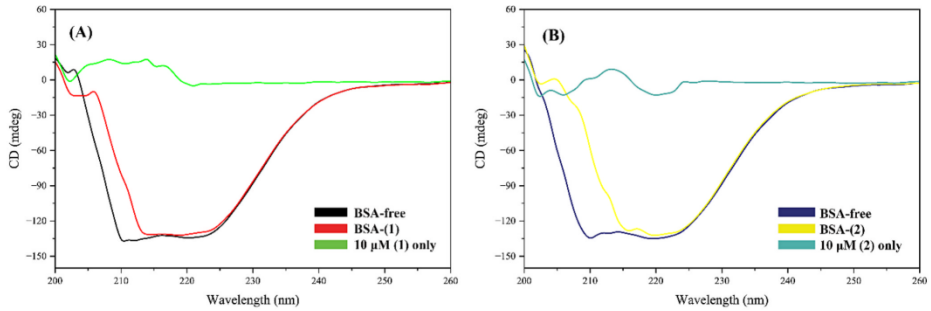

Fig. 5. The CD spectra of BSA in the absence and in the presence of **(1)** or **(2)**.

Table 2
Thermodynamic parameters for the interaction of BSA with **(1)** and **(2)** at different temperatures.

Temperature (K)	ΔH (kJ mol^{-1})		ΔS (kJ mol^{-1})		ΔG (kJ mol^{-1})	
	(1)	**(2)**	**(1)**	**(2)**	**(1)**	**(2)**
298	−42.65	−52.08	−53.48	−83.29	−26.43	−27.38
308					−26.78	−26.18
318					−25.32	−25.74

To understand the effects of new synthesized compounds on the secondary structure of BSA, CD spectral measurement of BSA in the absence and presence of **(1)** or **(2)** was performed, and the results are shown in Fig. 5.

As shown in Fig. 5, the CD spectra of free BSA revealed two distinctive negative bands at 208 and 222 nm (Fig. 5A black line and Fig. 5B blue line), which are the indicative of the typical α-helix structure in protein [34]. Upon addition of compound **(1)** or **(2)** to the BSA solution, the intensity of negative absorption band was decreased (Fig. 5A red line and Fig. 5B yellow line, respectively), suggesting that the binding process led to modifications in the secondary structure of BSA. Compounds **(1)** and **(2)** did not exhibit CD spectra (green lines).

3.5. Determination of thermodynamic parameters and binding mode

In order to investigate the nature of binding force between new synthesized compounds and BSA, thermodynamic parameters, including the Gibb free energy (ΔG), enthalpy changes (ΔH) and entropy changes (ΔS), were calculated by using Eqs. (3) and (4) [16,35].

$$\ln K_b = -\frac{\Delta H}{RT} + \frac{\Delta S}{R} \quad (3)$$

$$\Delta G = -RT\ln K_b = \Delta H - T\Delta S \quad (4)$$

where K_b is the binding constant and R is the gas constant. The values of ΔH and ΔS for the binding reaction are important information to elucidate the main binding force, which consists of 4 types: electrostatic interaction (ΔH < 0 and ΔS > 0), hydrophobic interaction (ΔH > 0 and ΔS > 0), van der Waals force (ΔH < 0 and ΔS < 0), and hydrogen bond (ΔH < 0 and ΔS < 0). According to the equation (3), the values of ΔH and ΔS of BSA-**(1)** and BSA-**(2)** were estimated from the slope and intercept of the plot of ln K_b versus 1/T, respectively. As shown in Table 2, the values of ΔH and ΔS of BSA-**(1)** and BSA-**(2)** were negative, indicating that hydrogen bond and van der Waals force play a major role in the binding process of **(1)** and **(2)** to BSA. Additionally, the negative values of ΔG at different temperatures supported that the binding interaction of both compounds to BSA was spontaneous process.

3.6. Identification of the binding site

BSA consists of three main binding sites (sites I, II and III) which are located on the structure of BSA in subdomain IIA, IIIA and IB, respectively. Warfarin, ibuprofen and digitoxin are well-known site markers for binding to BSA at site I, site II and site III, respectively [16]. Therefore, to investigate the binding location of **(1)** and **(2)** on BSA structure, the competitive experiments were performed by using warfarin, ibuprofen and digitoxin as site probes. During the competitive experiment, **(1)** or **(2)** was gradually added to the mixture solution of BSA and each marker. The binding constants of BSA-site marker system in the absence and presence of **(1)** or **(2)** were determined by analyzing the fluorescence intensity using Eq. (2). The results are shown in Table 3.

From the data in Table 3, the binding constants of BSA with **(1)** and **(2)** dramatically changed upon addition of digitoxin from 2.76 ± 0.12, 2.84 ± 0.14 to 1.78 ± 0.13, 1.65 ± 0.13, respectively. In contrast, in the presence of warfarin and ibuprofen, the binding constants were not significantly altered. These results suggested that the binding location of **(1)** and **(2)** on BSA was positioned at site III, in subdomains IB.

3.7. Synchronous fluorescence studies

The exploration of microenvironmental changes around fluorescent amino acid residues of the protein upon interaction with small molecules was conducted using synchronous fluorescence spectroscopy [34,36]. Synchronous fluorescence spectra provide spectral information of tyrosine (Tyr) and tryptophan (Trp) residues when wavelength intervals (Δλ) between emission and excitation are fixed at 15 nm and 60 nm,

Table 3
Binding constants of BSA-**(1)** and BSA-**(2)** in the absence and presence of site markers.

System	Without the site marker		Site I marker (Warfarin)		Site II marker (Ibuprofen)		Site III marker (Digitoxin)	
	log K_b	R^2	log K_b	R^2	log K_b	R^2	log K_b	R^2
BSA – (1)	2.76 ± 0.12	0.9880	2.64 ± 0.13	0.9809	2.87 ± 0.13	0.9806	1.78 ± 0.13	0.9779
BSA – (2)	2.84 ± 0.14	0.9836	2.61 ± 0.14	0.9868	2.64 ± 0.13	0.9817	1.65 ± 0.13	0.9881

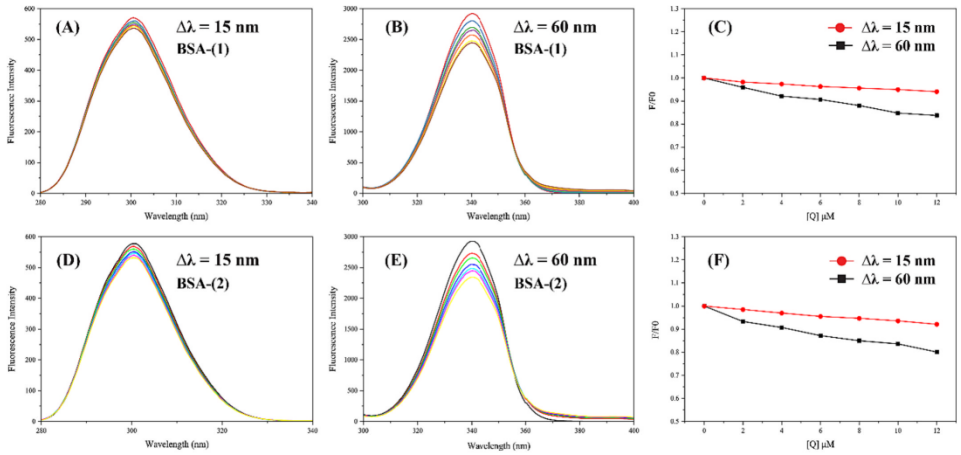

Fig. 6. The synchronous fluorescence spectra of BSA with and without **(1)** or **(2)** at different Δλ values of 15 nm ((A) and (D)) and 60 nm ((B) and (E)), and the effects of **(1)** or **(2)** on the synchronous fluorescence spectra of BSA-**(1)** (C) and BSA-**(2)** (F).

Table 4
Binding information of BSA-**(1)** and BSA-**(2)** from molecular docking studies.

System	Binding site on BSA	Binding energy (kcal/mol)	Surrounding amino acid within 5 Å	
			H-bond	π-π stacking
BSA – (1)	Site I	−7.97	Arg194, Arg256	His287
	Site II	−7.67	Arg409, Arg484	–
	Site III	−10.48	Lys116, Tyr137	Phe133, Tyr160
BSA – (2)	Site I	−8.15	Arg198, Arg217	Trp213
	Site II	−7.74	Arg409, Lys413	–
	Site III	−10.53	Tyr137	Tyr160

respectively [37,38]. The influence of **(1)** and **(2)** on synchronous fluorescence spectra of BSA is presented in Fig. 6C and 6F, respectively. A slightly blue shift in maximum emission peak of tryptophan residue (Δλ = 60 nm) was observed upon addition of **(1)** or **(2)** as shown in Fig. 6B and E, respectively, and almost no spectral shift was seen in the emission peak of tyrosine residue (Δλ = 15 nm) (Fig. 6A and D, respectively), suggesting that the two compounds had more effect on tryptophan residue compared to tyrosine residue. Moreover, the results also demonstrated that the presence of **(1)** or **(2)** induced a conformational change in BSA, and the microenvironments surrounding tryptophan residue demonstrated an increase in the hydrophobicity.

3.8. Molecular docking studies

In order to support the results from competitive experiment, molecular docking technique was applied to examine the binding interaction between new synthesized compounds and BSA. This docking method helps in predicting the binding location and binding affinity of **(1)** and **(2)** inside the BSA structure. **(1)** and **(2)** were docked to BSA (PDB ID: 4F5S) using Autodock program (version 4.2). The docking results with minimum binding free energy are presented in Table 4. Docking studies showed that the estimated binding free energy of both compounds within subdomain IB (site III) of BSA was lower than that in subdomain IIA (site I) and subdomain IIIA (site II). These indicated that **(1)** and **(2)** bound to BSA at site III in subdomain IB (Figs. 7A and 8A, respectively), which corresponded to the experimental data obtained from the competitive experiment.

As shown in Fig. 7B, the location of **(1)** in subdomain IB (site III) of BSA within 5 Å was surrounded by Lys114, Leu115, Lys116, Pro117, Asp118, Thr121, Leu122, Glu125, Phe133, Lys136, Tyr137, Glu140, Ile141, Tyr160, Ile181, Met184, Arg185 and Val188. The hydrogen bonding interactions were observed between the aldehyde group in **(1)** and the nitrogen atom on Lys116 residue, and also between the cyanide group in **(1)** and the oxygen atom on Tyr137 residue in BSA. In case of **(2)**, the amino acid residues of BSA encircling **(2)** within 5 Å consisted of Leu115, Lys116, Pro117, Asp118, Leu122, Glu125, Phe126, Asp129, Lys132, Phe133, Lys136, Tyr137, Glu140, Ile141, Tyr160, Ile181, Met184, Arg185 and Val188 (Fig. 6B). The cyanide group of **(2)** formed hydrogen bonds with the oxygen atom on Tyr137 residue in BSA structure. These results suggested that the binding mode of new synthesized compounds to BSA was dominated by hydrogen bonding interactions, which are the agreement to the results from thermodynamic parameter analysis. In addition, **(1)** demonstrated π-π stacking interactions with residues Phe133 and Tyr160 in site III of BSA, and **(2)** also bound to the same domain via π-π stacking interaction with Tyr160. The π-π stacking interaction is consistent with results obtained from UV–Vis absorption studies in which the absorption intensities of BSA enhanced with increasing concentration of **(1)** and **(2)**.

Comparisons of the binding energies at site III for BSA-**(1)** and BSA-**(2)** systems, BSA bound to **(2)** with lower binding energy than bound to **(1)**. These results indicated that BSA-**(2)** was more stable than BSA-**(1)**, which agreed well with the results obtained from thermodynamic studies. The cause for the greater stability of BSA-**(2)** system was further studied in molecular dynamics simulation.

3.9. Molecular dynamics (MD) simulation

The structural stability of BSA-**(1)** and BSA-**(2)** complexes in three different binding sites (site I, site II and site III) were evaluated under simulated physiological conditions by MD simulations. The dynamic properties were investigated based on several parameters such as root

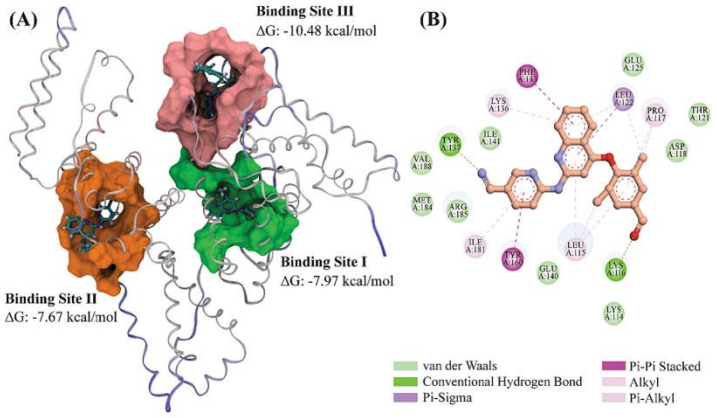

Fig. 7. The docking conformation of **(1)** in BSA (A). Two-dimensional diagram of **(1)** upon binding to BSA in the subdomain IB (B). The dotted green line displays the hydrogen bonding between BSA and **(1)**.

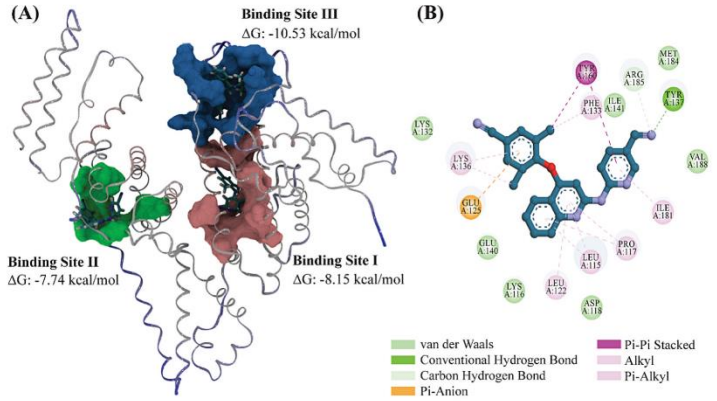

Fig. 8. The docking conformation of **(2)** in BSA (A). Two-dimensional diagrams of **(2)** upon binding to BSA in the subdomain IB (B). The dotted green line displays the hydrogen bonding between BSA and **(2)**.

mean square deviations (RMSD), root mean square fluctuation (RMSF) and radius of gyration (Rg).

RMSD is one of the parameters used to measure the stability of the protein in the presence of ligand as a function of time. The RMSD calculations of BSA-**(1)** and BSA-**(2)** complexes at three different binding sites are presented in Fig. 9C and 9D, respectively. The presence of **(1)** or **(2)** affected the structural stability of BSA at all sites. Interestingly, the binding site III of the bound BSA-**(1)** and BSA-**(2)** slightly fluctuated, compared to BSA-free, indicating that the two simulated systems had reached an equilibrium state. The binding interactions of BSA-**(1)** and BSA-**(2)** complexes at site III are the most stable in comparison to sites I and II, supporting the results from the competitive experiment, and docking study. When comparing the fluctuations of both complexes at three different binding sites, **(2)** exhibited the greatest structural stability when bound to BSA at site III.

The RMSF calculation provides information about the fluctuation of amino acid residues in the BSA structure during the simulation process. The observed higher RMSF fluctuations indicated greater structural flexibility, implying relative instability of the complex [39,40]. The fluctuations of RMSF plots for BSA-free, BSA-**(1)** and BSA-**(2)** at three different binding sites are illustrated in Fig. 9E and 9F, respectively. The results showed that the amino acids located at site III have lower fluctuation than unbound form, which indicated that BSA was found to form a stable complex with **(1)** and **(2)**. Therefore, both compounds showed the most structural stability upon binding to BSA structure at site III.

Furthermore, Rg is another parameter used to analyze the binding stability and equilibrium of the protein–ligand complex to indicate the fluctuated protein backbone in the simulated system [24,41]. Fig. 9G and 9H show the Rg plots of BSA-**(1)** and BSA-**(2)** complexes at all three bindings sites in comparison to the unbound BSA. The fluctuation of Rg could be reduced for BSA-**(1)** and BSA-**(2)** complexes at site III when compared to the free form. The results suggested that the

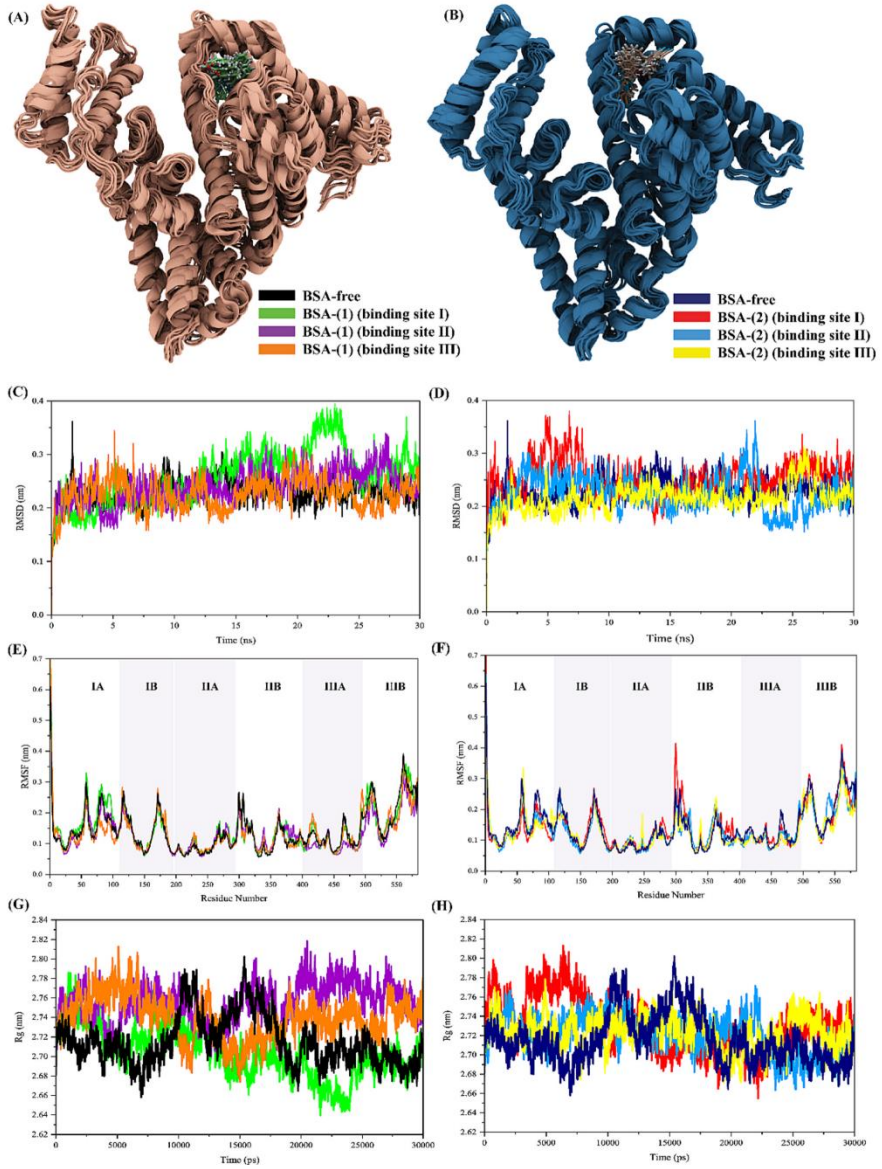

Fig. 9. Superimposed structure of BSA from MD simulations of BSA-**(1)** (A) and BSA-**(2)** (B). MD simulation plots of BSA-**(1)** in three different binding sites based on RMSD (C), RMSF (E), and R_g (G). MD simulation plots of BSA-**(2)** in three different binding sites based on RMSD (D), RMSF (F), and R_g (H).

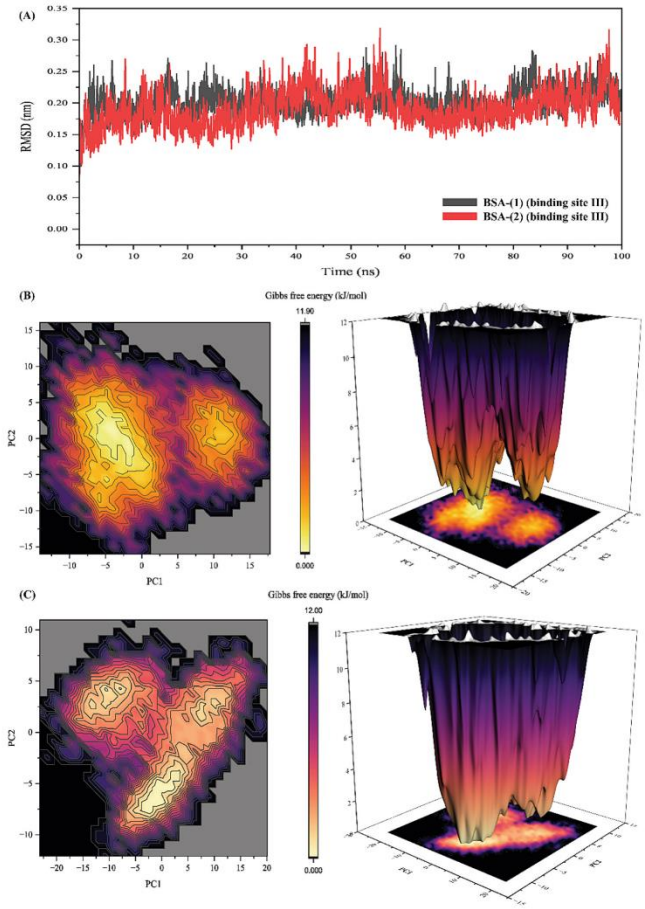

Fig. 10. The RMSD plot of BSA-**(1)** and BSA-**(2)** at site III in the period of 100 ns (A). 2D and 3D the Gibbs free energy landscape of BSA-**(1)** (B) and BSA-**(2)** (C) complexes at site III.

conformational change led to the stability of the complex. This increased stability is notably reflected in the backbone-RMSD plot, portraying a structural adjustment due to the presence of the ligand, rendering a greater stability compared to the BSA-free state.

In order to confirm the structural stability of both complexes at site III along with simulation times, we therefore extended the MD simulations to 100 ns. The Gibbs free energy landscape (FEL) indicated the global minimum of protein–ligand complex states space concerning energy function and time [42]. The obtained FEL for BSA-**(1)** and BSA-**(2)** at site III was demonstrated by using 2D and 3D color maps, as shown in Fig. 10B and 10C, respectively. In Fig. 10B, the color map illustrated the global energy minimum region of BSA-**(1)** complex, where a bright yellow shade indicated the lowest energy state. Similarly, BSA-**(2)** complex (Fig. 10C) exhibited a light beige contour map representing the global energy minimum state, signifying the stability state of the complex. Additionally, these results indicated the global minimal regions which have been observed in the periods of 70–80 and 81–90 ns for BSA-**(1)** and BSA-**(2)** complexes, respectively. Therefore, these time intervals were used to calculate the binding free energy of both complexes using the MM-PBSA approach.

3.10. Binding free energy calculations

To investigate the binding energies of BSA-**(1)** and BSA-**(2)** complexes, extracted from 500 frames of the global energy minimum state based on the MD trajectories, the MM-PBSA method was used for calculation. This method has been widely employed to calculate the binding free energy and per-residue free energy decomposition for understanding of the deeper insight into the molecular interactions and mechanism [24,42,43]. The estimation of individual component free

Table 5
Binding energies and individual component energy values obtained from the MM-PBSA calculation of BSA-**(1)** and BSA-**(2)** complexes.

Energetic terms (kcal/mol)	BSA-(1)	BSA-(2)
ΔE_{vdw}	−42.87 ± 2.62	−47.38 ± 2.89
ΔE_{ele}	−3.82 ± 0.95	−2.82 ± 1.66
ΔE_{MM}	−46.69 ± 2.52	−50.19 ± 3.20
ΔG_{PB}	10.76 ± 1.52	9.72 ± 1.70
$\Delta G_{non\text{-}polar}$	−4.20 ± 0.10	−4.58 ± 0.11
$\Delta G_{solv/PB}$	6.56 ± 1.48	5.14 ± 1.66
ΔG_{IE}	5.25 ± 0.21	4.62 ± 1.79
ΔG_{bind}	−34.89 ± 2.64	−40.44 ± 3.62

energies for both complexes was summarized in Table 5.

From the data in Table 5, **(1)** and **(2)** were bound to BSA with binding energy of −34.89 ± 2.64 kcal/mol and −40.44 ± 3.62 kcal/mol, respectively. The calculated binding energies of these complexes demonstrated that the binding interaction of BSA-**(2)** was more stable than BSA-**(1)**, which was correlated to the binding constant (K_b) obtained from the fluorescence study (Table 1). The consistency between experimental and computational outcomes highlights the reliability of molecular modeling in confirming experimental observations and predicting variations in binding affinity, as well as providing insights into the conformational changes within the complexes. The van der Waals interaction energies of BSA-**(1)** and BSA-**(2)** are observed to be −42.87 ± 2.62 kcal/mol and −47.38 ± 2.89 kcal/mol, respectively. The contribution of van der Waals energy component for two systems was higher than the other components, which explained that van der Waals force was a driving force for the binding interaction between BSA and new synthesized compounds which clearly explained in Fig. 11. In order to investigate deeper insights into the interactions of individual residues for both complexes, the MD trajectory was used to extract structures. These results revealed strong hydrogen bonds and van der Waals interactions involved in BSA binding with **(1)** and **(2)**, and this corresponded to the binding mode data obtained from the thermodynamic parameter, as illustrated in Fig. 12.

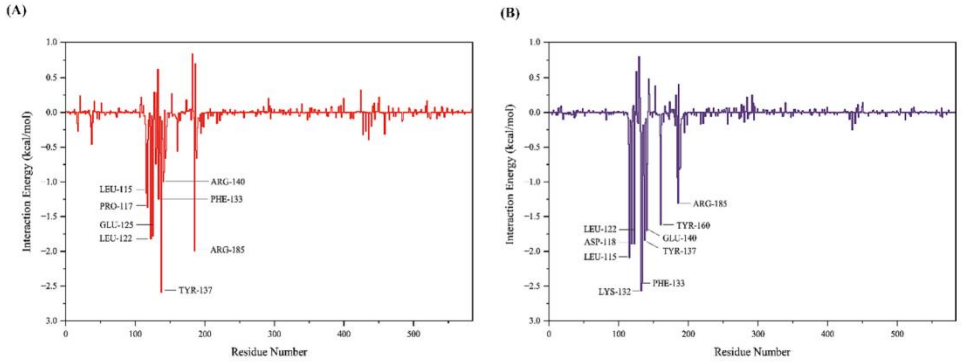

Fig. 11. The per-residues decomposition of binding energy showed the contributions to the binding and stability of the binding site III on the BSA complex, shown in (A) BSA-**(1)** and (B) BSA-**(2)**.

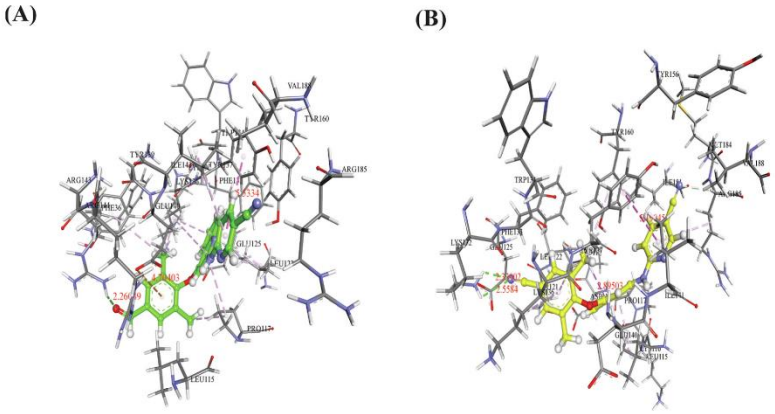

Fig. 12. The interactions extracted from MD simulations, covering periods of 73 ns and 82 ns for (A) BSA-**(1)** and (B) BSA-**(2)** complexes. The figure illustrates the interactions through lines and distances, highlighting both hydrogen bonding and hydrophobic interactions.

4. Conclusions

In this study, multiple spectroscopic and computational methods were employed to estimate the binding interaction of BSA with new synthesized compounds (**1** and **2**) under physiological conditions. The experimental results obtained from this study suggested that **(1)** and **(2)** bound to BSA at site III (subdomain IB), and quenched BSA fluorescence intensity through a static quenching process. The binding interactions of BSA-**(1)** and BSA-**(2)** systems were moderate with one binding site, based on the binding constant values of 4.43 x 10^4 and 6.45 x 10^4 $Lmol^{-1}$, respectively. The main interaction forces in the binding process of BSA with both compounds were van der Waals force and hydrogen bonding, and the conformation of BSA structure was changed upon interaction with **(1)** and **(2)**. Additionally, molecular docking and molecular dynamics simulation demonstrated that the binding of BSA-**(2)** was more stable than BSA-**(1)**. This study will be helpful for elucidation of binding mechanisms of drug-ligand interaction and novel probe design for development of therapeutic agents in the future.

CRediT authorship contribution statement

Natchaphon Ngueanngam: Methodology, Investigation, Data curation. **Benchawan Jityuti:** Writing – review & editing, Writing – original draft, Data curation. **Suwicha Patnin:** Resources. **Pornthip Boonsri:** Writing – original draft, Formal analysis. **Arthit Makarasen:** Resources. **Apinya Buranaprapuk:** Writing – review & editing, Writing – original draft, Supervision.

Declaration of competing interest

The authors declare that they have no known competing financial interests or personal relationships that could have appeared to influence the work reported in this paper.

Data availability

No data was used for the research described in the article.

Acknowledgements

Financial support from the Fundamental Fund (FF) (Grant No. 035/2566) and facilities from Faculty of Science, Srinakharinwirot University are gratefully acknowledged. Thailand Science Research and Innovation (TSRI) and Chulabhorn Research Institute for financial support (Grant No. 48295/4691986) during this study.

References

[1] Y. Zhang, S. Shi, X. Chen, W. Zhang, K. Huang, M. Peng, Investigation on the interaction between ilaprazole and bovine serum albumin without or with different C-ring flavonoids from the viewpoint of food-drug interference, J. Agric. Food Chem. 59 (2011) 8499–8506, https://doi.org/10.1021/jf201796x.

[2] X. Li, S. Wang, Binding of glutathione and melatonin to human serum albumin: a comparative study, Colloids Surf. B Biointerfaces. 125 (2015) 96–103, https://doi.org/10.1016/j.colsurfb.2014.11.023.

[3] J. Lazniewska, M. Agostino, S.M. Hickey, E. Parkinson-Lawrence, S. Stagni, M. Massi, D.A. Brooks, S.E. Plush, Spectroscopic and molecular docking study of the interaction between neutral Re(I) tetrazolate complexes and bovine serum albumin, Chem. Eur. J. 27 (2021) 11406–11417, https://doi.org/10.1002/chem.202101307.

[4] S. Anitha, V. Saranya, R. Shankar, V. Sasirekha, Structural exploration of interactions of (+) catechin and (-) epicatechin with bovine serum albumin: insights from molecular dynamics and spectroscopic methods, J. Mol. Liq. 348 (2022) 118026, https://doi.org/10.1016/j.molliq.2021.118026.

[5] Y. Sohrabi, V. Panahi-Azar, A. Barzegar, J.E.N. Dolatabadi, P. Dehghan, Spectroscopic, thermodynamic and molecular docking studies of bovine serum albumin interaction with ascorbyl palmitate food additive, BioImpacts. 7 (2017) 241-246. 10.15171/bi.2017.28.

[6] F. Dangkoob, M.R. Housaindokht, A. Asoodeh, O. Rajabi, Z.R. Zaeri, A.V. Doghaei, Spectroscopic and molecular modeling study on the separate and simultaneous bindings of alprazolam and fluoxetine hydrochloride to human serum albumin (HSA): With the aim of the drug interactions probing, Spectrochim. Acta A Mol. Biomol. Spectrosc. 137 (2015) 1106–1119, https://doi.org/10.1016/j.saa.2014.08.149.

[7] Z. Omidvar, A. Asoodeh, J. Chamani, Studies on the antagonistic behavior between cyclophosphamide hydrochloride and aspirin with human serum albumin: time-resolved fluorescence spectroscopy and isothermal titration calorimetry, J Solution Chem. 42 (2013) 1005–1017, https://doi.org/10.1007/s10953-013-0009-7.

[8] R.J. Zhang, S.B. Kou, L. Hu, L. Li, J.H. Shi, S.L. Jiang, Exploring binding interaction of baricitinib with bovine serum albumin (BSA): multi-spectroscopic approaches combined with theoretical calculation, J. Mol. Liq. 354 (2022) 118831, https://doi.org/10.1016/j.molliq.2022.118831.

[9] Y. Liu, M. Chen, Z. Luo, J. Lin, L. Song, Investigation on the site-selective binding of bovine serum albumin by erlotinib hydrochloride, J. Biomol. Struct. Dyn. 31 (2013) 1160–1174, https://doi.org/10.1080/07391102.2012.726532.

[10] B.C. Swain, S.K. Mukherjee, J. Rout, P.P. Sakshi, M. Mishra, U.T. Mukherjee, A spectroscopic and computational intervention of interaction of lysozyme with 6-mercaptopurine, Anal. Bioanal. Chem. 412 (2020) 2565–2577, https://doi.org/10.1007/s00216-020-02483-1.

[11] T. Xu, X. Guo, L. Zhang, F. Pan, J. Lv, Y. Zhang, H. Jin, Multiple spectroscopic studies on the interaction between olaquindox, a feed additive, and bovine serum albumin, Food Chem. Toxicol. 50 (2012) 2540–2546, https://doi.org/10.1016/j.fct.2012.04.007.

[12] M.A. Abdelaziz, M. Shaldam, R.A. El-Domany, F. Belal, Multi-spectroscopic, thermodynamic and molecular dynamic simulation studies for investigation of interaction of dapagliflozin with bovine serum albumin, Spectrochim. Acta A Mol. Biomol. Spectrosc. 264 (2022) 120298, https://doi.org/10.1016/j.saa.2021.120298.

[13] S. Dhar, D.K. Rana, A. Pal, S.C. Bhattacharya, Photobehavior and docking simulations of drug within macromolecules: binding of an antioxidative isoquinolindione to a serine protease and albumin proteins, J. Photochem. Photobiol. B. 129 (2013) 69–77, https://doi.org/10.1016/j.jphotobiol.2013.09.007.

[14] A. Jahanban-Esfahlan, A. Ostadrahimi, R. Jahanban-Esfahlan, L. Roufegarinejad, M. Tabibiazar, R. Amarowicz, Recent developments in the detection of bovine serum albumin, Int. J. Biol. Macromol. 138 (2019) 602–617, https://doi.org/10.1016/j.ijbiomac.2019.07.096.

[15] W. Li, Y. Fan, C. Yan, Y. Du, T. Liang, C. Wang, L. Wang, L. Han, Q. Li, T. Liang, Triptolide and methotrexate binding competitively to bovine serum albumin: a study of spectroscopic experiments, molecular docking, and molecular dynamic simulation, J. Mol. Liq. 367 (2022) 120300, https://doi.org/10.1016/j.molliq.2022.120300.

[16] K. Phopin, W. Ruankham, S. Prachayasittikul, V. Prachayasittikul, T. Tantimongcolwat, Insight into the molecular interaction of cloxyquin (5-chloro-8-hydroxyquinoline) with bovine serum albumin: biophysical analysis and computational simulation, Int. J. Mol. Sci. 21 (2020) 249, https://doi.org/10.3390/ijms21010249.

[17] D. Agudelo, P. Bourassa, J. Bruneau, G. Bérubé, É. Asselin, H.A. Tajmir-Riahi, Probing the binding sites of antibiotic drugs doxorubicin and N-(trifluoroacetyl) doxorubicin with human and bovine serum albumins, PLoS ONE. 7 (2012) e43814.

[18] A. Makarasen, M. Kuno, S. Patnin, N. Reukngam, P. Khlaychan, S. Deeyohe, P. Intachote, B. Saimanee, S. Sengsai, P. Boonsri, A. Chaivisuthangkura, W. Sirithana, S. Techasakul, Molecular docking studies and synthesis of amino-oxydiarylquinoline derivatives as potent non-nucleoside HIV-1 reverse transcriptase inhibitors, Drug Res. 69 (2019) 671–682, https://doi.org/10.1055/a-0968-1150.

[19] S. Paul, P. Roy, P.S. Sardar, A. Majhi, Design, synthesis, and biophysical studies of novel 1,2,3-triazole-based quinoline and coumarin compounds, ACS Omega. 4 (2019) 7213–7230, https://doi.org/10.1021/acsomega.9b00414.

[20] A. Makarasen, S. Patnin, P. Vijitphan, N. Reukngam, P. Khlaychan, M. Kuno, P. Intachote, B. Saimanee, S. Sengsai, S. Techasakul, Structural basis of 2-Phenyl-amino-4-Phenoxyquinoline derivatives as potent HIV-1 non-nucleoside reverse transcriptase inhibitors, Molecules. 27 (2022) 461, https://doi.org/10.3390/molecules27020461.

[21] G.M. Morris, R. Huey, W. Lindstrom, M.F. Sanner, R.K. Belew, D.S. Goodsell, A. J. Olson, AutoDock4 and AutoDockTools4: automated docking with selective receptor flexibility, J. Comput. Chem. 30 (2009) 2785–2791, https://doi.org/10.1002/jcc.21256.

[22] M. Manjushree, H.D. Revanasiddappa, A diversified spectrometric and molecular docking technique to biophysical study of interaction between bovine serum albumin and sodium salt of risedronic acid, a bisphosphonate for skeletal disorders, Bioinorg. Chem. Appl. (2018) 6954951, https://doi.org/10.1155/2018/6954951.

[23] BIOVIA, Dassault Systèmes, Discovery studio visualizer, v20.1.0.19295, Dassault Systèmes, San Diego, 2020.

[24] F. Ding, W. Peng, Biophysical evaluation of protein structural flexibility for ligand biorecognition in solid solution, Phys. Chem. Chem. Phys. 18 (2016) 6595–6606, https://doi.org/10.1039/C5CP07385E.

[25] M.J. Abraham, T. Murtola, R. Schulz, S. Páll, J.C. Smith, B. Hess, E. Lindahl, GROMACS: high performance molecular simulations through multi-level parallelism from laptops to supercomputers, SoftwareX 1 (2015) 19–25, https://doi.org/10.1016/j.softx.2015.06.001.

[26] L. Wickstrom, A. Okur, C. Simmerling, Evaluating the performance of the ff99SB force field based on NMR scalar coupling data, Biophys. J. 97 (2009) 853–856, https://doi.org/10.1016/j.bpj.2009.04.063.

[27] A.W. Sousa da Silva, W.F. Vranken, ACPYPE - AnteChamber PYthon Parser interfacE, BMC Res. Notes 5 (2012) 367, https://doi.org/10.1186/1756-0500-5-367.

[28] P. Mark, L. Nilsson, Structure and dynamics of the TIP3P, SPC, and SPC/E water models at 298 K, J. Phys. Chem. A. 105 (2001) 9954–9960, https://doi.org/10.1021/jp003020w.
[29] W. Humphrey, A. Dalke, K. Schulten, VMD: visual molecular dynamics, J. Mol. Graph. 14 (1996) 33–38, https://doi.org/10.1016/0263-7855(96)00018-5.
[30] M.S. Valdés-Tresanco, M.E. Valdés-Tresanco, P.A. Valiente, E. Moreno, gmx_MMPBSA: a new tool to perform end-state free energy calculations with GROMACS, Chem. Theory Comput. 17 (2021) 6281–6291, https://doi.org/10.1021/acs.jctc.1c00645.
[31] Q. Zhang, Y. Ni, S. Kokot, Molecular spectroscopic studies on the interaction between Ractopamine and bovine serum albumin, J. Pharm. Biomed. Anal. 52 (2010) 280–288, https://doi.org/10.1016/j.jpba.2010.01.006.
[32] M. Sarkar, S.S. Paul, K.K. Mukherjea, Interaction of bovine serum albumin with a psychotropic drug alprazolam: physicochemical, photophysical and molecular docking studies, J. Lumin. 142 (2013) 220–230, https://doi.org/10.1016/j.jlumin.2013.03.026.
[33] T. Madrakian, H. Bagheri, A. Afkhami, M. Soleimani, Spectroscopic and molecular docking techniques study of the interaction between oxymetholone and human serum albumin, J. Lumin. 155 (2014) 218–225, https://doi.org/10.1016/j.jlumin.2014.06.047.
[34] J. Guan, X. Yan, Y. Zhao, Y. Sun, X. Peng, Binding studies of triclocarban with bovine serumalbumin: Insights from multi-spectroscopy and molecular modeling methods, Spectrochim. Acta A Mol. Biomol. Spectrosc. 202 (2018) 1–12, https://doi.org/10.1016/j.saa.2018.04.070.
[35] X. Zhang, Y. Lin, L. Liu, C. Lin, Study on the synthesis of sulfonamide derivatives and their interaction with bovine serum albumin, Luminescence. 30 (2015) 269–279, https://doi.org/10.1002/bio.2725.
[36] M.Z. Kabir, H. Tayyab, C. Erkmen, S. Kurbanoglu, S.B. Mohamad, B. Uslu, Characterization of Climbazole-Bovine serum albumin interaction by experimental and in silico approaches, Spectrochim. Acta A Mol. Biomol. Spectrosc. 288 (2023) 122197, https://doi.org/10.1016/j.saa.2022.122197.
[37] Y. Lu, R. Zhao, C. Wang, X. Zhang, C. Wang, Deciphering the non-covalent binding patterns of three whey proteins with rosmarinic acid by multi-spectroscopic, molecular docking and molecular dynamics simulation approaches, Food Hydrocoll. 132 (2022) 107895, https://doi.org/10.1016/j.foodhyd.2022.107895.
[38] H. Tang, L. Huang, D. Zhao, C. Sun, P. Song, Interaction mechanism of flavonoids on bovine serum albumin: Insights from molecular property-binding affinity relationship, Spectrochim. Acta A Mol. Biomol. Spectrosc. 239 (2020) 118519, https://doi.org/10.1016/j.saa.2020.118519.
[39] M. Kooravand, S. Asadpour, H. Haddadi, S. Farhadian, An insight into the interaction between malachite green oxalate with human serum albumin: molecular dynamic simulation and spectroscopic approaches, J. Hazard. Mater. 407 (2021) 124878, https://doi.org/10.1016/j.jhazmat.2020.124878.
[40] I. Aier, P.K. Varadwaj, U. Raj, Structural insights into conformational stability of both wild-type and mutant EZH2 receptor, Sci. Rep. 6 (2016) 34984, https://doi.org/10.1038/srep34984.
[41] S. Farhadian, B. Shareghi, F. Tirgir, S. Reiisi, N.G. Dehkordi, L. Momeni, E. Heidari, Design, synthesis, and anti-gastric cancer activity of novel 2,5-diketopiperazine, J. Mol. Liq. 294 (2019) 111585, https://doi.org/10.1016/j.molliq.2019.111585.
[42] K. Al-Khafaji, T.T. Tok, Molecular dynamics simulation, free energy landscape and binding free energy computations in exploration the anti-invasive activity of amygdalin against metastasis, Comput. Methods Programs Biomed. 195 (2020) 105660, https://doi.org/10.1016/j.cmpb.2020.105660.
[43] B.R. Miller III, T.D. McGee Jr, J.M. Swails, N. Homeyer, H. Gohlke, A.E. Roitberg, MMPBSA.py: an efficient program for end-state free energy calculations, Chem. Theory Comput. 8 (2012) 3314–3321, https://doi.org/10.1021/ct300418h.

VITA

PUBLICATION

[1]. Ngueanngam, N., Jityuti, B., Patnin, S., Boonsri, P., Makarasen, A., Buranaprapuk, A. Multiple spectroscopic and computational studies on binding interaction of 2-phenylamino-4-phenoxyquinoline derivatives with bovine serum albumin. Spectrochimica Acta Part A: Molecular and Biomolecular Spectroscopy, 310 (2024) 123948. https://doi.org/10.1016/j.saa.2024.123948, (Q2, impact factor 4.4).

[2]. Ngueanngam, N., Chaivisuthangkura, T., Asawutmangkul, N., Jityuti, B., Boonsri, P. Molecular Design of the Triphenylamine Substitution on Isoindigo-Based as Promising Hole Transport Materials for Perovskite Solar Cell. SWU Sci J, 38 (2022) 48-61, (TCI1).

[3]. Suksangiamkul, P., Choolert, C., Ngueanngam, N., Pasookhush, P., Vaniksampanna, A., Longyant, S., Chaivisuthangkura, P. Molecular cloning and tissue expression analysis of tumor necrosis factor (TNF) gene from Macrobrachium rosenbergii in response to pathogen infections, Sci. Ess. J. 40 (2024) 37-60, (TCI1).

AWARD RECEIVED

[1]. Bronze Prize (Young Rising Stars of Science Award 2020) entitled "Molecular Docking Study of Drug Molecules against SARS-CoV-2 in Silico" at the 46th International Congress on Science, Technology, and Technology-based Innovation (STT46), organized by the Science Society of Thailand under the Patronage of His Majesty the King,

October 5-7, 2020.

[2]. Outstanding Oral Presentation (Chemistry, Applied Chemistry, and Industrial Chemistry Group) entitled "Intermolecular Interactions of Quinoline Derivatives to Human Serum Albumin Using Fluorescence Spectroscopy, Molecular Docking, and Molecular Dynamics Simulations" at the 14th National Science Research Conference (The 14th Science Research Conference), May 25-26, 2023, University of Phayao.